Design and synthesis of quinazolin-4-one derivatives as potential anticancer agents and investigation of their interaction with RecQ helicases

Hanan S Haggag, Shaimaa M Aboukhatwa, Mohamed S Nafie, Anju Paul, Nabaweya Sharafeldin, Antony Oliver, Mervat H El-Hamamsy

Published in
Bioorganic Chemistry

Link to external publisher version
https://doi.org/10.1016/j.bioorg.2023.107086

Design and Synthesis of Quinazolin-4-one Derivatives as Potential Anticancer Agents and Investigation of their Interaction with RecQ Helicases

Hanan S. Haggag,[a, #,*] Shaimaa M. Aboukhatwa,[a, b, #,*] Mohamed S. Nafie,[c,d] Anju Paul,[e] Nabaweya Sharafeldin,[a] Antony W. Oliver,[e] Mervat H. El-Hamamsy [a,*]

- ***Hanan S. Haggag***
  MSc. Student, Department of Pharmaceutical Chemistry, Faculty of Pharmacy, Tanta University, El Giesh street, Tanta, 31527, Egypt. Email: hanan.soliman@pharm.tanta.edu.eg
- ***Shaimaa M. Aboukhatwa, PhD***
  Assistant Professor, Department of Pharmaceutical Chemistry, Faculty of Pharmacy, Tanta University, El Giesh Street, Tanta 31527, Egypt. Email: shaymaa.aboukhatwa@pharm.tanta.edu.eg
  Current Affiliation: Postdoctoral Research Associate, Department of Pharmaceutical Sciences, University of Illinois at Chicago, Chicago 60608, IL, USA.
- ***Mohamed S. Nafie, PhD***
  Department of Chemistry, College of Sciences, University of Sharjah (P. O. Box 27272), Sharjah, United Arab Emirates.
  Assistant Professor, Chemistry Department (Biochemistry program), Faculty of Science, Suez Canal University, Ismailia 41522, Egypt. Email: mohamed_nafie@science.suez.edu.eg
- ***Anju Paul, PhD***
  Research Fellow: Genome Damage and Stability Centre, School of Life Sciences, University of Sussex, Falmer BN1 9RQ, UK. Email: anju.paul@icr.ac.uk
  Current Affiliation: Hit Discovery and Structural Design Team, Division of Cancer Therapeutics, The Institute of Cancer Research, London SM2 5NG, UK.
- ***Nabaweya Sharafeldin, PhD***
  Associate Professor Emeritus, Department of Pharmaceutical Chemistry, Faculty of Pharmacy, Tanta University, El Giesh Street, Tanta 31527, Egypt. Email: nabawia.eldeen@pharm.tanta.edu.eg
- ***Antony W. Oliver, PhD***
  Faculty Senior Research Fellow: Genome Damage and Stability Centre, School of Life Sciences, University of Sussex, Falmer BN1 9RQ, UK. Email: antony.oliver@sussex.ac.uk
- ***Mervat H. El-Hamamsy, PhD***
  Associate Professor and Acting Head, Department of Pharmaceutical Chemistry, Faculty of Pharmacy, Tanta University, El Giesh street, Tanta, 31527, Egypt. Email: mhamamsy@pharm.tanta.edu.eg

Design and Synthesis of Quinazolin-4-one Derivatives as Potential Anticancer Agents and Investigation of their Interaction with RecQ Helicases

Hanan S. Haggag,[a, #,*] Shaimaa M. Aboukhatwa,[a, b, #,*] Mohamed S. Nafie,[c,d] Anju Paul,[e] Nabaweya Sharafeldin,[a] Antony W. Oliver,[e] Mervat H. El-Hamamsy [a,*]

a *Department of Pharmaceutical Chemistry, Faculty of Pharmacy, Tanta University, Tanta, 31527, Egypt.*

b *Department of Pharmaceutical Sciences, College of Pharmacy, University of Illinois at Chicago, Chicago 60608, IL, USA.*

c *Department of Chemistry, College of Sciences, University of Sharjah (P. O. Box 27272), Sharjah, United Arab Emirates.*

d *Chemistry Department (Biochemistry program), Faculty of Science, Suez Canal University, Ismailia 41522, Egypt.*

e *Genome Damage and Stability Centre, Science Park Road, University of Sussex Falmer, Brighton, BN1 9RQ.*

 # Both authors contributed equally to this work.

** To whom correspondence might be addressed*

Graphical abstract

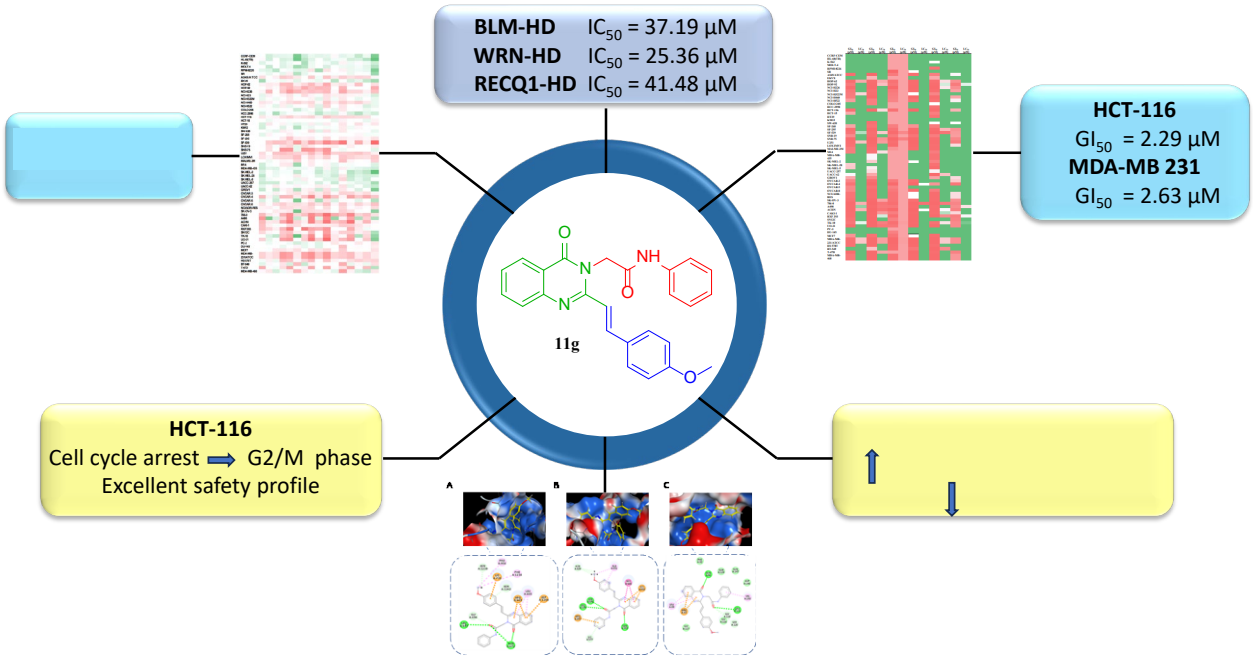

Keywords:

Anticancer, RecQ helicases, Colorectal carcinoma, DNA repair, Quinazolinones.

Abstract

The upregulation of RecQ helicases has been associated with cancer cell survival, making them appealing targets for TREATMENT. In this study, 29 quinazolinone derivatives were designed and synthesized. The cytotoxic activity of all compounds was evaluated against 60 cancer cell lines at the NCI, with 6 compounds being promoted to a five-dose screen. The compounds were further assayed for BLM helicase inhibition, where **11g**, **11q**, and **11u** showed moderate activity. These compounds were counter-screened against WRN and RECQ1 helicases, where **11g** moderately inhibited both enzymes. An ATP competition assay confirmed that the compounds bound to the ATP site of RecQ helicases, and molecular docking simulations were used to study the binding mode within the active site of the 3 enzymes. **11g** induced apoptosis in both HCT-116 and MDA-MB-231 cell lines, but also caused an G2/M phase cell cycle arrest in HCT-116 cells. This data revealed the potential of **11g** as a modulator of cell cycle dynamics and supports its interaction with RecQ helicases. In addition, **11g** displayed non-significant toxicity against FCH normal colon cells at doses up to 100 μM, confirming its selectivity on cancer cells. Overall, these findings suggest **11g** as a potential pan RecQ helicase inhibitor with high anticancer potency and a favorable safety margin and selectivity.

Highlights:

- Novel quinazolinone derivatives were designed and synthesized as anticancer agents.
- Target compounds showed promising cytotoxic activity against NCI-60 cancer cell lines.
- The compounds demonstrated ATP competitive inhibitory activity against BLM, WRN, and RECQ1 helicases.
- Molecular docking simulations revealed the binding modes of the compounds within helicase active sites.
- Target compounds induced apoptosis in colon cancer cells and arrested the cell cycle at G2/M phase and disclosed selectivity by being non-toxic to normal colon cell lines.

1. Introduction

RecQ helicases are a family of highly conserved ATP-dependent DNA helicases that play a crucial role in maintaining genomic integrity and DNA repair. [1, 2] In humans, there are five known RecQ helicases: RecQ1, Bloom syndrome protein (BLM), Werner syndrome protein (WRN), RecQ4, and RecQ5. [1-3] RecQ helicases are involved in a variety of cellular processes, including DNA replication, recombination, repair, and transcription regulation. [1, 2] The overexpression of RecQ helicases has been implicated in cancer cell survival and resistance to chemotherapy, making them attractive therapeutic targets in certain cancer types. [1-5]

RecQ1 is the most abundant RecQ helicase and is involved in DNA repair, recombination, and replication. [1, 2] BLM and WRN are associated with Bloom and Werner syndromes, respectively, which are rare genetic disorders with increased incidence. [1] BLM helicase is involved in the resolution of recombination intermediates, and its mutations are associated with the development of several types of cancer, including colorectal, breast, and ovarian cancer. [6-9] BLM helicase is involved in DNA replication and repair and is also associated with telomere maintenance. [1] Mutations in the BLM gene result in Bloom syndrome, characterized by premature aging and an increased risk of cancer. [1]

Structurally, RecQ helicases contain several domains, the most conserved is the ATPase domain, which consists of two Rec-A like subdomains, referred to as D1 and D2. [10] These subdomains are involved in ATP binding and hydrolysis, which powers the unwinding of DNA by the helicase. [7, 10] Another domain found in RecQ helicases is the zinc-binding domain, followed the two RecA-like domains and stabilizes the structure of the helicase. [7, 10, 11] The RecQ C-terminal (RQC) domain is involved in protein-protein interactions and plays a role in regulating helicase activity. [7, 10, 11] The winged helix (WH) domain is found in some RecQ helicases and is involved in DNA binding and recognition. [10] Finally, some RecQ helicases also contain a helicase-and-ribonuclease D C-terminal (HRDC) domain, which may play a role in DNA binding and recognition as well as in regulating helicase activity. [1, 7, 10]

Although helicases play a well-established role in cancer pathogenesis, and substantial research efforts have been made to develop specific inhibitors targeting these enzymes for potential anticancer treatments, no such therapies have progressed to the late-stage development phases. The discovery of a thiadiazolyl urea BLM helicase inhibitor, ML216 (**I**, **Figure 1**), suggested a non-

ATP competitive inhibition mechanism. ML216 (**I**) was found to impede the ability of BLM helicase to attach to DNA, initially indicating competition with DNA for binding to BLM helicase. [12, 13] However, subsequent studies by Chen *et al.* revealed that **I** directly interacts with the DNA substrate rather than the BLM helicase DNA binding site. [14] Additionally, they discovered an allosteric mode of action for a selective inhibitor of human BLM helicase (**II**, **Figure 1**). This inhibitor (**II**) did not interfere with ATP binding even with an excess of ATP, indicating a non-competitive mode of action. [14] Further X-ray crystallographic data confirmed **II** as an allosteric inhibitor of BLM helicase. [14]

In another study, Yin *et al*. discovered a class of isaindigotone derivatives as BLM helicase inhibitors with inhibitory activity against human colon cancer cells (**III**, **Figure 1**). [15] The quinazolinone core of compound **III** was found to be crucial for binding to BLM helicase, while the amine side chain and styryl part had partial effects. [15] Molecular docking and dynamic simulation revealed that compound **III** binds to the 3′-tailed duplex DNA binding pocket of the RQC domain of BLM helicase. [15] Further research by Wang, *et al*. to expand the understanding of the structure activity relationship for BLM helicase inhibitors, confirmed that the quinazolinone core was the main structural requirement for BLM inhibition. [16]

Quinazolinone scaffold is an established privileged scaffold in medicinal chemistry. Several pharmacologically active compounds with a quinazolinone structure are known for anticancer, among other activities. [17-19] The anticancer potential for quinazolinone derivatives was observed in multiple cancer types.

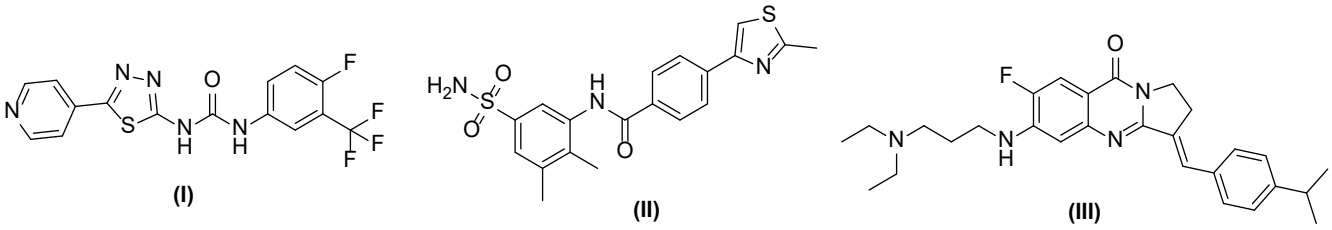

Figure 1. Examples of literature reported small molecules with BLM helicase inhibitory activity.

In this study, our objective was to expand our understanding of the structure-activity relationship (SAR) of quinazolinone derivatives as potential anticancer compounds. Additionally, we aimed to test their inhibitory activity against BLM helicase and validate their binding mode through biochemical assays.

The overexpression of RecQ helicase isoforms in certain cancer types supports the anticancer potential of RecQ helicases. [20, 21] On another hand, some genetic disorders with loss of RecQ function demonstrate an increased incidence of tumors. [22] This controversy suggests that targeting RecQ helicases may be a double-edged sword and it might be necessary to categorize RecQ helicase inhibitors as "personalized/individualized" treatment option for certain cancer types. There remains a lot to be investigated about those attractive targets and we hope our study would contribute to further understanding of the RecQ helicases functions.

Design Rationale

The design strategy for the target compounds is illustrated in **Figure 2**. The design of compounds (**6a-c** and **11a-w**) was guided by the structural features of a previously reported BLM helicase inhibitor (**IV**). [23] Generally, all compounds were designed with preserving the quinazolinone core structure, and excluding the amine linker at position seven of the quinazolinone ring, as it might interfere via non-specific interaction with the negatively charged DNA substrate under physiological conditions. Specifically, compounds **6a-c** were designed via replacing the 2-styryl group with a phenyl group, and incorporating an imine linker, flanking hydrophobic substituents at position three of the quinazolinone ring.

Meanwhile, analogues **11a-w** were built by conserving the styryl group, with varying the substituents on the phenyl *meta* or/and *para* with fluctuating electronic and steric properties, and incorporation of an amide linker at the N-3 position of the quinazolinone ring. The inclusion of the amide linker aimed to expand the molecular space at this position by constructing a hydrophobic arm. The hydrophobic arm is expected to facilitate additional binding interactions within the pocket in the active site of BLM helicase.

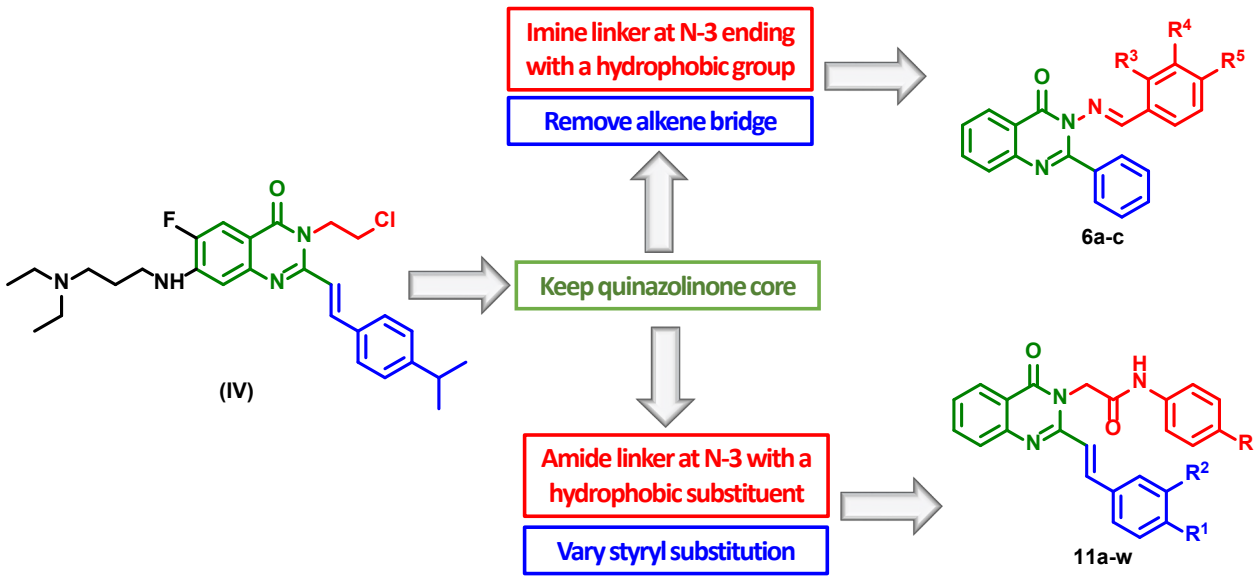

Figure 2. Design rationale of target compounds **6a-c** and **11a-w** as BLM helicase inhibitors.

2. Results and discussion

2.1. Chemical synthesis and characterization

The synthetic pathways for the designed compounds are depicted in **Scheme 1** and **Scheme 2**. In **Scheme 1**, cyclization reaction of anthranilic acid (**1**) and benzoyl chloride under basic conditions as reported in references, [24, 25] yielded 2-phenyl-4*H*-benzoxazin-4-one (**2**). Upon reaction of intermediate **2** with 99% hydrazine hydrate in ethanol at 80 °C, an unexpected formation of the open-ring structure *N*-(2-(hydrazinecarbonyl)phenyl)benzamide (**3**) was observed. The formation of diamide **3** instead of the ring structure **5** was also observed in previous studies, [26, 27] under similar reaction conditions. To avoid this ring opening, compound **2** was reacted with 99% hydrazine hydrate in absolute ethanol, at a higher temperature of 250 °C to provide compound **5**. [28-31] The elevated temperature would provide enough energy for elimination of a water molecule, leading to ring closure of the diamide intermediate (**Scheme S1**, Supplementary information). Both compounds **3** and **5** were obtained with identical melting points of 195-196 °C. [32, 33] However, their differentiation was confirmed by analyzing their ^{1}H NMR spectra. The ^{1}H NMR spectrum of **3** exhibited a singlet at δ 12.56 ppm for the amide proton (N**H**C=O) and another singlet at 10.21 ppm for the hydrazine group N**H**NH$_2$, whereas both these peaks were absent in **5**. Condensation reaction of intermediate **3** or **5** with suitable aldehydes resulted in the formation of compounds **4a-b** and **6a-c**, respectively. In the reaction of **5** with 3-pyridinecarboxyaldehyde,

followed by precipitation with ice-water, generated the open ring structure **4c**. The chemical structures of the synthesized compounds were confirmed through ^{1}H NMR, ^{13}C NMR, mass spectral data analysis, and elemental analysis as detailed in the experimental section. The ^{1}H NMR spectra of compounds **4a-c** indicated the disappearance of the NH_2 singlet peak at δ 4.70 ppm and the appearance of a singlet for N=C**H** in the range of δ 8.37-8.89 ppm. Similarly, the ^{1}H NMR spectra of compounds **6a-c** demonstrated the disappearance of the NH_2 singlet at δ 5.08 ppm and the emergence of a singlet for N=C**H** in the range from δ 8.88 to 9.66 ppm.

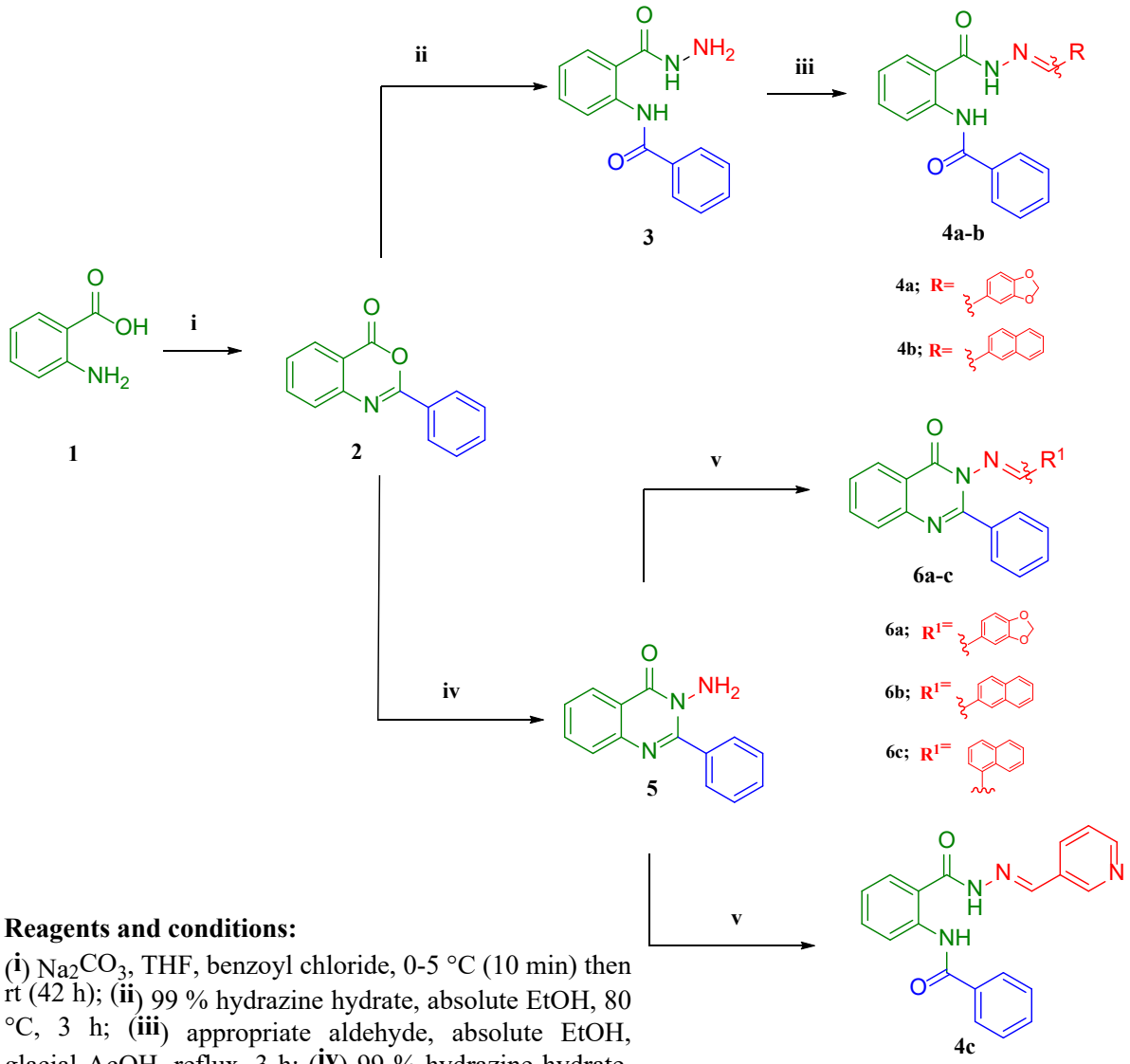

Reagents and conditions:

(**i**) Na_2CO_3, THF, benzoyl chloride, 0-5 °C (10 min) then rt (42 h); (**ii**) 99 % hydrazine hydrate, absolute EtOH, 80 °C, 3 h; (**iii**) appropriate aldehyde, absolute EtOH, glacial AcOH, reflux, 3 h; (**iv**) 99 % hydrazine hydrate, absolute EtOH, 250 °C, 18 h; (**v**) appropriate aldehyde, absolute EtOH, glacial AcOH, reflux, 26-72 h.

Scheme 1. Synthesis and chemical structures of compounds **4a-c** and **6a-c**.

The convergent synthetic pathway of compounds **11a-w** is illustrated in **Scheme 2**. The synthesis begins with the reaction of anthranilic acid (**1**) with acetic anhydride to form 2-methyl-4*H*-benzo[*d*][1,3]oxazin-4-one (acetanthranil), which is unstable and prone to hydrolysis by water. [27] The instability of acetanthranil intermediate arises from water attacking the carbonyl group of the cyclic ester, leading to ring opening as shown in **Scheme S2** (Supplementary Information). The 2-aryl substitution on the benzoxazinone ring in intermediate **2** (**Scheme 1**) imparted some degree of stability of the carbonyl group to water hydrolysis, in comparison to the acetanthranil intermediate (**Scheme 2**). [27] To avoid ring opening and diamide formation during the synthesis of **7**, a two-step approach was employed. First, the cyclization reaction of **1** with acetic anhydride was achieved and yielded acetanthranil as an intermediate, followed by evaporation of the solvent under vacuum. Then, 32% ammonia was added to the resulting residue under air-tight conditions to give compound **7 (Scheme 2)**. [34]

Nucleophilic acyl substitution reactions of substituted aromatic amines **8a-c** with 2-chloroacetyl chloride were performed to obtain compounds **9a-c**. [35] Subsequently, the nucleophilic substitution reaction between compound **7** and compounds **9a-c** afforded analogues **10a-c**. [36] Finally, the condensation reactions of **10a-c** with suitable aldehydes in the presence of acetic anhydride and zinc chloride catalyst were accomplished by heating under reflux conditions at 150 °C to yield the desired compounds, **11a-w**.

The chemical structures of target compounds, **11a-w** were confirmed by ^{1}H NMR spectral analysis and elemental analysis as reported in the experimental section. The ^{1}H NMR spectra of **11a–w**, revealed the disappearance of the -CH_3 singlet at δ 2.56 ppm, observed in compounds **10a–c**. Simultaneously, appearance of two doublet signals at approximately δ 8.0 and 7.5 ppm, which were assigned to the styryl alkene protons (quinazolinone-**CH**=**CH**-Ar). Styryl alkene protons recorded a coupling constant (*J* value) of ca. 15 Hz, which indicated that compounds **11a-w** exist in the (*E*) isomer rather than the (*Z*) isomer.

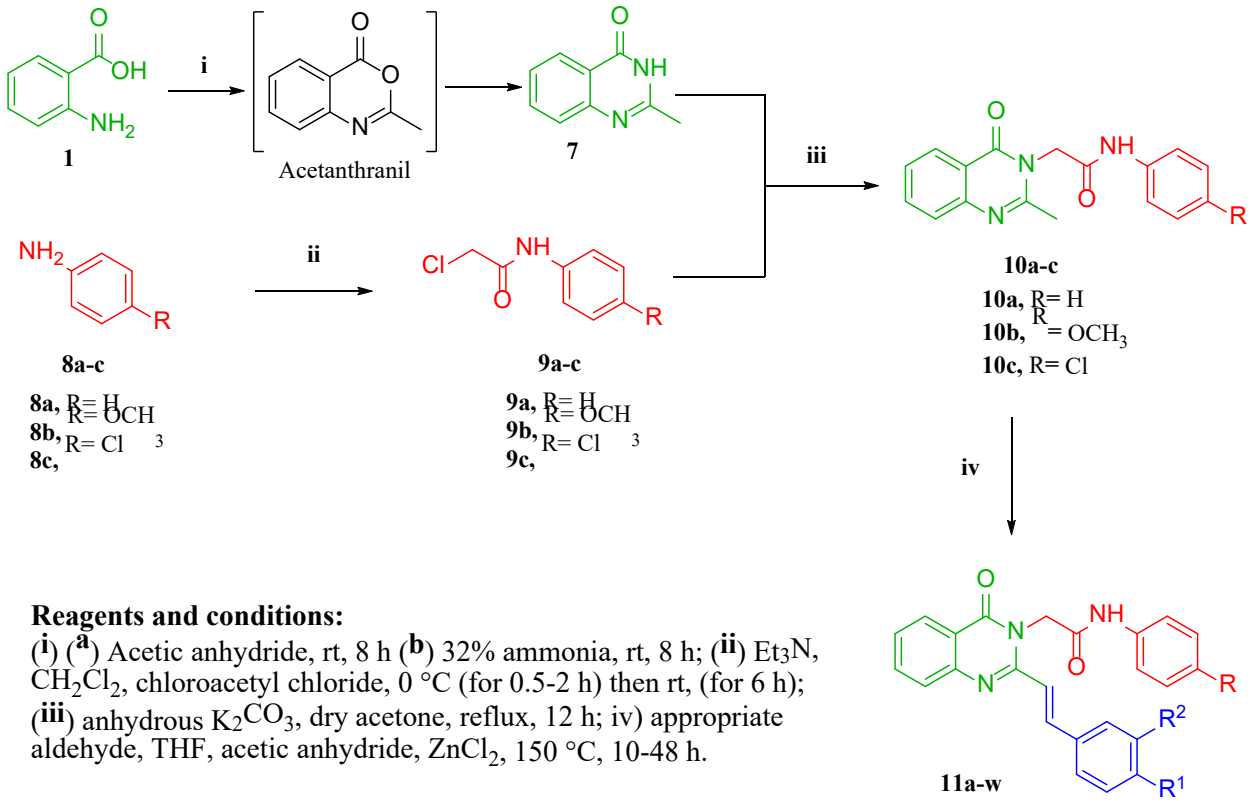

Reagents and conditions:
(**i**) (**a**) Acetic anhydride, rt, 8 h (**b**) 32% ammonia, rt, 8 h; (**ii**) Et_3N, CH_2Cl_2, chloroacetyl chloride, 0 °C (for 0.5-2 h) then rt, (for 6 h); (**iii**) anhydrous K_2CO_3, dry acetone, reflux, 12 h; iv) appropriate aldehyde, THF, acetic anhydride, $ZnCl_2$, 150 °C, 10-48 h.

11a: R= H, R_1= H, R^2= H

11b: R= H, R_1= NO_2, R^2= H

11c: R= H, R_1= H, R^2= Br

11d: R= H, R^1= H, R^2= NO_2

11e: R= H, R_1, R_2= OCH_2O

11f: R= H, R_1= H, R^2= OCH_3

11g: R= H, R^1= OCH_3, R^2= H

11h: R= H, R_1= $N(CH_3)_2$, R^2= H

11i: R= OCH_3, R_1= H, R^2= H

11j: R= OCH_3, R_1= NO_2, R^2= H

11k: R= OCH_3, R_1= H, R^2= Br

11l: R= OCH_3, R^1= H, R^2= NO_2

11m: R= OCH_3, R_1, R_2= OCH_2O

11n: R= OCH_3, R_1= H, R^2= OCH_3

11o: R= OCH_3, R_1= OCH_3, R^2= H

11p: R= OCH_3, R_1= $N(CH_3)_2$, R^2= H

11q: R= Cl, R_1= H, R^2= H

11r: R= Cl, R^1= H, R^2= NO_2

11s: R= Cl, R_1= H, R^2= Br

11t: R= Cl, R^1, R^2= OCH_2O

11u: R= Cl, R^1= OCH_3, R^2= H

11v: R= Cl, R_1= H, R^2= OCH_3

11w: R= Cl, R_1= $N(CH_3)_2$, R^2= H

Scheme 2. Synthesis of compounds **11a-w**.

2.2. Biological evaluation

2.2.1. *In vitro* anticancer activity in NCI 60 single-dose screening

The newly synthesized derivatives (**4a-c**, **6a-c**, and **11a-w**) were screened for potential activity against 60 cancer cell lines, at the National Cancer Institute (NCI) Developmental Therapeutic Program (DTP). [37-41] Target compounds were initially evaluated at a single dose of 10 μM against nine different cancer types, including leukaemia, non-small cell lung cancer, melanoma, CNS cancer, ovarian cancer, renal cancer, prostate cancer, and breast cancer. The single-dose screening outcomes for **4a-c**, **6a-c**, and **11a-w** against 60 cancer cell lines were presented as a mean-graph showing the growth percentages (G%) of treated cancer cells relative to the no-drug control. The individual NCI-60 reports for tested compounds are provided in the Supplementary Information (**Figures S94-S123**) The corresponding growth inhibition percentages (GI%) were calculated for each screened compound by subtracting the G% from 100, according to the formula (GI% = 100 – G%) and the results were summarized in **Table 1.**

Compounds, **4a**, **4c**, **11r**, **11s**, and **11t** exhibited poor cytotoxic activity in all examined cancer cell lines, with a mean GI% less than zero except **4c** with a mean GI% = 1% (**Table S1**, Supplementary Information). Compounds **4b, 11c**, **11e**, **11m**, and **11i** showed moderate anticancer activity against most tested cell lines, with a mean GI% of 13, 11.4, 13.8, 16.1, and 14.2%, respectively (**Table S1**, Supplementary Information).

Thirteen compounds exhibited moderate to strong growth inhibition activity against the examined cell lines with mean GI% ranging from 25% to 50%, namely **6a** and **6c** (mean GI% = 28), **6b** (mean GI% = 47), **11a** (mean GI% = 35), **11b** (mean GI% = 30), **11d** (mean GI% = 27), **11j** (mean GI% = 42), **11l** (mean GI% = 34), **11o** (mean GI% = 32), **11q** (mean GI% = 47), **11u** (mean GI% = 36), **11v** (mean GI% = 34), **11w** (mean GI% = 49) (**Table 1**).

Six of the tested compounds showed moderate to lethal anticancer activity against the examined cell lines, with a mean growth inhibition above 50%; namely **11f** (mean GI% = 53), **11g** (mean GI% = 60), **11k** (mean GI% = 65), **11n** (mean GI% = 68), **11p** (mean GI% = 60), and **11h** (mean GI% = 52). Compound **11n,** with the highest GI% among all tested derivatives, showed lethality in 14 cancer cell lines, with GI% ranging from 112% to 174%, and strong growth inhibitory activity in 12 other cancer cell lines ranging from 62% to 99% GI. Compound **11k** with a mean GI% of 65,

exposed the second-highest GI% (**Table 1**). **11k** disclosed lethality in 12 cancer cell lines, with a GI% ranging from 102% to 161% and strong growth inhibitory activity in other 14 cancer cell lines ranging from 64% to 100%. Both **11g** and **11p** (mean GI% = 60) exhibited lethality in 6 cancer cell lines ranging from 102% to 160% (**Table 1**). Strong cancer cell growth inhibition was observed with **11g** in 14 cancer cell lines ranging from 63% to 100% and with **11p** in 18 cancer cell lines ranging from 61% to 97% (**Table 1**). Compound **11f** (mean GI% = 53) with the fourth highest GI% exhibited lethality in 6 cancer cell lines ranging from 102% to 136% and strong activity in 15 other cancer cell lines ranging from 60% to 100% (**Table 1**).

To our notice, the inhibition profile of several compounds demonstrated high selectivity towards renal cancer over the other tested cancer cell lines. For example, compounds **11g, 11k**, **and 11n** displayed lethal activity against almost all examined renal cell lines. Compound **11g** reported 110% to 160% value of GI%, compound **11k** recorded 116% to 161% value of GI% and compound **11n** GI% was from 124% to 174% against renal cancer cells (**Table 1**). One of the most sensitive cell lines was the ACHN cell line with a GI% of 160, 151, 161, 102, 101, and 166 % for compounds **11g**, **11k**, **11n**, **11p**, **11v**, and **11q**, respectively (**Table 1**). Compounds **11g**, **11k**, **11n**, **11o**, and **11q** exhibited excellent and lethal activity against the 786-0 cell line in which GI% was 143, 144, 171, 113, and 149%, respectively (**Table 1**). Compounds **11f**, **11g**, **11k**, **11n**, and **11q** showed lethal activity against UO-31 with GI% of 125, 133, 161, 174, and 125%, respectively. Compounds **11g**, **11k**, **11n**, and **11q** resulted in growth inhibitory activity against A498 with GI% = 143, 151, 143, and 116%, respectively. Compounds **11g** and **11j** showed remarkable activity against RXF 393 with GI% = 155 and 158%, respectively (**Table 1**).

The other highly susceptible cancer cell lines were CNS cancer cells. For example, compounds **11p**, **11w** and **11n** resulted in GI% = 160, 164 and 146%, respectively, against SF-539 cells. Moreover, the OVCAR-4 ovarian cancer cell growth was inhibited by compounds **11n** and **11k** with a GI% of 130 and 146%, respectively (**Table 1**). The MDA-MB-231 breast cancer cells responded to compounds **11k** and **11n** with a GI% of 138 and 130%, respectively (**Table 1**).

Due to their significant cancer cell growth inhibitory activity and lethality observed during the single-dose screening against multiple cell lines, the NCI-DTP selected six quinazolinone derivatives, namely **11f**, **11g**, **11k**, **11n**, **11p**, and **11q**, for further detailed screening. These

compounds were chosen for evaluation at five different concentrations to gain a more comprehensive investigation of their anticancer potential, as presented in **Table 2**.

Table 1. NCI-60 single dose screening results for analogues with GI % Mean > 25%.

Cell lines	Growth Inhibition Percentage (GI %)[a]																		
	6a	6b	6c	11a	11b	11d	11f	11g	11h	11j	11k	11l	11n	11o	11p	11q	11u	11v	11w
Leukemia																			
CCRF-CEM	---[b]	48	---	29	---	---	---	12	10	---	13	---	11	36	---	14	---	14	11
HL-60(TB)	nd[c]	64	---	35	---	nd	---	---	---	---	---	nd	---	18	18	---	---	---	---
K-562	nd	73	26	---	20	nd	---	16	44	---	14	nd	16	---	41	15	33	15	31
MOLT-4	nd	81	11	27	---	nd	---	13	20	---	13	nd	---	22	15	13	18	---	25
RPMI-8226	---	61	---	---	---	---	29	18	36	---	58	---	59	24	43	13	16	12	12
SR	nd	89	15	20	12	nd	10	45	25	11	22	nd	22	21	27	12	29	20	19
Non-Small Cell Lung Cancer																			
A549/ATCC	---	58	39	62	24	44	83	73	66	24	84	15	87	53	85	66	77	71	56
EKVX	41	20	18	---	20	20	15	37	36	26	18	12	20	---	29	---	11	---	20
HOP-62	47	44	61	42	51	46	95	98	63	67	98	59	112	48	61	42	92	29	75
HOP-92	66	20	28	nd	48	36	80	100	85	112	89	100	96	nd	103	nd	nd	nd	114
NCI-H226	49	48	60	40	101	24	86	126	107	79	93	87	99	39	115	70	70	45	98
NCI-H23	24	32	22	---	45	23	41	57	41	65	41	18	59	46	50	40	39	17	33
NCI-H322M	10	20	16	12	33	16	28	53	51	30	42	---	58	17	54	25	11	25	38
NCI-H460	31	91	49	57	47	33	49	63	83	58	68	37	85	49	80	61	77	53	38
NCI-H522	42	37	25	43	21	---	47	11	51	27	57	---	73	30	56	23	36	---	38
Colon Cancer																			
COLO 205	---	42	nd	21	33	19	25	29	30	15	30	---	28	12	53	22	25	14	43
HCC-2998	---	42	---	---	20	---	10	20	42	33	15	---	---	---	37	---	---	---	32
HCT-116	31	78	34	55	39	42	64	79	69	64	74	45	86	68	71	70	65	62	43
HCT-15	35	87	22	23	14	34	32	20	48	26	29	22	29	12	43	22	25	12	58
HT29	---	80	---	---	54	29	42	17	36	15	48	12	48	27	55	24	61	36	68
KM12	13	55	---	---	23	25	6	33	24	17	12	22	18	20	50	16	39	22	45
SW-620	---	nd	10	24	16	---	49	38	42	30	68	---	59	16	52	28	26	32	38
CNS Cancer																			
SF-268	71	50	40	---	41	21	31	46	43	35	35	28	34	29	27	25	39	18	42
SF-295	52	53	38	29	28	32	51	87	65	44	51	21	65	25	50	41	47	39	72
SF-539	45	73	75	30	79	91	88	68	127	70	123	93	146	119	160	41	113	47	164
SNB-19	44	43	78	32	63	19	60	71	37	68	51	27	44	48	29	47	23	24	65

Cell lines	Growth Inhibition Percentage (GI %)[a]																		
	6a	6b	6c	11a	11b	11d	11f	11g	11h	11j	11k	11l	11n	11o	11p	11q	11u	11v	11w
SNB-75	70	34	nd	nd	62	30	136	135	37	133	130	98	134	nd	16	nd	nd	nd	36
U251	65	69	31	64	31	88	93	84	84	68	102	64	127	74	77	80	89	72	60
Melanoma																			
LOX IMVI	59	nd	22	57	42	67	73	73	98	38	71	49	78	35	86	75	63	60	91
MALME-3M	27	41	55	30	15	25	44	39	84	28	51	23	37	26	93	41	24	33	84
M14	11	43	18	---	19	29	52	54	19	31	50	23	39	---	19	18	22	24	35
MDA-MB-435	---	45	---	---	---	---	29	15	40	16	33	---	41	---	46	15	---	---	31
SK-MEL-2	21	---	nd	---	25	12	19	19	29	21	20	---	12	---	23	---	---	---	---
SK-MEL-28	39	38	12	---	24	15	24	21	64	19	30	---	11	---	54	---	---	---	34
SK-MEL-5	nd	62	71	---	17	nd	26	28	38	47	22	nd	---	---	69	---	11	---	44
UACC-257	---	51	11	---	---	---	32	---	40	14	29	---	19	---	32	16	---	---	21
UACC-62	---	64	---	---	30	49	33	21	56	27	32	48	42	25	59	---	27	---	29
Ovarian Cancer																			
GROV1	---	44	22	---	25	---	39	50	24	40	50	---	62	6	53	32	---	23	12
OVCAR-3	51	33	nd	22	19	45	25	51	74	40	64	49	72	37	73	71	50	65	58
OVCAR-4	36	14	45	100	43	---	102	99	65	84	146	55	130	91	41	122	83	111	93
OVCAR-5	---	31	---	---	20	---	34	39	11	24	52	---	60	---	34	31	---	27	25
OVCAR-8	71	49	41	56	34	64	78	56	74	54	86	57	90	41	79	42	73	51	97
NCI/ADR-RES	36	46	33	42	46	35	67	63	70	61	69	29	65	24	68	33	44	31	78
SK-OV-3	15	31	13	39	28	51	46	55	---	66	64	58	55	21	75	60	21	23	15
Renal Cancer																			
786-0	67	47	71	98	53	40	109	143	80	91	144	116	171	113	92	149	72	90	72
A498	---	---	---	130	---	---	72	143	29	14	151	---	143	---	43	116	---	75	24
ACHN	68	58	52	98	52	56	116	160	81	48	151	80	161	86	102	166	49	101	57
CAKI-1	39	52	32	92	43	20	28	65	76	37	44	50	49	53	81	80	57	39	47
RXF 393	49	19	56	91	73	45	100	155	Nd	158	116	106	132	29	nd	109	51	16	nd
SN12C	---	47	---	69	38	25	82	92	61	38	94	24	124	43	76	81	45	61	24
TK-10	29	27	---	24	---	---	88	110	---	74	139	27	143	52	37	112	---	68	17
UO-31	---	42	17	75	---	23	125	133	46	77	161	77	174	53	97	125	21	84	13
Prostate Cancer																			
PC-3	15	47	47	24	15	22	24	15	32	10	21	---	26	54	36	27	52	24	70
DU-145	27	44	30	25	21	31	12	22	58	11	21	---	26	23	93	29	34	31	63

Cell lines	Growth Inhibition Percentage (GI %)[a]																		
	6a	**6b**	**6c**	**11a**	**11b**	**11d**	**11f**	**11g**	**11h**	**11j**	**11k**	**11l**	**11n**	**11o**	**11p**	**11q**	**11u**	**11v**	**11w**
Breast Cancer																			
MCF7	47	66	26	nd	21	58	58	45	74	26	66	53	70	nd	79	nd	nd	nd	72
MDA-MB-231/ATCC	44	42	71	75	53	66	129	119	67	118	138	84	130	73	81	96	51	72	65
HS 578T	36	nd	57	17	46	13	97	90	55	70	100	33	91	44	34	62	77	67	83
BT-549	nd	48	16	---	37	nd	56	---	101	---	44	nd	26	28	110	11	36	13	73
T-47D	23	44	28	111	20	17	63	120	51	44	117	31	115	34	56	111	34	94	25
MDA-MB-468	---	33	46	38	55	---	17	44	105	48	22	16	29	---	125	43	---	---	69
GI % Mean	28	47	28	35	30	27	53	60	53	42	65	34	68	32	60	47	36	34	49

[a] GI% coded on the green-white-red color scale from minimum to maximum, [b] "---" refers to the GI% less than 10%, [c] nd; not determined.

Min **Max**

2.2.2. Structure Activity relationship (SAR)

The structure Activity relationship (SAR) of quinazolinone derivatives (**11a-w**) was investigated to understand how their activity in the NCI-60 screen correlates with their structural features. **Figure 3** presents a summary of the SAR analysis, highlighting the most active derivatives and their corresponding mean growth inhibition percentage

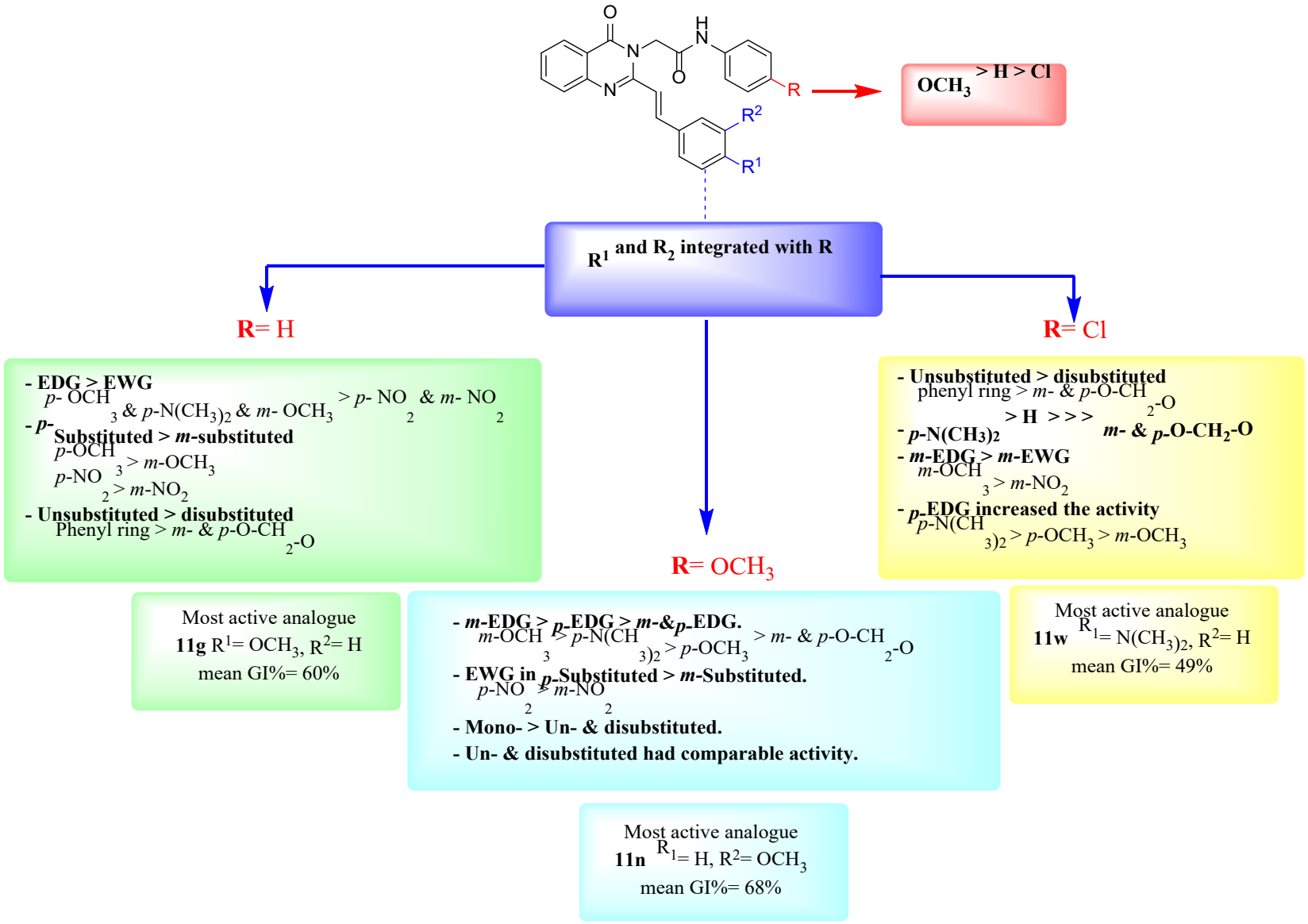

Figure 3. Summary of SAR and the most active analogues for target quinazolinone derivatives (**11a-w**) as *in vitro* growth inhibitors of 60 human cancer cell lines based on the mean GI% values.

Analysis of the structure-activity relationship for **11a-w** revealed that firstly, the methoxy (OCH_3) substitution at the *para* position of the phenylacetamide ring resulted in derivatives with higher activity compared to the unsubstituted ring. Conversely, the chloro (Cl) substitution at the at *para* position of phenylacetamide ring led to derivatives with lower activity. This trend is exemplified by comparing the three *N,N*-dimethylaminostyryl derivatives in which **11p** (R = OCH_3) which exhibited a higher mean GI% of 60%; **11h** (R = H) which showed a mean GI% of 53%, and **11w** (R = Cl) which displayed a mean GI% of 49%.

Secondly, regarding unsubstituted phenylacetamide derivatives (R = H), it was observed that electron-donating groups in the *ortho* or *meta* positions on the styryl ring exhibited higher cytotoxicity compared to electron-withdrawing groups. For instance, **11g** ($R^1 = OCH_3$, R^2 = H) with a mean GI% = 60%, **11h** ($R^1 = N(CH_3)_2$, R^2 = H) with mean GI% = 53%, and **11f** (R^1 = H, $R^2 = OCH_3$) with a mean GI% = 53% demonstrated greater activity compared to **11b** ($R^1 = NO_2$, R^2 = H) with a mean GI% = 30% and **11d** (R^1 = H, $R^2 = NO_2$) with a mean GI% = 27%. In addition, the presence of *para*- substituents on the styryl ring appeared to contribute to higher cytotoxicity compared to the corresponding *meta*- substitution. For example, compound **11g** ($R^1 = OCH_3$, R^2 = H) with a mean GI% of 60% and **11b** ($R^1 = NO_2$, R^2 = H) with a mean GI% of 30% exhibited greater activity than their respective counterparts, **11f** (R^1 = H, $R^2 = OCH_3$) with a mean GI% of 53% and **11d** (R^1 = H, $R^2 = NO_2$) with a mean GI% of 27%. Also, the unsubstituted styryl ring as in compound **11a** ($R^1 = R^2$ = H) with mean GI% of 35% resulted in higher activity compared to the disubstituted (fused ring) compound **11e** (R^1, $R^2 = OCH_2O$) with mean GI% of 14%.

Thirdly, concerning the *para*- methoxy substituted phenylacetamide derivatives (R = OCH_3), it was found that in the beginning, the *meta*- methoxy substituent on the styryl ring showed an increase in activity among other derivatives substituted with electron-donating group in other positions. For example, **11n** (R^1 = H, $R^2 = OCH_3$) with a mean GI% of 68% had higher activity than **11p** ($R^1 = N(CH_3)_2$, R^2 = H) with a mean GI% of 60%, **11o** ($R^1 = OCH_3$, R^2 = H) with a mean GI% of 32% and **11m** (R^1, $R^2 = OCH_2O$) with a mean GI% of 16%. Then, electron-withdrawing groups at the *para* position of the styryl ring resulted in higher activity compared to the *meta*-substituted ones. **11j** ($R^1 = NO_2$, R^2 = H) with a mean GI% of 42% was more active than **11l** (R^1 = H, $R^2 = NO_2$) with a mean GI% of 34%. In addition to, the monosubstituted compounds showed higher activity than the unsubstituted and the disubstituted one. For example, **11n** (R^1 = H, R^2 =

OCH_3) with a mean GI% of 68% and **11l** (R^1 = H, R^2 = NO_2) with a mean GI% of 34% were more active compared to **11m** (R^1, R^2 = OCH_2O) with a mean GI% of 16% and **11i** (R^1 = R^2 = H) with a mean GI% of 14%. On the other hand, the unsubstituted compound **11i** (R^1 = R^2 = H) with a mean GI% of 14% and the disubstituted **11m** (R^1, R^2 = OCH_2O) with a mean GI% of 16% had comparable activity.

Finally, in the *para*- chloro substituted phenylacetamide derivatives (R = Cl), firstly, the plain styryl derivatives seemed to produce superior activity than the disubstituted one. **11q** (R^1 = R^2 = H) with a mean GI% of 47% was more active than **11t** (R^1, R^2 = OCH_2O) with mean GI% less than zero%. In addition, the plain styryl derivative **11q** (R^1 = R^2 = H) with mean GI%= 47% showed comparable activity to **11w** (R^1 = $N(CH_3)_2$, R^2 = H) with mean GI% = 49% and both were superior to other derivatives. Secondly, electron-donating styryl substitution resulted in an increase in activity compared to electron-withdrawing groups. For example, **11v** (R^1 = H, R^2 = OCH_3) with a mean GI% of 34% was more active than **11r** (R^1 = H, R^2 = NO_2) with a mean GI% less than zero%. Also, electron-donating groups in the *para* position of the styryl ring resulted in higher activity than in the *meta* position. **11w** (R^1 = $N(CH_3)_2$, R^2 = H) with a mean GI% of 49% is more active than *p*-OCH_3 **11u** (R^1 = OCH_3, R^2 = H) with mean GI% of 36% and **11v** (R^1 = H, R^2 = OCH_3) with a mean GI% of 34%.

The SAR for derivatives **6a-c** and **4a-c** is outlined in **Figure 4**. Analyzing the structural features in relation to their activity (mean GI%), the following remarks were made, in the beginning, the presence of the quinazolinone core is essential for activity, as demonstrated by the comparison of quinazolinone derivatives **6a** (R = 5-benzo[d][1,3]dioxole) with a mean GI% of 28% and **6b** (R = 2-naphthyl) with a mean GI% of 48% to the corresponding open ring compounds **4a** (R = 5-benzo[d][1,3]dioxolo) with a mean GI% less than zero% and **4b** (R = 2-naphthyl) with a mean GI% of 13%. This indicates that the ring opening and formation of the diamide in compounds **4a** and **4b** abolished or significantly diminished their activity, highlighting the importance of the intact quinazolinone core for anticancer activity. Then, **4b** (R = 2-naphthyl) with a mean GI% = 13% was more active than **4c** (R = 3-pyridyl) with a mean GI% of 1% and, (*m, p)*-O-CH_2-O-, **4a** (1-naphthyl) with a mean GI% of less than zero%. Finally, among the quinazolinone derivatives (**6a**-**6c**), **6b** (R = 2-naphthyl) exhibited the highest activity with a mean GI% of 48%. In comparison, **6a** (R = 5-benzo[*d*][1,3]dioxole) showed a lower activity with a mean GI% of 28%.

Compound **6c** (R = 1-naphthyl) also displayed a mean GI% of 28%, signifying a comparable activity to **6a**. This suggests that the substitution of the quinazolinone core with different groups can influence the anticancer activity, with 2-naphthyl being the most favourable substitution in this case.

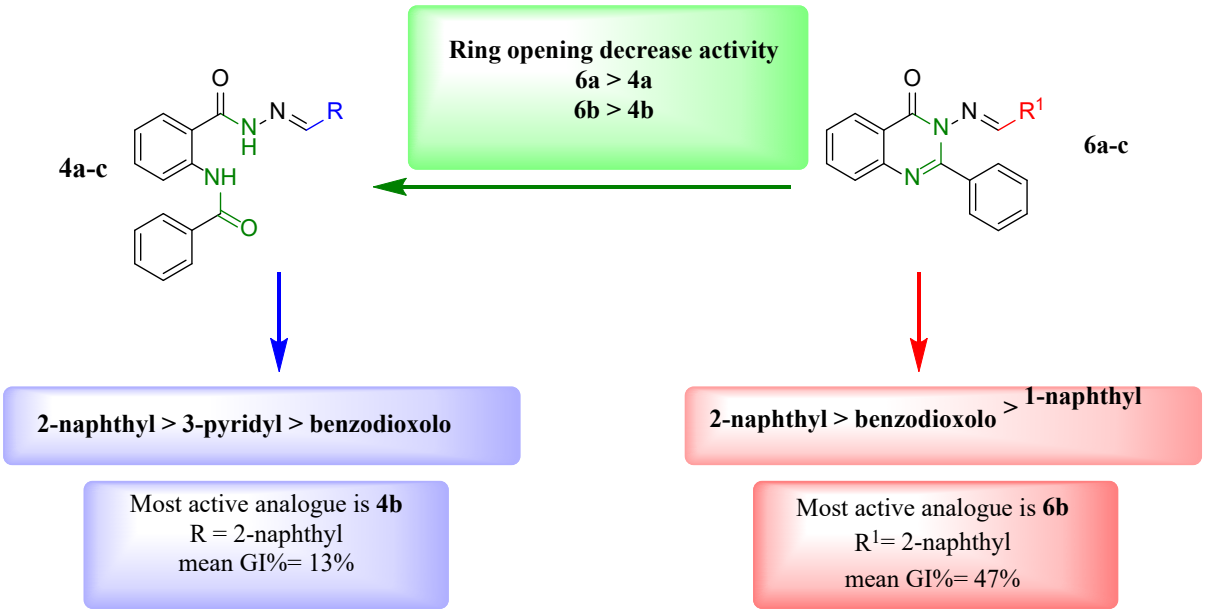

Figure 4. Summary of SAR and the most active analogues for target compounds, **6a-c** and **4a-c,** as *in vitro* cytotoxic agents against 60 human cancer cell lines depending on mean GI % values.

2.2.3. *In vitro* screening at 5-dose against NCI-60 cell panel

Among the compounds evaluated in the single-dose NCI-60 screen, a subset of quinazolinone derivatives demonstrated significant inhibition in a minimum number of cell lines, meeting the predetermined threshold criteria. Consequently, these six quinazolinone derivatives, namely **11f (**NSC: D-834383), **11g** (NSC: D-834609), **11k** (NSC: D-834384), **11n** (NSC: D-834385), **11p** (NSC: D-835926) and **11q** (NSC: D-836907) were selected for further evaluation in the 5-dose NCI-60 assay. At this stage, the six selected derivatives were screened and evaluated against sixty cancer cell lines at five different concentrations ranging from 0.01 to 100 µM in 10-fold dilutions. [39] The 5-dose mean graphs are provided in the supporting information file (**Figures S124 - S147**). Two response parameters for each cell of the sixty cancerous cell lines, GI_{50} (molar concentration at which the growth was inhibited by 50%, µM) and LC_{50} (molar concentration at which 50% of the cancer cells are killed, µM), are used to express the outcomes of the 5-dose

assay from the given dose-response curves. [38, 39] The achieved GI_{50} and LC_{50} results for **11f**, **11g**, **11k**, **11n**, **11p**, and **11q** are summarized in **Table 2**.

The five-dose assay results indicated that the compounds exhibited selectivity towards renal cancer cells, followed by CNS, non-small cell lung cancer, ovarian cancer, and breast cancer to a lesser extent. Among the tested derivatives, compound **11g** displayed remarkable activity against various cancer cell lines, except for leukemia and prostate cancer.

The tested compounds exhibited poor activity against leukemia cell lines with few exceptions. Notably, compound **11k** demonstrated growth inhibitory activity with a GI_{50} of 1.06 μM, and high cytotoxic activity with an LC_{50} of >36 μM in the SR cell line. Compound **11p** exhibited anticancer activity against the B-lymphocyte plasmacytoma, RPMI-8226 cells, with a GI_{50} of 7.14 μM. In non-small cell lung cancer, compounds **11f** and **11g** exhibited greater activity against A549 cell line with GI_{50} of 3.81 and 0.85 μM, respectively. For the NCI-H226 cell lines, compounds **11k**. **11p**, **11f**, **11g**, and **11n** showed GI_{50} values of 1.69, 2.31, 3.22, 2.46, and 2.17 μM, respectively.

The most sensitive among the colon cancer subpanel cell lines was HCT-116. Compounds **11f**, **11g**, **11k**, **11n**, **11p**, and **11q** displayed GI_{50} values of 5.48, 2.29, 5.67, 0.86, 3.05, and 46 μM, respectively, in HCT-116. Compound **11p** showed activity in multiple colon cancer cells, including HCC-2998, HCT-116, HCT-15, and HT29 with GI_{50} values of 6.21, 3.05, 13.60, and 6.32 μM, respectively. Compound **11g** exhibited anticancer activity in three colon cancer cell lines, namely COLO 205, HCT-116, and SW-620 with GI_{50} values of 13.80, 2.29, and 4.57 μM, respectively.

In melanoma cancer cell lines, compound **11p** demonstrated high activity against most of the examined cells, with GI_{50} values ranging from 2.69 to 16.10 μM. The SK-MEL-5 and UACC-62 cells were the most sensitive melanoma cell lines, both exhibiting a GI_{50} of 2.69 μM for compound **11p**. LOX IMVI and MALME-3M cells showed inhibited cell growth, with GI_{50} values of 5.94 and 12.10 μM for compound **11f**, 2.95 and 5.25 μM for compound **11g**, 3.02 and 27 μM for compound **11k**, 166 and 3.01 μM for compound **11n**, and 4.48 and 3.95 μM for compound **11p**, respectively.

For CNS cancer cells, **11g** demonstrated a GI_{50} value ranging from 1.71 to 6.92 μM, while **11k** showed a GI_{50} of 0.80 to 13.90 μM. SNB-75 and U251 were the most susceptible CNS cancer

cells, with a GI_{50} of 3.15 and 4.87 μM for **11f**, 1.17 and 1.58 μM for **11g**, 0.80 and 4.96 μM for **11k**, 1.50 and 0.76 μM for **11n** and 3.39 and 3.72 μM for **11p**. The superior GI_{50} of 0.76 μM for U251 in response to **11n**, followed by SNB-75 with a GI_{50} of 0.80 μM for **11k.** Among the ovarian cancer cell lines, OVCAR-4 cell line was noticed to report superior GI_{50} compared, with a GI_{50} of 6.87, 0.85, 2.17, and 0.77 for **11f**, **11g**, **11k**, and **11n**, respectively.

Renal cancer showed the highest sensitivity among the nine cell types to all six compounds. For compound **11f**, the GI_{50} values ranged from 2.89 to 9.51 μM, for compound **11g** GI_{50} ranged from 0.72 to 2.45 μM, for compound **11k**, GI_{50} ranged from 1.75 to 14.78 μM for **11k**, GI_{50} ranged from 1.14 to 2.49 μM for **11n**, GI_{50} ranged from 2.03 to 6.22 μM for **11p**. The LC_{50} value of **11g** in renal cancer cell lines was as low as 7.0 μM in the case of ACHN cells. Compound **11n** showed superior cytotoxicity against 786-0 cells with a GI_{50} of 1.58 μM and an LC_{50} of 6.33 μM. Compound **11p** displayed its highest cytotoxic activity against the 786-0 cells and the RXF 393 cells, with a GI_{50} of 2.03 and 2.09 μM, respectively, and LC_{50} of 11.70 and 22 μM, respectively. ACHN was the most sensitive among renal cancer cell lines, with compounds **11g**, **11k**, and **11n** exhibiting GI_{50} values of 0.72, 1.75, and 1.14 μM, respectively.

Compound **11k** displayed the highest activity against prostate cancer DU-145 cells, with a GI_{50} of 15.50 μM. For breast cancer cell lines, compounds **11g**, **11k**, **11n**, **11p**, and **11q** showed high inhibitory activity against MDA-MB-231 with GI_{50} ranging from 1.40 to 5.97 μM. For the T-47D, GI_{50} values ranged from 1.99 to 4.27 μM excluding **11k** which had a GI_{50} greater than 36 μM. The HS 578T cell lines exhibited GI_{50} values ranging from 2.10 to 5.91 μM, for all screened compounds.

Table 2. NCI-60 five dose screening results of derivatives **11f**, **11g**, **11k**, **11n**, **11p**, and **11q**.

Subpanel cell lines	11f		11g		11k		11n		11p		11q	
	GI_{50} (μM)	LC_{50} (μM)	GI_{50} (μM)	LC_{50} (μM)	GI_{50} (μM)	LC_{50} (μM)	GI_{50} (μM)	LC_{50} (μM)	GI_{50} (μM)	LC_{50} (μM)	GI_{50} (μM)	LC_{50} (μM)
Leukemia												
CCRF-CEM	> 100	> 100	> 100	> 100	> 36	> 36	> 100	> 100	> 100	> 100	> 100	> 100
HL-60(TB)	> 100	> 100	> 100	> 100	> 36	> 36	> 100	> 100	> 100	> 100	> 100	> 100
K-562	> 100	> 100	> 100	> 100	> 36	> 36	> 100	> 100	nd	> 100	> 100	> 100
MOLT-4	> 100	> 100	> 100	> 100	> 36	> 36	> 100	> 100	> 100	> 100	> 100	> 100
RPMI-8226	> 100	> 100	> 100	> 100	> 36	> 36	> 100	> 100	7.14	> 100	> 100	> 100
SR	> 100	> 100	> 100	> 100	1.06	> 36	nd	> 100	> 100	> 100	> 100	> 100
Non-Small Cell Lung Cancer												

Subpanel cell lines	11f		11g		11k		11n		11p		11q	
	GI_{50} (μM)	LC_{50} (μM)	GI_{50} (μM)	LC_{50} (μM)	GI_{50} (μM)	LC_{50} (μM)	GI_{50} (μM)	LC_{50} (μM)	GI_{50} (μM)	LC_{50} (μM)	GI_{50} (μM)	LC_{50} (μM)
A549/ATCC	3.81	> 100	0.85	> 100	11.40	> 36	3.89	> 100	13.9	> 100	87.20	> 100
EKVX	> 100	> 100	47.86	> 100	> 36	> 36	> 100	> 100	40.30	> 100	> 100	> 100
HOP-62	3.89	40	4.27	42	6.47	> 36	3.14	> 100	5	72.60	24.70	> 100
HOP-92	11	> 100	3	53	8.66	> 36	2.81	> 100	3.65	93.10	12.20	92.10
NCI-H226	3.22	> 100	2.46	> 100	1.69	> 36	2.17	> 100	2.31	78.50	23.90	> 100
NCI-H23	8.91	> 100	5.25	> 100	10.50	> 36	3.40	> 100	3.79	> 100	34.40	> 100
NCI-H322M	11.70	67.60	3.80	> 100	13.60	> 36	nd	> 100	18.10	> 100	> 100	> 100
NCI-H460	12.60	> 100	2.45	> 100	15.70	> 36	1.55	> 100	3.63	> 100	39.60	> 100
NCI-H522	31.60	> 100	14	> 100	17.60	> 36	6.72	> 100	5.69	> 100	83.40	> 100
Colon Cancer												
COLO 205	> 100	> 100	13.80	> 100	> 36	> 36	> 100	> 100	nd	> 100	> 100	> 100
HCC-2998	> 100	> 100	> 100	> 100	> 36	> 36	> 100	> 100	6.21	> 100	> 100	> 100
HCT-116	5.48	> 100	2.29	70	5.67	> 36	0.86	> 100	3.05	> 100	46	> 100
HCT-15	39.90	> 100	> 100	> 100	> 36	> 36	> 100	> 100	13.60	> 100	> 100	> 100
HT29	> 100	> 100	> 100	> 100	> 36	> 36	> 100	> 100	6.32	> 100	> 100	> 100
KM12	> 100	> 100	> 100	> 100	> 36	> 36	> 100	> 100	> 100	> 100	> 100	> 100
SW-620	> 100	> 100	4.57	> 100	> 36	> 36	> 100	> 100	nd	> 100	nd	> 100
CNS Cancer												
SF-268	36.8	> 100	6.92	> 100	13.90	> 36	25.80	> 100	12.4	> 100	> 100	> 100
SF-295	5.23	> 100	2.14	> 100	6.79	> 36	1.97	> 100	3	48.6	26.80	> 100
SF-539	7.51	95.10	4.57	60	2.94	19.70	1.59	> 100	1.79	7.51	30.90	> 100
SNB-19	21.70	> 100	3.98	> 100	11.40	> 36	8.58	> 100	13.10	> 100	32.70	> 100
SNB-75	3.15	> 100	1.17	28	0.80	15.10	1.50	> 100	3.86	> 100	19.40	> 100
U251	4.87	54.5	1.58	32	4.69	> 36	0.75	> 100	3.72	> 100	13.90	> 100
Melanoma												
LOX IMVI	5.94	> 100	2.95	> 100	3.02	> 36	1.66	> 100	4.48	> 100	71.30	> 100
MALME-3M	12.10	> 100	5.25	> 100	27	> 36	3.01	> 100	3.95	> 100	> 100	> 100
M14	12.50	> 100	7.94	74	> 36	> 36	> 100	> 100	12.90	> 100	> 100	> 100
MDA-MB-435	> 100	> 100	87.09	> 100	> 36	> 36	> 100	> 100	7.19	> 100	> 100	> 100
SK-MEL-2	> 100	> 100	60.26	> 100	> 36	> 36	nd	> 100	16.10	> 100	> 100	> 100
SK-MEL-28	61.4	> 100	> 100	> 100	> 36	> 36	> 100	> 100	6.07	> 100	> 100	> 100
SK-MEL-5	59.30	> 100	83.18	> 100	> 36	> 36	> 100	> 100	2.96	> 100	> 100	> 100
UACC-257	> 100	> 100	72.44	> 100	> 36	> 36	> 100	> 100	84.5	> 100	> 100	> 100
UACC-62	88.5	> 100	38.90	> 100	> 36	> 36	> 100	> 100	2.96	54.60	> 100	> 100
Ovarian Cancer												
GROV1	39.10	> 100	18.62	> 100	> 36	> 36	> 100	> 100	36.70	> 100	70.10	> 100
OVCAR-3	17.80	> 100	3.89	> 100	10.60	> 36	3.81	> 100	> 100	> 100	60.60	> 100
OVCAR-4	6.87	> 100	0.85	> 100	2.17	> 36	0.77	nd	28	> 100	9.54	> 100
OVCAR-5	19.30	> 100	6.46	> 100	15.60	> 36	> 100	> 100	> 100	> 100	> 100	> 100
OVCAR-8	18.80	> 100	3.39	> 100	10.50	> 36	4.34	> 100	13.50	> 100	> 100	> 100

Subpanel cell lines	11f		11g		11k		11n		11p		11q	
	GI_{50} (μM)	LC_{50} (μM)	GI_{50} (μM)	LC_{50} (μM)	GI_{50} (μM)	LC_{50} (μM)	GI_{50} (μM)	LC_{50} (μM)	GI_{50} (μM)	LC_{50} (μM)	GI_{50} (μM)	LC_{50} (μM)
NCI/ADR-RES	7.72	> 100	3.98	> 100	7.10	> 36	nd	> 100	3.51	> 100	71.40	> 100
SK-OV-3	5.87	> 100	2.45	35	7.25	> 36	5.52	> 100	3.22	> 100	24.80	> 100
Renal Cancer												
786-0	3.08	44.2	1.17	9	4.9	> 36	1.58	6.33	2.03	11.70	18.4	> 100
A498	3.19	97.1	1.99	11	9.70	> 36	2.10	> 100	4.19	> 100	22.20	75.3
ACHN	3.47	47.4	0.72	7	1.75	> 36	1.14	nd	3.25	90.5	16	> 100
CAKI-1	4.30	> 100	1.62	29	14	> 36	2.49	> 100	4.12	95.1	69	> 100
RXF 393	4.23	> 100	2.45	93	4.39	> 36	1.84	> 100	2.09	22	14.40	86.7
SN12C	6.58	> 100	1.45	> 100	14.80	> 36	1.72	> 100	> 100	> 100	16.70	> 100
TK-10	9.51	91.7	1.91	14	5.39	33.30	2.37	> 100	6.22	76.5	21.40	98.6
UO-31	2.89	> 100	1.45	9	9.41	> 36	1.54	> 100	2.92	> 100	21.30	> 100
Prostate Cancer												
PC-3	> 100	> 100	> 100	> 100	> 36	> 36	> 100	> 100	> 100	> 100	> 100	> 100
DU-145	> 100	> 100	> 100	> 100	15.50	> 36	> 100	> 100	> 100	> 100	> 100	> 100
Breast Cancer												
MCF7	27	> 100	6.76	> 100	8.56	> 36	nd	> 100	4.35	> 100	> 100	> 100
MDA-MB-231/ATCC	5.97	57.70	2.63	34	1.93	34	1.40	> 100	2.61	60.40	25.10	> 100
HS 578T	5.91	> 100	2.57	> 100	2.73	> 36	2.10	> 100	4.88	> 100	> 100	> 100
BT-549	> 100	> 100	56.23	> 100	3.62	> 36	8.86	> 100	2.01	22.60	> 100	> 100
T-47D	2.76	> 100	1.99	39	> 36	> 36	2.17	> 100	4.27	> 100	15.80	> 100
MDA-MB-468	9.17	> 100	2.29	> 100	6.25	> 36	2.59	> 100	3.11	> 100	29.20	> 100

Abbreviation of nd; not determined.

2.2.4. Screening for RecQ helicase inhibitory activity and selectivity profiling

A total of fifteen compounds, namely **6b**, **11a**, **11f-h**, **11j-l**, **11n-q**, and **11u-w**, were blind-tested for their inhibitory activity against the helicase domain of human BLM (BLM-HD) using a malachite-green based assay. This assay quantifies inorganic phosphate liberated from the turnover of ATP, when the protein is incubated with a short single-stranded 20-base oligonucleotide. [14] Among the DMSO-soluble compounds tested, thirteen compounds displayed clear dose-response curves, with calculated IC_{50} values ranging between 15 and 134 μM (**Figure S148**, Supplementary Information). The obtained results are summarized in **Table 3**. Compound **11n** exhibited no inhibition of BLM-HD within the tested concentration range, likely due to its poor DMSO solubility, which led to assay artifacts at high concentrations. Similarly, Compound **6b** did not demonstrate inhibition of BLM-HD across the tested concentration range.

Three compounds, namely **11g**, **11u**, and **11q** were chosen as exemplars for a limited selectivity screen. This screen aimed to evaluate their efficacy against the helicase domains of both RECQ1 and WRN as depicted in **Figure S149,** Supplementary Information. Compound **11g** exhibited similar inhibition of the ATP turnover for all three enzymes. In contrast, compounds **11u** and **11q** displayed selectivity towards BLM over both WRN and RECQ1. Notably, while compound **11u** demonstrated relatively little discrimination between WRN and RECQ1, compound **11q** exhibited more effective inhibition of WRN compared to RECQ1 as shown in **Table 4**.

To establish a likely mode-of-action for the three compounds, two experiments were conducted. First, the malachite-green assay was repeated using a 5-fold excess concentration of ATP (80 mM). In this assay, all three compounds failed to inhibit BLM-HD, suggesting that they operate as ATP-competitive inhibitors. Secondly, a commercial assay utilizing recombinant Topoisomerase I (Topo I) was employed to assess the ability of the compounds to relax a supercoiled plasmid. [14] Compounds that interact with the minor or major groove of DNA, or intercalate within the DNA, hinder the relaxation process. This was demonstrated by the control compound m-Amsacrine (m-AMSA) in **Figure 5A**. The three selected compounds did not affect the ability of Topo I to relax DNA, indicating that they do not directly bind to dsDNA. Taken together, these results collectively support the notion that the inhibitory effects of the compounds on the RecQ helicases are not a result of direct binding to dsDNA, but rather through ATP-competitive inhibition.

	95% C.I.

Compound	IC_{50} (μM)	Lower	Upper
11a	91.17	73.53	111.5
11f	32.74	22.69	47.35
11g	37.19	25.46	53.82
11h	86.11	74.27	98.84
11j	83.63	80.47	86.1
11k	133.90	76.52	408.4
11l	94.63	79.17	111.7
11o	32.99	25.96	42.15
11p	99.77	72.04	146.8
11q	21.78	16.36	28.68
11u	15.17	13.35	17.20
11v	76.89	53.45	107.3
11w	34.91	27.45	44.03

Table 3. Summary of inhibition data against BLM-HD**.** IC_{50} values were determined by fitting of experimental data to an [inhibitor] vs. normalised response — Variable slope model provided in GraphPad Prism (version 9.6.1). Calculated values for IC_{50} and 95% confidence intervals(C.I)(Lower and Upper) are given in each case. Data correspond to at least three technical replicates for each experiment.

			95% C.I.	
Target	**Compound**	**IC_{50} (μM)**	**Lower**	**Upper**
BLM-HD	**11g**	37.19	25.46	53.82
WRN-HD		25.36	18.54	34.61
RECQ1-HD		41.48	29.74	56.91
BLM-HD	**11q**	21.78	16.36	28.68
WRN-HD		124.5	105.4	148.2
RECQ1-HD		303.3	222.1	563.5
BLM-HD	**11u**	15.17	13.35	17.20
WRN-HD		40.03	26.38	62.14
RECQ1-HD		20.56	14.93	28.44

Table 4. Summary of selectivity data**.** All data were calculated as in **Table 3**. Data correspond to at least three technical replicates for each experiment.

Assessment of the unwinding inhibitory activity of 11g on BLM-HD

Compound **11g** was selected for additional assay due to its superior cytotoxic activity against the majority of examined cell lines in NCI-60 screening. To ascertain the mechanism of action, a Fluorescence-based DNA unwinding assay was employed to evaluate the impact of compound **11g** on BLM-HD's ability to unwind double-stranded DNA (dsDNA). The results revealed that **11g** hinders the unwinding activity of BLM-HD on a forked-dsDNA template, as evidenced by a reduction in the change of fluorescent signal over time (**Figure 5B**). The compound was included at a final concentration of 280 μM, the maximum achievable under assay conditions still compatible with robust unwinding (helicase) activity and in an excess over ATP as depicted in **Figure 5B**. Collectively, these findings suggest that the target compounds operate by impeding the ability of RecQ helicases to unwind the dsDNA through ATP-competitive inhibition.

To further validate the mechanism of action of our compounds within cells by interacting with RecQ helicases, we employed a Western blot assay to assess the relationship between expression levels of RecQ helicases represented by WRN helicase in the examined cell lines (HCT-116 and PC3), and the cell growth inhibitory activity of the compounds. The results, presented in the Supplementary Information (**Figure S150** and **Table S2**), indicated a 1.5±0.2-fold increase in WRN helicase expression in HCT-116 compared to PC3. In addition, we utilized different databases including the Human Protein Atlas (https://www.proteinatlas.org/) and DepMap (https://depmap.org/portal/) databases to predict the WRN and BLM helicases expression levels (Supplementary Information **Pages 107-108).** These findings substantiate the correlation between RecQ helicases expression levels and the activity observed in the *in vitro* screening in the NCI-DTP60 program. For compound **11g**, HCT-116 had higher expression level and better GI_{50} than PC3 as detailed in **Table S3** (Supporting Information). Also, we can't exclude that the molecules have other off-target effects especially being ATP-binding site competitive inhibitors.

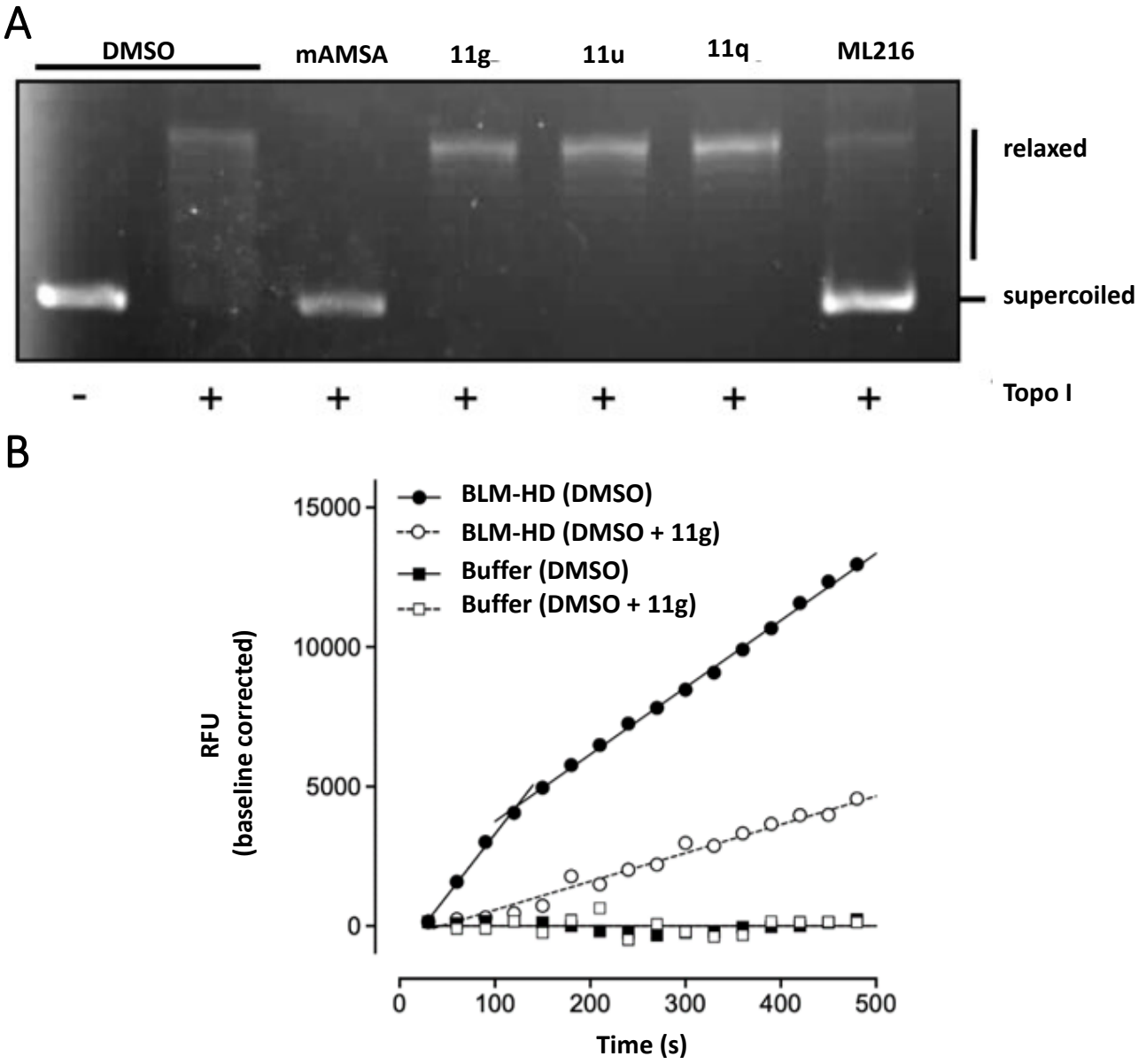

Figure 5. Mechanistic investigation of RecQ helicases inhibition. **(A)** Effect of compounds **11g, 11u** and **11q** on the ability of Topo I to relax DNA compared to ML216 and m-AMSA. **(B)** Fluorescence-based DNA unwinding assay, RFU, relative fluorescence units.

2.2.5. The apoptotic effect of 11g on HCT-116 and MDA-MB-231 cells

Real-Time quantitative Polymerase Chain Reaction (RT-qPCR) was utilized to examine the impact of compound **11g** on the induction of apoptosis-related genes (P53, Bax, Bcl-2, CASP-3,8,9) in both HCT-116 and MDA-MB-231. In HCT-116, compound **11g** demonstrated an increase in the expression of apoptosis-related genes compared to the control (**Figure 6**). Specifically, P53, Bax,

CASP-3, CASP-8 and CASP-9 exhibited approximately 6.39-fold, 8.29-fold, 7.8-fold, 1.23-fold and 8.2- fold increases, respectively. On the other hand, the expression of Bcl-2 was decreased by approximately 0.34-fold (**Figure 6**).

Similarly, in MDA-MB-231 cells, compound **11g** led to increased expression of the apoptosis-related genes compared to the control. P53, Bax, CASP-3, and CASP-9 showed approximately 4.31-fold, 4.19- fold, 6.34- fold and 6.31-fold increases, respectively. However, there was no change in the expression of CASP-8 after treatment with **11g**, Bcl-2 expression decreased by approximately 0.64-fold (**Figure6**). Based on these observations, it can be concluded that compound **11g** induces apoptosis more effectively in HCT-116 compared to MDA-MB-231. Consequently, Flow cytometry (Annexin V/PI + CCA) was performed on HCT-116 to further investigate the apoptotic induction effect.

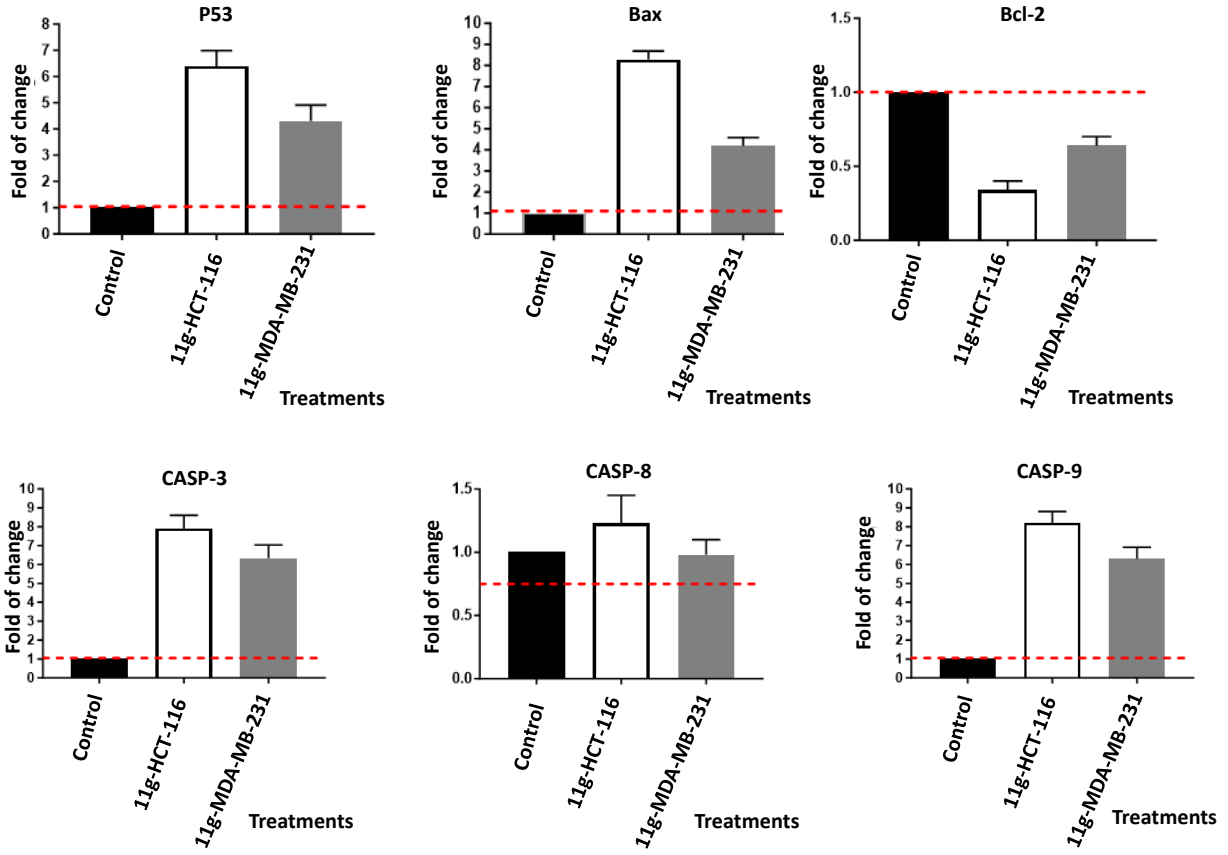

Figure 6. Gene expression for the expression of apoptosis-related genes in HCT-116 and MDA-MB-231 cells treated with compound **11g** (IC_{50} = 2.29 µM, 48h) and (IC_{50} = 2.63 µM, 48h) using RT-qPCR. Values are expressed as Mean ± SD for three independent experimental runs. The red dashed line represents the β-actin as the housekeeping gene.

To assess the apoptotic and necrotic effects of compound **11g** on HCT-116 cells, a flow cytometry analysis using Annexin V/ Propidium iodide (AV/PI) staining was conducted. This allowed for the detection and differentiation of apoptotic and necrotic cell populations in both untreated and treated cells, results are illustrated in **Figure 7**.

Figure 7A shows that it was observed that the percentage of necrotic cells (upper left UL quadrant, AV-/PI+) was lower in the treated HCT-116 cells compared to the untreated cells. Specifically, the untreated cells exhibited 11.6% necrosis, while the **11g**-treated cells showed a necrotic population of 4.6%. There was no significant change observed in the early apoptotic population (lower right LR quadrant, AV+/PI) between the untreated and treated cells. However, a substantial increase in late apoptosis was observed in the **11g**-treated cells (upper right UR quadrant, AV+/PI+), with a percentage of 43.3% compared to 10.6% in the untreated cells.

Figure 7B confirms the statistical significance of the results using an unpaired t-test ($P \leq 0.001$) between the untreated and treated HCT-116 cells, as analyzed in GraphPad Prism. The flow cytometry analysis results demonstrated that compound **11g** predominantly induces apoptosis rather than necrosis in HCT-116 cells, as evidenced by the significant increase in late apoptotic cells and the reduced necrotic cell population.

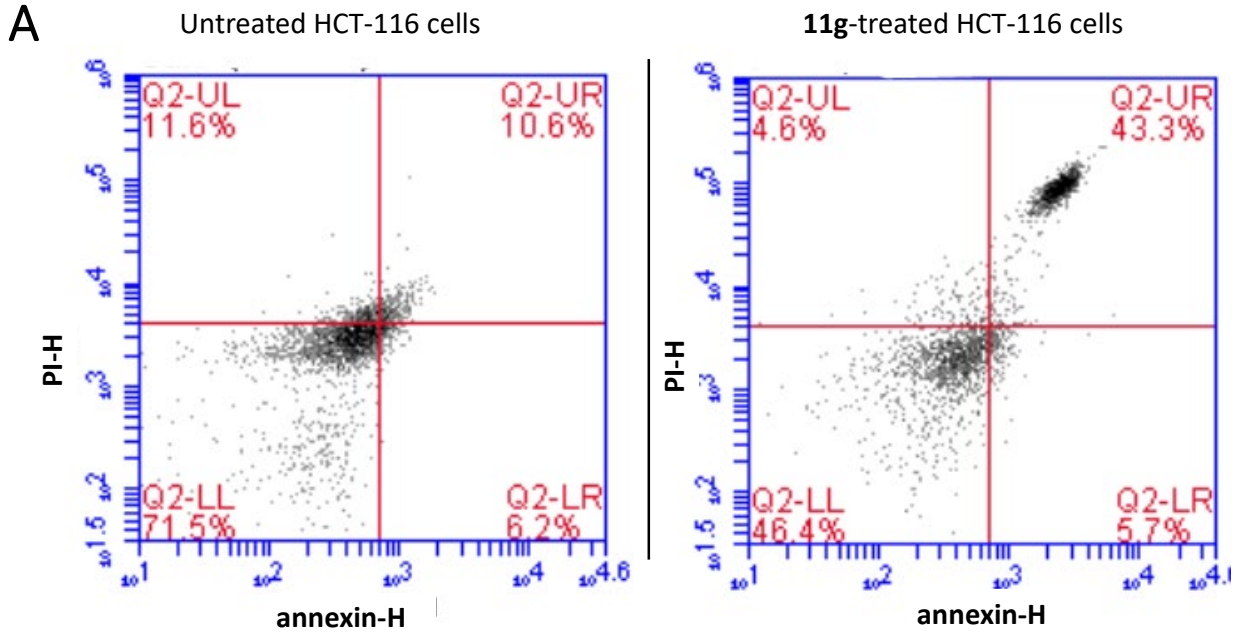

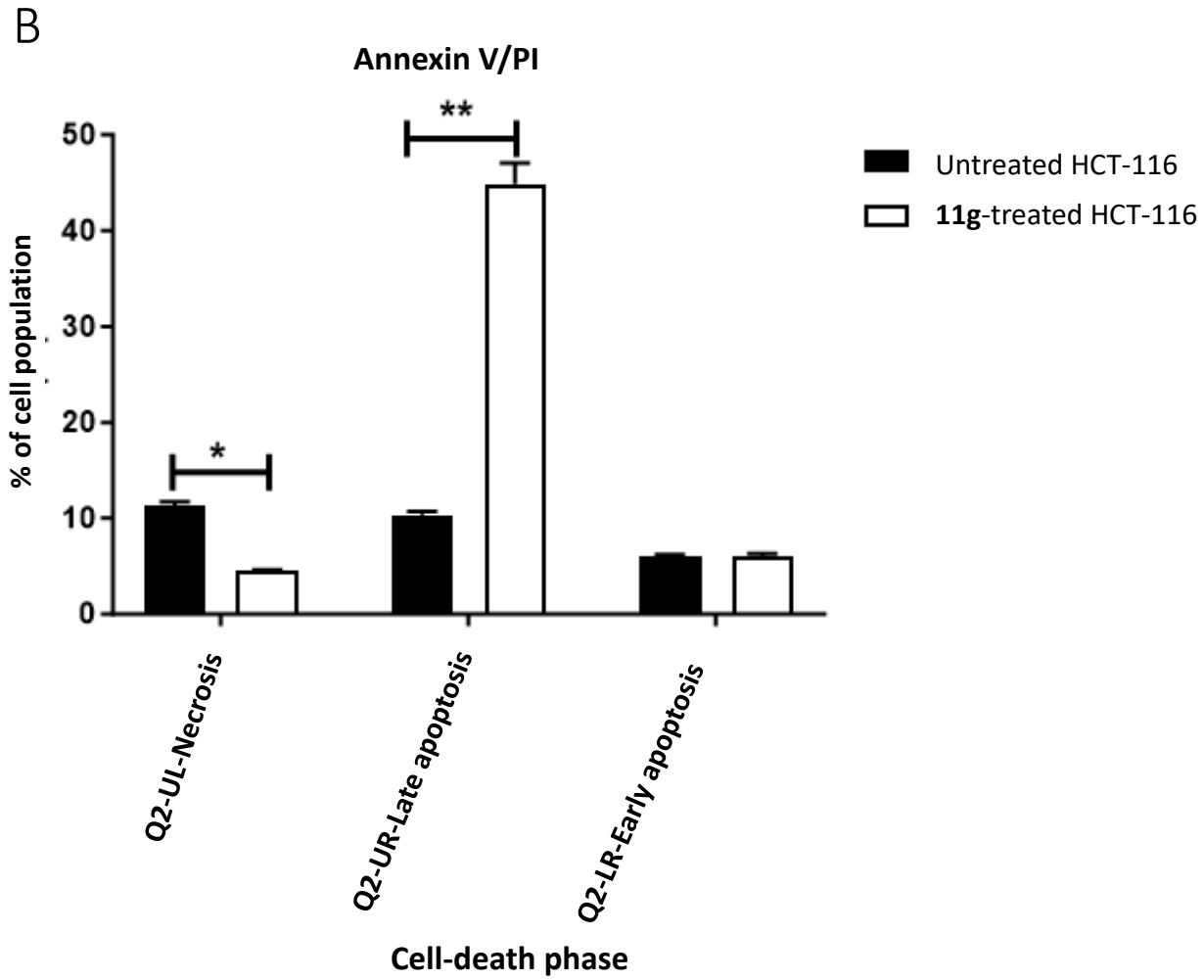

Figure 7. (A) Cytograms showing annexin-V/Propidium Iodide stained in both untreated and **11g**-treated HCT-116 cells (IC_{50}=2.29 μM, 48h). "Q2-UL (necrosis, AV-/PI+), Q2-UR (late apoptotic cells, AV+/PI+), Q2-LL (normal cells, AV-/PI-), Q2-LR (early apoptotic cells, AV+/PI-)". **(B)** Bar representation for quantification for cell population at each phase. ** ($P \leq 0.001$) between untreated and treated HCT-116 cells using unpaired t-test in GraphPad prism.

2.2.6. Cell cycle analysis of HCT-116 cells in response to compound 11g treatment

Further analysis was conducted to investigate the impact of compound **11g** on cell cycle progression in the HCT-116 cell line compared to untreated cells. The results as depicted in **Figure 8**, revealed that compound **11g** significantly interfered with the distribution of cell population across the different phases of the cell cycle. Notably, there was a significant increase in the G2/M phase population (33.5% in **11g**-treated cells versus 20.7% in untreated cells). Conversely, there was a non-significant decrease in the S phase population (26.6% in **11g**-treated cells versus 30.5% in untreated cells). **Figure 8B** confirms the statistical significance of these observations using an unpaired t-test in GraphPad Prism. The differences were found to be significant ($P \leq 0.05$) for the

G2/M phase between the untreated and treated HCT-116 cells. These findings suggest that compound **11g** interferes with the normal progression of the cell cycle in HCT-116 cells and arrests the cell cycle at the G2/M phase.

RecQ helicases are involved in DNA repair using homologous recombination where the sister chromatid, available in mid-S to the early G2 phase of the cell cycle, is used as a template for DNA repair. [1] Moreover, the highest expression of BLM helicase is typically observed in the late S and G2 phases of the cell cycle. [7, 42, 43] Additionally, HCT-116 cell is one of the high microsatellite instability (MSI-High) cell lines, which survival was found to be dependent on WRN helicase. [44-46] In HCT-116 WRN silencing reduced the proportion of microsatellite instability (MSI) cells in S phase. [46] In MSI cells, WRN silencing led to decrease the population of the cells in S phase and increase the cells in both phases G1 or G2/M, i.e., the cell cycle is arrested at G1 or G2/M phases. [47] WRN helicase may possess a G1 or G2-specific function as a recruitment factor for p53 to the damaged sites of DNA. [48] Also, depletion of RECQ1 helicase promotes the accumulation of cells in G1 and G2/M phases. [49] These are consistent with the *in vitro* inhibitory activity of compound **11g** on RecQ helicases which lead to cell cycle arrest at the G2/M phase.

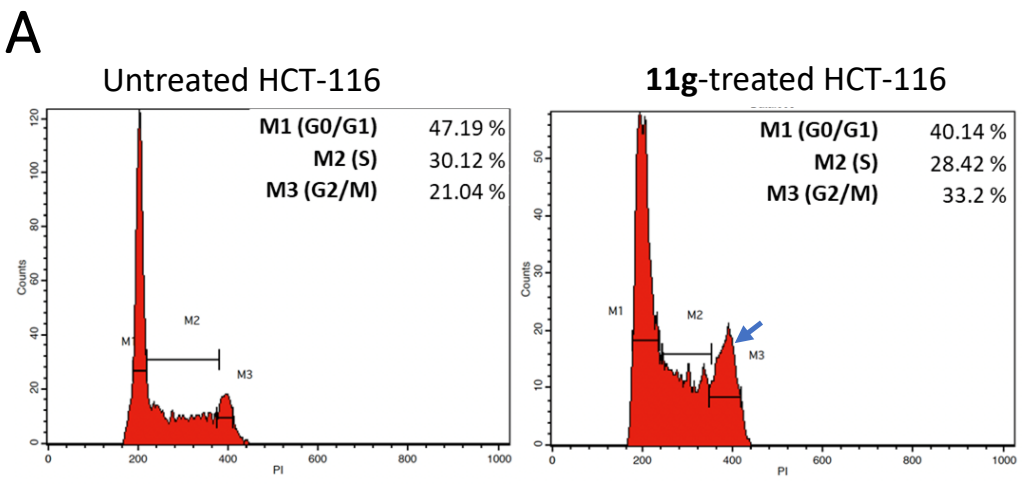

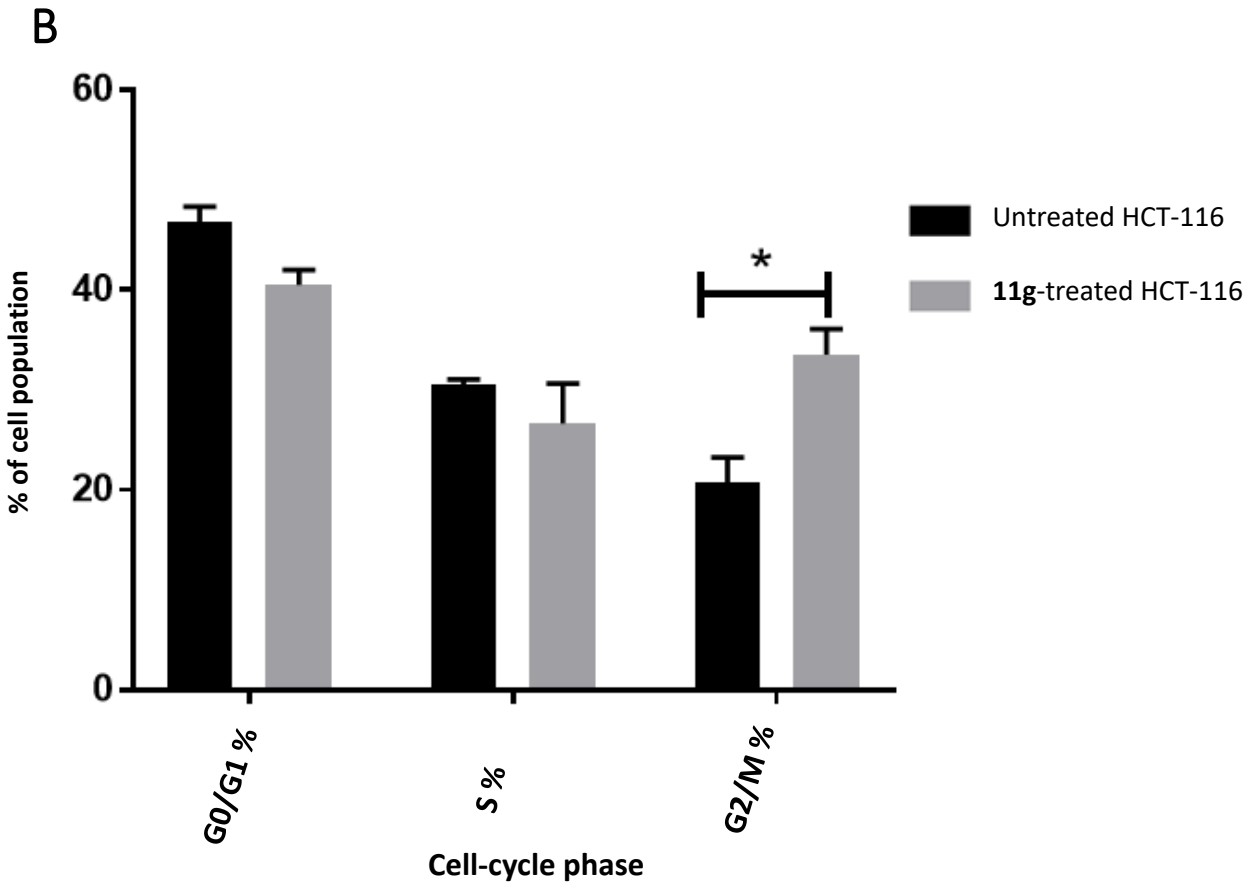

Figure 8. (A) Cytogram reflecting cell cycle distribution at each cell cycle phase of HCT-116 cells in both untreated and **11g**-treated cells. **(B)** Bar representation for quantification for cell population at each cell cycle. * ($P \leq 0.05$) significantly different between untreated and treated HCT-116 cells using unpaired t-test in GraphPad prism.

2.2.5. In vitro cytotoxicity of compound 11g on normal colon cells (FHC cells)

To evaluate the safety of compound **11g** on normal cells and its selectivity towards cancer cells, the viability of normal colon cancer FHC cells was assessed in response to **11g** treatment. The results as depicted in **Figure 9**, demonstrates that compound **11g** did not show significant cytotoxicity on FHC cell. At the highest tested concentration (100 μM), the cell viability remained high at approximately 82% compared to the control cells. This further supports the safety and selectivity of compound **11g** towards cancer cell lines.

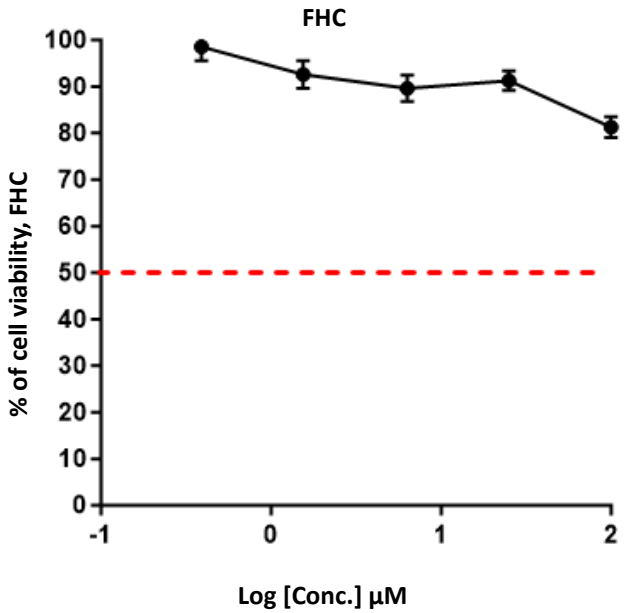

Figure 9. Percentage of cell viability of FHC (normal colon cells) against the tested serial concentration of **11g** [100, 25, 6.25, 1.6, and 0.4 µM]. IC_{50} was calculated as non-determined.

3. In silico studies

3.1. Predicted ADME properties

The pharmacokinetic profile of the newly synthesized quinazolinone and diamide derivatives was predicted using the Swiss ADME predictor, an online web-based tool. [50, 51] The outcomes were described in **Table S5,** Supplementary Information**.** The polarity estimate, the total polar surface area (TPSA) within the range of 20 and 130 $Å^2$, lipophilicity, the consensus log P values did not exceed 5.0, [52] the solubility estimate; log S values did not exceed 6 and Synthetic Accessibility (SA) Score is ca. 3, indicating ease of synthesis, on the scale from 1 to 10. Pan-assay Interference alerts (PAINS) predicted that compounds **11p**, **11h** and **11w** have PAINS alerts due to presence of dialkylated aniline group, which may lead to aniline-derived toxicity through the formation of reactive imine metabolites (RM). [53, 54]

Passive human gastrointestinal absorption and brain penetration assessed using the BOILED-Egg (Brain Or IntestinaL EstimateD permeation predictive model) model, which is a plot of WLOGP (octanol-water partition coefficient) versus TPSA. The BOILED-Egg analysis predicted high human intestinal absorption of all compounds. Sixteen compounds (**4b**, **6a-c**, **11a**, **11c**, **11f-i**, **11p-q**, **11s** and **11u-w**) were predicted to have the potential to cross the blood-brain barrier (BBB)

(**Figure S151**, Supporting Information). Compound **11m** was predicted to be effluxed out by P-Glycoprotein (**Figure S151**, Supporting Information).

These predictions delivered insights into the pharmacokinetic properties of the compounds as explained. Experimental studies would be however required to validate these predictions and assess the actual pharmacokinetic behaviour of the compounds.

3.2. Molecular docking analysis

The BLM, WRN, and RECQ1 are highly conserved RecQ family helicases, involved in DNA metabolism.. [1, 7] They share structured ATPase and RQC (helicase core) domains, with the ATPase domain being the largest and most conserved component. [10]

According to the results obtained from the biological evaluation of the RecQ helicases inhibitory effect and ATP competition assay which confirmed that the target compounds are ATP-competitors. So, the docking simulation analysis was performed at the ATP-binding site rather than DNA-binding site. To understand the molecular binding interactions of the synthesized quinazolinone derivatives against BLM, WRN, and RECQ1 helicases, molecular docking analysis was performed to examine the amino acids involved in their interaction with each isoform. The protein data bank files (PDB ID: 4CGZ, 6YHR, and 2V1X) were chosen for docking of BLM, WRN, and RECQ1, respectively. [55-57] The docking analysis was performed using the Molecular Operating Environment software (MOE 2020). [58]

The quinazolinone ring structure in the target compounds was found to mimic the ATP purine ring, which is crucial for making key interactions with the active site residues of the helicases. In BLM helicase, interactions were observed with Gln672, Leu665, and Arg669, [55] including hydrogen bonds, hydrophobic interactions, and electrostatic interactions **(Figure S154**, Supplementary Information). In the case of WRN helicase, interactions of ATP were observed with His546, Lys550, and Gln553, involving hydrogen bonds, π-π stacking interaction, and electrostatic/hydrophobic interactions **(Figure S155**, Supplementary Information). [56] For RecQ1 helicase, interactions were observed with Arg93, Leu89, and Gln93, including hydrogen bonds, hydrophobic interactions, and electrostatic interactions **(Figure S156**, Supplementary Information). [57]

As an example of the docking results for the novel derivatives, compound **11g** demonstrated favourable energy score (S) in its interaction with the active sites of BLM, WRN, and RecQ1 helicases. The energy scores (S) and amino acids involved in interaction of helicases with compound **11g** are shown in **Table 5**. 2D and 3D interaction diagrams of compound **11g** in the active sites of BLM, WRN, and RecQ1 helicases are illustrated in **Figure 10**.

Table 5. Molecular docking simulation results for compound **11g** in the active sites of BLM, WRN, and RECQ1 helicases (PDB ID: 4CGZ, 6YHR, and 2V1X, respectively).

Enz/ compound	S (kcal/mol)	Amino acids involved		
		Quinazolinone core	Phenylacetamide linker	Styryl tail
BLM (PDB: 4CGZ**)**				
11g	-7.67	Arg669, Leu665, Gln672, Asp 1264	Gln672, Leu697, Gly694	Lys726, Asn1242, Phe1238, Pro956 and Asn1239
WRN (PDB: 6YHR**)**				
11g	-6.48	His546, Lys550, Gln553	Arg857, Lys577, Ser578, Leu579	Ala831, Asn829
RECQ1 (PDB: 2V1X**)**				
11g	-6.59	Arg93, Leu89, Gln96, Phe92	Leu121, Val150, Gly118, Ser120, Gln124, Gln147, Asp146	Gly116, Gly117

In **Figure 10A**, it is depicted that compound **11g** interacts favourably within the active site of BLM helicase. Specifically, the quinazolinone ring of **11g** forms two hydrophobic interactions with Leu665. Additionally, the quinazolinone ring forms electrostatic interactions with Arg669 and Asp1246. Furthermore, a hydrogen bond is formed between Gln672 and the carbonyl group of the quinazolinone ring. The amide group in the phenylacetamide linker of **11g** hydrogen bonds with Gln672, Leu697, and Gly694. The 4-methoxy substituent on the styryl group of **11g**, forms hydrophobic interactions with Pro956 and Phe1238. The styryl phenyl group in **11g** forms electrostatic interactions with Lys726.

Figure 10B shows compound **11g** in the active site of WRN helicase. In this setting, the quinazolinone ring of **11g** forms π-π stacking interactions with His546, electrostatic and hydrophobic interactions with Lys550. The carbonyl group of the quinazolinone ring forms a hydrogen bond with Gln553. The carbonyl group in the phenylacetamide linker forms two

hydrogen bonds with Ser578 and Leu579. The phenyl ring extended from the linker forms electrostatic interaction with Arg857 and non-classical bond interactions with Lys577. The styryl phenyl group forms hydrophobic interaction with Ala831.

In **Figure 10C** compound **11g** is modelled in the active site of RecQ1 helicase. The quinazolinone ring forms hydrophobic interactions with Leu89, electrostatic interactions with Arg93, and van der Waals interaction with Phe92. The carbonyl group of the quinazolinone ring forms a hydrogen bond with Gln96. The phenyl ring extended from the acetamide linker forms hydrophobic interaction with Val154 and the amide group in the linker forms a hydrogen bond with Leu121, and van der Waals interactions with Gln124, Gln147, and Asp146. The styryl group exhibits van der Waals interactions with Gly117 and Gly116.

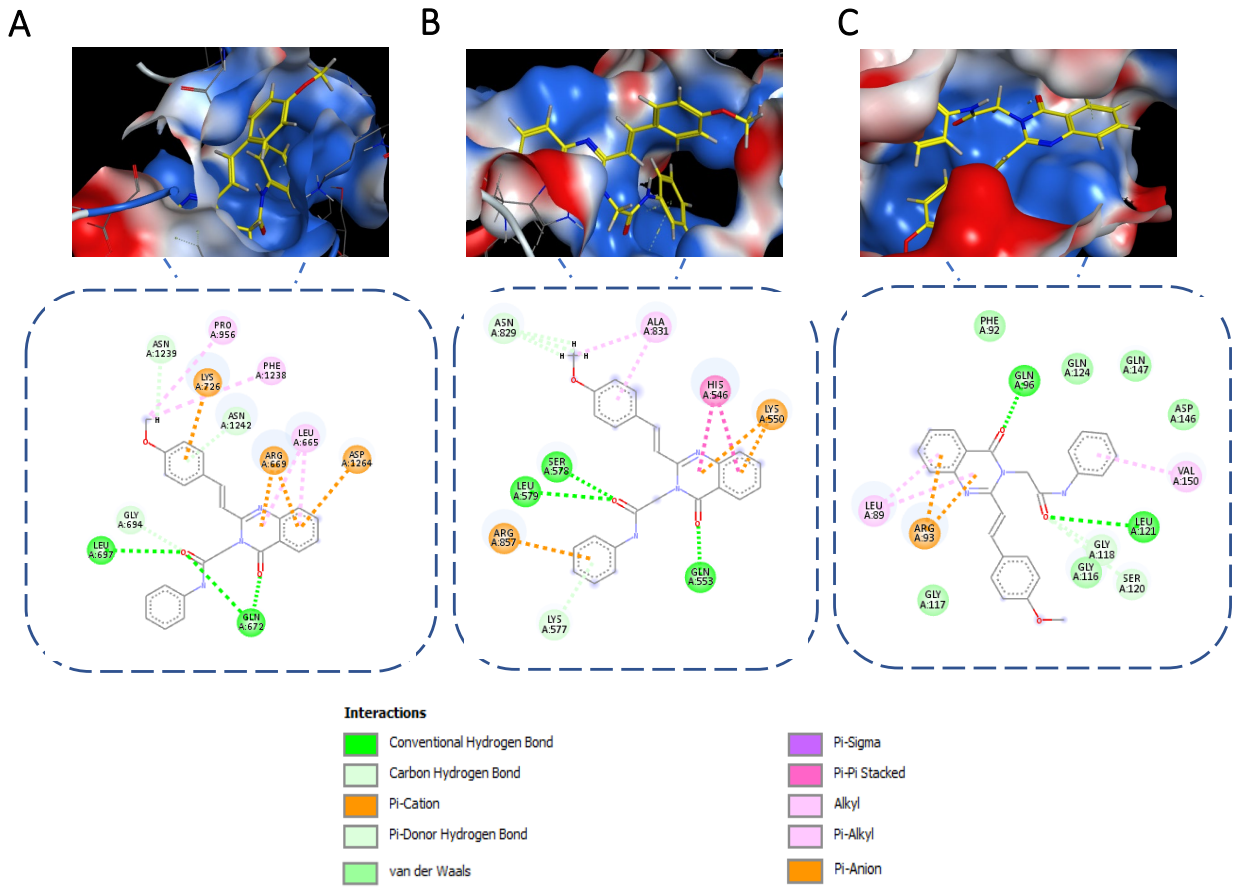

Figure 10. Interaction diagrams of compound **11g** docked in the active site of BLM, WRN and RecQ1 helicases. **(A)** 2D and 3D pose show ligand interactions diagram of compound **11g** inside the active site of BLM helicase (PDB: 4CGZ). **(B)** 2D and 3D pose show ligand interactions diagram of compound **11g** inside the active site of WRN helicase (PDB: 6YHR). **(C)** 2D and

3D pose show ligand interactions diagram of compound **11g** inside the active site of RECQ1helicase (PDB: 2V1X).

4. Conclusions

In this study, twenty-nine novel quinazolinone derivatives (**11a-w**, **4a-c**, and **6a-c**) were designed, synthesized, and evaluated for their potential as antitumor agents. Two synthetic schemes were developed, involving different modifications to the quinazolinone core. **Scheme 1** incorporated an imine linker at N3 and phenyl group at position 2 of quinazolinone ring and was employed for synthesis of derivatives **6a-c**. **Scheme 2** was developed to access derivatives **11a-w**, *via* incorporating an *N*-phenylacetamide linker at the N3 position and a styryl group at position 2 of the quinazolinone ring. The synthesized compounds were screened for *in vitro* cytotoxic activity against the NCI-DTP sixty cancer cell lines. Compounds **11a-w** showed superior cytotoxic activity compared to **4a-c** and **6a-c.** Six compounds, namely **11f**, **11g**, **11k**, **11n**, **11p**, and **11q** were selected for the 5-dose assay. Among them, compound **11g** exhibited superior cytotoxic activity against most examined cell lines.

Fifteen compounds were then blind-tested for their ability to inhibit ATP turnover by the helicase domain of BLM. Compounds **11u** and **11q** exhibited the best activity (as judged by IC_{50}), while compound **11g** showed pan-inhibitory activity against all three RECQ helicases tested, in an ATP-competitive mechanism. The compounds may have off-target effects being ATP competitive.

Further investigation of the anticancer activity of compound **11g** revealed its apoptotic activity in both HCT-116 and MDA-MB-231 cells. Compound **11g** arrested the cell cycle of HCT-116 cells in the G2/M phase. Compound **11g** was found to be safe on the normal colon FHC cells with a selectivity greater than 100. To gain insights into the binding mode and rationalize the activity, molecular docking simulations were performed for compound **11g** within the active sites of BLM, WRN, and RECQ1 helicases. Overall, this study presents novel quinazolinone compounds as potential antitumor agents with a comprehensive evaluation of their cytotoxic activity and mechanistic insights into their helicase inhibitory activity.

5. Experimental

5.1. Chemistry

5.1.1. General

All reagents and solvents were obtained from commercial sources and used without further purification. Melting points were determined in open-glass capillaries using a Stuart SMP30 apparatus and were uncorrected. Analytical thin layer chromatography (TLC): pre-coated aluminum sheets, 0.2 mm silica gel (Supelco Co., Silica 60 F_{254}) employed routinely to follow the progress of the reactions and to check the purity of the products using developing system: *n*-hexane: ethyl acetate as eluent and was visualized by exposure to UV lamp at λ 254 nm. ^{1}H NMR and ^{13}C NMR spectra were carried out using the Bruker instrument at 400 MHz for ^{1}H NMR and at 100 MHz for ^{13}C NMR spectrophotometer, (Faculty of Pharmacy, Mansoura University, Mansoura, Egypt), using TMS as an internal standard and chemical shifts were recorded in ppm on the δ scale using DMSO-d_6 or $CDCl_3$ as a solvent. Coupling constant (*J*) values were estimated in Hertz (Hz). Splitting patterns are designated as follows: s, singlet; d, doublet, t, triplet; m, multiplet. The electron impact (EI) mass spectra were recorded using a Thermo Scientific, ISQ Single Quadruple MS (The regional center for mycology and biotechnology, Al-Azhar University, Nasr City, Cairo, Egypt). Microanalysis was performed for C, H, N on PerkinElmer 2400 (The regional center for mycology and biotechnology, Al-Azhar University, Nasr City, Cairo, Egypt) and was within ± 0.4% of theoretical values.

5.1.2. 2-Phenyl-4*H*-benzoxazin-4-one 2

To a stirred mixture of compound **1** (0.686 g, 5.0 mmol) in THF (10 mL) at 0-5 °C, sodium carbonate powder (1.059 g, 10.0 mmol) was added followed by benzoyl chloride (1.757 g, 12.5 mmol). After 10 min, the cold bath was removed, and the mixture was stirred at rt for 42 h. Distilled water (10 mL) was added, and the mixture was stirred for 10 min prior to filtration. The precipitated solid was then washed with distilled water, followed by 50% aqueous MeOH. The additional precipitated solid from the filtrate was collected by filtration and washed. The combined crops were dried. [24, 25] The product was obtained as a white powder (1.039 g, 93%), m.p.118-120 °C (119 °C) (lit). [25]

5.1.3. *N*-(2-(Hydrazinecarbonyl)phenyl)benzamide 3

Equimolar quantities of compound **2** (0.223 g, 1 mmol) and 99% hydrazine hydrate (0.050 g, 1 mmol) in absolute ethanol (10 mL) were heated under reflux at 80 °C for 3 h. The reaction was monitored by TLC (*n*-hexane: ethyl acetate 1.5: 1). The reaction mixture was concentrated and allowed to cool. The solid product was filtered off, washed with distilled water, dried, and

recrystallized from ethanol. The product was obtained as a white powder (0.195 g, 76 %), m.p.195-196 °C [32]. ^{1}H NMR (400 MHz, DMSO-*d*$_6$) δ (ppm): 12.56 (1H, s, N**H**C=O), 10.21 (1H, s, N**H**NH$_2$), 8.67 (1H, d, *J* = 8.0 Hz, 3-**H** phenyl), 7.98 (2H, d, *J* = 7.3 Hz, 2,6-**H$_2$** benzamide), 7.80 (1H, d, *J* = 8.0 Hz, 6-**H** phenyl), 7.72-7.48 (4H, m, 3,4,5-**H$_3$** benzamide and 5-**H** phenyl), 7.19 (1H, s, 4-**H** phenyl), 4.70 (2H, s, NHN**H$_2$**).

5.1.3.1 *N*-(2-(2-(Benzo[*d*][1,3]dioxol-5-ylmethylene)hydrazine-1-carbonyl)phenyl)benzamide **4a**

Compound **3** (0.230 g, 0.9 mmol) and 1,3-benzodioxole-5-carbaldehyde (piperonal) (0.151 g, 1.0 mmol) were dissolved in absolute ethanol. The pH was adjusted to Ca. 4.5 with glacial acetic acid. The mixture was heated under reflux for 3 h and the reaction mixture was monitored by TLC (*n*-hexane: ethyl acetate 1: 1). After completion of reaction, the reaction mixture was poured into ice cooled water, the precipitated solid was filtered, dried, and recrystallized from absolute ethanol. **4a** was obtained as a white powder (0.276 g, 79.16 %), m.p. 228-233 °C. ^{1}H NMR (400 MHz, CDCl$_3$) δ (ppm): 11.63 (1H, s, N**H**N=C), 10.43 (1H, s, N**H**C=O), 8.45 (1H, d, *J* = 8.0 Hz, 3-**H** benzamide), 8.37 (1H, s, N=C**H**), 8.06 (2H, d, *J* = 8.0 Hz, 2,6-**H$_2$** phenyl), 7.65-7.45 (5H, m, 6-**H** benzamide, 6-**H** benzodioxol and 3,4,5-**H$_3$** phenyl), 7.41 (1H, t, *J* = 8.0 Hz, 4-**H** benzamide), 7.20 (1H, d, *J* = 8.0 Hz, 7-**H** benzodioxol), 6.92-6.81 (2H, m, 5-**H** benzamide and 4-**H** benzodioxol), 6.04 (2H, s, OC**H**$_2$O). ^{13}C NMR (100 MHz, CDCl$_3$) δ (ppm): 166.51, 165.39, 150.16, 149.23, 148.44, 139.24, 134.35, 134.16, 132.61, 132.27, 128.92, 127.93, 127.52, 127.20, 124.43, 123.21, 122.02, 120.16, 108.26, 106.41, 102.13, 101.64. EI-MS: *m/z*: 387.38 [M$^+$]. Anal. calcd. for $C_{22}H_{17}N_3O_4$: C, 68.21; H, 4.42; N, 10.85. Found: C, 68.45; H, 4.61; N, 10.76.

5.1.3.2 *N*-(2-(2-(Naphthalen-2-ylmethylene)hydrazine-1-carbonyl)phenyl)benzamide **4b**

Compound **3** (0.230 g, 0.9 mmol) and 2-naphthaldehyde (0.156 g, 1.0 mmol) were dissolved in absolute ethanol (10 mL) then glacial acetic acid (3 mL) was added. The mixture was heated under reflux for 16 h. The reaction was monitored by TLC (*n*-hexane: ethyl acetate 2: 1). After completion of the reaction, the precipitated solid was filtered off and washed with minimum amount of distilled water, then with absolute ethanol and dried under vacuum. **4b** was obtained as a white powder (0.227 g, 64.11 %), m.p. 227-230 °C. ^{1}H NMR (400 MHz, DMSO-*d*$_6$) δ (ppm): 12.25 (1H, s, N**H**N=C), 11.97 (1H, s, N**H**C=O), 8.65 (1H, s, N=C**H**), 8.61 (1H, d, *J* = 8.0 Hz, 3-**H** naphthalene), 8.21 (1H, s, 1-**H** naphthalene), 8.10-7.91 (7H, m, 3,6-**H$_2$** benzamide, 4,5,8-**H$_3$** naphthalene and 2,6-**H$_2$** phenyl), 7.73-7.54 (6H, m, 4-**H** benzamide, 6,7-**H$_2$** naphthalene and 3,4,5-

H₃ phenyl), 7.33 (1H, t, *J* = 8.0 Hz, 5-**H** benzamide). ^{13}C NMR (100 MHz, DMSO-*d₆*) δ (ppm): 165.49, 165.04, 149.47, 139.78, 134.88, 134.35, 133.32, 133.13, 132.62, 132.25, 129.60, 129.43, 129.16, 129.05, 128.89, 128.28, 127.78, 127.54, 127.30, 123.67, 123.19, 121.57, 121.08. EI-MS: *m/z*: 393.46 [M^+]. Anal. calcd. for $C_{25}H_{19}N_3O_2$: C, 76.32; H, 4.87; N, 10.68. Found: C, 76.09; H, 5.12; N, 10.94.

5.1.3.3 *N*-(2-(2-(Pyridin-3-ylmethylene)hydrazine-1-carbonyl)phenyl)benzamide **4c**

Compound **5** (0.237 g, 1.0 mmol) and 3-pyridinecarboxyaldehyde (0.107 g, 1.0 mmol) were dissolved in absolute ethanol. Then glacial acetic acid (3 mL) was added. The mixture was heated under reflux for 18 h. The reaction mixture was monitored by TLC (*n*-hexane: ethyl acetate 2: 1). After completion of reaction, the reaction mixture was poured into ice cooled water, the precipitated solid was filtered, dried, and recrystallized from absolute ethanol.

4c was obtained as a white powder (0. 200 g, 58.08 %), m.p. 216-219 °C. ^{1}H NMR (400 MHz, DMSO-*d₆*) δ (ppm): 12.31 (1H, s, N**H**N=C), 11.86 (1H, s, N**H**C=O), 8.90 (1H, s, N=C**H**), 8.79 - 8.40 (3H, m, 6-**H** benzamide and 2,4-**H₂** pyridine), 8.29-7.17 (10 H, m, 3,4,5-**H₃** benzamide, 2,3,4,5,6-**H₅** phenyl and 5,6-**H₂** pyridine). ^{13}C NMR (100 MHz, DMSO-*d₆*) δ (ppm): 165.55, 165.08, 151.47, 149.41, 146.73, 139.75, 134.86, 134.12, 133.20, 132.62, 130.45, 129.42, 129.16, 127.56, 124.55, 123.72, 121.71, 121.10. EI-MS: *m/z*: 344.04 [M^+]. Anal. calcd. for $C_{20}H_{16}N_4O_2$: C, 69.76; H, 4.68; N, 16.27. Found: C, 69.98; H, 4.85; N, 16.41.

5.1.4 3-Amino-2-phenylquinazolin-4(3*H*)-one 5

Equimolar quantities of compound **2** (0.223 g, 1 mmol) and 99% hydrazine hydrate (0.050 g, 1 mmol) in absolute ethanol (10 mL) were heated under reflux at 250 °C for 18 h. The reaction was monitored by TLC (*n*-hexane: ethyl acetate 1: 2). The reaction mixture was concentrated and allowed to cool. The solid product was filtered off, washed with distilled water, and dried under vacuum. [26, 28-31]

5 was obtained as white threads (0.973 g, 82 %), m.p. 195-196 °C [33]. ^{1}H NMR (400 MHz, $CDCl_3$) δ (ppm): 8.33 (1H, d, *J* = 8.0 Hz, 5-**H** quinazolinone), 7.90-7.78 (4H, m, 2,6-**H₂** phenyl and 7,8-**H₂** quinazolinone), 7.60-7.50 (4H, m, 3,4,5-**H₃** phenyl and 6-**H** quinazolinone), 5.08 (2H, s, N**H₂**).

5.1.5 General procedure for the preparation of compounds 6a-c

Compound **5** (1.0 mmol) and appropriate aldehydes with different ratios (1: 1.75) were dissolved in absolute ethanol (10 mL) then glacial acetic acid (3 mL) was added. The mixture was heated under reflux for 26-72 h. The reaction was monitored by TLC (*n*-hexane: ethyl acetate 2: 1). After completion of the reaction, the obtained solid was filtered off and washed with minimum amount of distilled water, then with absolute ethanol.

5.1.5.1 (*E*)-3-((Benzo[*d*][1,3]dioxol-5-ylmethylene)amino)-2-phenylquinazolin-4(3*H*)-one **6a**

Ratio of compound **5**: piperonal was 1: 1.75 and heated under reflux for 26 h. **6a** was obtained as a white powder (0.274 g, 74 %), m.p. 195-197 °C. ^{1}H NMR (400 MHz, $CDCl_3$) δ (ppm): 8.88 (1H, s, C**H**=N), 8.38 (1H, d, *J* = 8.0 Hz, 5-**H** quinazolinone), 7.93 (1H, d, *J* = 8.0 Hz, 8-**H** quinazolinone), 7.82 (1H, t, *J* = 8.0 Hz, 7-**H** quinazolinone), 7.78-7.72 (2H, m, 2,6-**H$_2$** phenyl), 7.56 (1H, t, *J* = 8.0 Hz, 6-**H** quinazolinone), 7.51-7.43 (3H, m, 3,4,5-**H$_3$** phenyl), 7.25 (1H, s, 4-**H** benzodioxol), 7.17 (1H, d, *J* = 8.0 Hz, 6-**H** benzodioxol), 6.87 (1H, d, *J* = 8.0 Hz, 7-**H** benzodioxol), 6.05 (2H, s, OC**H$_2$**O). ^{13}C NMR (100 MHz, $CDCl_3$) δ (ppm): 166.13, 159.15, 154.02, 151.48, 148.45, 146.79, 134.61, 134.48, 130.02, 129.84, 127.95, 127.72, 127.29, 127.13, 127.07, 126.72, 121.44, 108.34, 106.35, 101.79. EI-MS: *m/z*: 369.42 [M^+]. Anal. calcd. for $C_{22}H_{15}N_3O_3$: C, 71.54; H, 4.09; N, 11.38. Found: C, 71.76; H, 4.23; N, 11.59.

5.1.5.2 (*E*)-3-((Naphthalen-2-ylmethylene)amino)-2-phenylquinazolin-4(3*H*)-one **6b**

Ratio of compound **5**: 2-naphthaldehyde was 1: 1 and heated under reflux for 72 h. **6b** was obtained as a white powder (0.117 g, 31.16 %), m.p.184-186 °C.^{1}H NMR (400 MHz, DMSO-*d$_6$*) δ (ppm): 9.21 (1H, s, C**H**=N), 8.32 (1H, s, 1-**H** naphthalene), 8.28 (1H, d, *J* = 7.6 Hz, 3-**H** naphthalene), 8.07 (1H, d, *J* = 7.6 Hz, 5-**H** quinazolinone), 7.99 (2H, d, *J* = 8.0 Hz, 5,8-**H$_2$** naphthalene), 7.93 (1H, t, *J* = 7.4 Hz, 7-**H** quinazolinone), 7.86-7.72 (4H, m, 4-**H** naphthalene, 2,6-**H$_2$** phenyl and 8-**H** quinazolinone), 7.71-7.58 (3H, m, 6,7-**H$_2$** naphthalene and 6-**H** quinazolinone), 7.52-7.41 (3H, m, 3,4,5-**H$_3$** phenyl). ^{13}C NMR (100 MHz, DMSO-*d$_6$*) δ (ppm): 169.83, 158.32, 153.61, 146.80, 135.29, 135.16, 135.09, 132.95, 132.75, 130.45, 130.32, 130.26, 129.40, 129.37, 128.89, 128.37, 128.17, 128.09, 127.64, 127.31, 122.88, 121.55. EI-MS: *m/z*: 375.65 [M^+]. Anal. calcd. for $C_{25}H_{17}N_3O$: C, 79.98; H, 4.56; N, 11.19. Found: C, 80.17; H,4.68; N, 11.40.

5.1.5.3 (*E*)-3-((Naphthalen-1-ylmethylene)amino)-2-phenylquinazolin-4(3*H*)-one **6c**

Ratio of compound **5**: 1-naphthaldehyde was 1: 1 and heated under reflux for 26 h. **6c** was obtained as a white powder (0.320 g, 85%), m.p. 184-186 °C. ^{1}H NMR (400 MHz, DMSO-*d*$_6$) δ (ppm): 9.66 (1H, s, C**H**=N), 8.49 (1H, d, *J* = 8.0 Hz, 2-**H** naphthalene), 8.31 (1H, d, *J* = 8.0 Hz, 4-**H** naphthalene), 8.18 (1H, d, *J* = 8.0 Hz, 5-**H** quinazolinone), 8.06 (1H, d, *J* = 8.0 Hz, 8-**H** naphthalene), 7.99-7.87 (2H, m, 5-**H** naphthalene and 7-**H** quinazolinone), 7.83 (1H, d, *J* = 8.0 Hz, 8-**H** quinazolinone), 7.81-7.72 (2H, m, 2,6-**H$_2$** phenyl), 7.71-7.53 (4H, m, 3,6,7-**H$_3$** naphthalene and 5-**H** quinazolinone), 7.49 (3H, s, 3,4,5-**H$_3$** phenyl). ^{13}C NMR (100 MHz, DMSO-*d*$_6$) δ (ppm): 170.72, 158.32, 153.71, 146.86, 135.31, 135.12, 133.85, 133.51, 131.02, 130.48, 130.19, 130.04, 129.29, 128.31, 128.07, 127.62, 127.32, 127.11, 125.94, 124.78, 121.74. EI-MS: *m/z*: 375.47 [M$^+$]. Anal. calcd. for $C_{25}H_{17}N_3O$: C, 79.98; H, 4.56; N, 11.19. Found: C, 79.85; H, 4.77; N, 11.40.

5.1.6 2-Methylquinazolin-4(3*H*)-one 7

It was synthesized according to published literature with modifications [34]. Compound **1** (1.000 g, 7.3 mmol) was dissolved in excess acetic anhydride (10 mL) and the resulting reaction mixture was stirred at rt for 8 h. The reaction was monitored using TLC (*n*-hexane: ethyl acetate 1: 2). The solvent was evaporated under vacuum. Then**,** the resulting residue was stirred in 32% ammonia solution (22.5 mL) for 8 h. Upon completion, the precipitated solid was filtered off and dried under vacuum. N.B: (The flask of the reaction should be kept under air-tight conditions during all steps of reaction). The product was obtained as a white powder (0.907 g, 77.7%), m.p. 238-240 °C. [59, 60] ^{1}H NMR (400 MHz, $CDCl_3$) δ (ppm): 11.83 (1H, s, N**H**), 8.31 (1H, d, *J* = 8.0 Hz, 5-**H** quinazolinone), 7.80 (1H, t, *J* = 8.0 Hz, 7-**H** quinazolinone), 7.71 (1H, d, *J* = 8.0 Hz, 8-**H** quinazolinone), 7.50 (1H, t, *J* = 8.0 Hz, 6-**H** quinazolinone), 2.62 (3H, s, C**H$_3$**).

5.1.7 General procedure for the preparation of α-chloro-*N*-arylacetamide derivatives 9a-c

A mixture of substituted aromatic amines **8a-c** (10.0 mmol) and triethylamine (1.210 g, 12.0 mmol), in methylene chloride (10 mL) was kept at 0 °C in an ice bath. 2-Chloroacetyl chloride (1.360 g, 12.0 mmol) was slowly added. The ice bath was then removed, and the reaction mixture was stirred for 6 h at rt. The reaction mixture was monitored by TLC (*n*-hexane: ethyl acetate 1: 2.5). At the end of reaction, the reaction mixture was concentrated at reduced pressure and cold water was added to the reaction mixture. The precipitated solid was filtered off, washed with cold water and dried under vacuum. [35]

5.1.7.1 2-Chloro-*N*-phenylacetamide **9a**

A shiny buff powder, (1.510 g, 88.9%), m.p. 133-135 °C (133-135 °C (lit) [35, 61].

5.1.7.2 2-Chloro-*N*-(4-methoxyphenyl) acetamide **9b**

A shiny prussian blue powder, (1.780 g, 89.36%), m.p. 120-122 °C (119-120 °C (lit)). [35, 62]

5.1.7.3 2-Chloro-*N*-(4-chlorophenyl) acetamide **9c**

A beige powder (2.000 g, 98.45 %), m.p. 169-171°C (169-171 °C (lit)). [63]

5.1.8 General procedure for the preparation of 2-(2-Methyl-4-oxoquinazolin-3(4*H*)-yl)-*N*-phenylacetamide derivatives 10a-c

To a stirred solution of **7** (1.200 g, 7.5 mmol) in dry acetone (150 mL), anhydrous potassium carbonate (2.070 g, 15.0 mmol) was added followed by the corresponding substituted 2-chloro-*N*-phenylacetamide (7.5 mmol). The reaction mixture was heated under reflux for 18 h. Upon completion, the solvent was evaporated under reduced pressure then washed with distilled water several times and dried under vacuum. [36]

5.1.8.1 2-(2-Methyl-4-oxoquinazolin-3(4*H*)-yl)-*N*-phenylacetamide **10a**

A white powder (2.050 g, 93%), m.p. 262-263°C. (261-263°C lit). [64]

5.1.8.2 *N*-(4-Methoxyphenyl)-2-(2-methyl-4-oxoquinazolin-3(4*H*)-yl)acetamide **10b**

A light grey powder (2.300 g, 95%), m.p. 228-230°C. (229 °C (lit) [65])**.** ^{1}H NMR (400 MHz, DMSO-d_6) δ (ppm): 10.34 (1H, s, N**H**), 8.11 (1H, d, *J* = 8.0 Hz, 5-**H** quinazolinone), 7.84 (1H, t, *J* = 8.0 Hz, 7-**H** quinazolinone), 7.64 (1H, d, *J* = 8.0 Hz, 8-**H** quinazolinone), 7.59-7.44 (3H, m, 2,6-$\mathbf{H_2}$ phenyl and 6-**H** quinazolinone), 6.91 (2H, d, *J* = 8.4 Hz, 3,5-$\mathbf{H_2}$ phenyl), 4.96 (2H, s, C$\mathbf{H_2}$CO), 3.74 (3H, s, OC$\mathbf{H_3}$), 2.56 (3H, s, C$\mathbf{H_3}$).

5.1.8.3 *N*-(4-Chlorophenyl)-2-(2-methyl-4-oxoquinazolin-3(4*H*)-yl)acetamide **10c**

A yellowish white powder (2.390 g, 97.38%), m.p. 273-275 °C (258-260 °C (lit)) [66]. ^{1}H NMR (400 MHz, DMSO-d_6) δ (ppm): 10.63 (1H, s, N**H**), 8.11 (1H, d, *J* = 7.6 Hz, 5-**H** quinazolinone), 7.83 (1H, t, *J* = 8.0 Hz, 7-**H** quinazolinone), 7.68-7.58 (3H, m, 2,6-$\mathbf{H_2}$ phenyl and 8-**H** quinazolinone), 7.52 (1H, t, *J* = 8.0 Hz, 6-**H** quinazolinone), 7.40 (2H, d, *J* = 8.8 Hz, 3,5-$\mathbf{H_2}$ phenyl), 4.98 (2H, s, C$\mathbf{H_2}$CO), 2.56 (3H, s, C$\mathbf{H_3}$).

5.1.9 General procedure for the preparation of compounds 11a-w

To a solution of **10a-c** (1.0 mmol) in THF (6.5 mL), acetic anhydride (0.5 mL), appropriate aldehydes with different ratios (1.3: 21.6), and zinc chloride (0.354 g, 2.6 mmol) were added. The reaction mixture was heated under reflux at 150 °C for 10-48 h. The reaction was monitored by TLC (*n*-hexane: ethyl acetate; 1: 2). On cooling, the precipitated solid was filtered off and washed with distilled water. The collected solid was heated with ethanol at 70 °C, then filtered off, washed with cold ethanol, and recrystallized from DMF/acetone to yield the pure products **11a-w**.

5.1.9.1 (*E*)-2-(4-Oxo-2-styrylquinazolin-3(4*H*)-yl)-*N*-phenylacetamide **11a**

Ratio of compound **10a**: benzaldehyde 1: 14.1 and heated under reflux for 18 h. **11a** was obtained as a greenish white powder (0.306 g,73 %), m.p. 278-280 °C. ^{1}H NMR (400 MHz, DMSO-*d*$_6$) δ (ppm): 10.50 (1H, s, N**H**), 8.14 (1H, d, *J* = 8.0 Hz, 5-**H** quinazolinone), 7.98 (1H, d, *J* = 15.2 Hz, =C**H**-styryl), 7.91-7.72 (4H, m, 7,8-**H$_2$** quinazolinone and 2,6-**H$_2$** styryl), 7.61 (2H, d, *J* = 8.0 Hz, 2,6-**H$_2$** phenylacetamide), 7.53 (1H, t, *J* = 8.0 Hz, 6-**H** quinazolinone), 7.48-7.37 (4H, m, quinazolinone-C**H**= and 3,4,5-**H$_3$** styryl), 7.33 (2H, t, *J* = 8.0 Hz, 3,5-**H$_2$** phenylacetamide), 7.07 (1H, t, *J* = 8.0 Hz, 4-**H** phenylacetamide), 5.25 (2H, s, C**H$_2$**CO). ^{13}C NMR (100 MHz, DMSO-*d*$_6$) δ (ppm): 166.27, 161.86, 153.09, 147.71, 140.77, 139.19, 135.69, 135.21, 130.22, 129.33, 128.66, 127.58, 126.96, 126.81, 123.99, 120.21, 119.58, 46.77. EI-MS: *m/z*: 382.20 [M$^+$]. Anal. calcd. for $C_{24}H_{19}N_3O_2$: C, 75.57; H, 5.02; N, 11.02. Found: C, 75.27; H, 5.25; N, 11.28.

5.1.9.2 *(E)*-2-(2-(4-Nitrostyryl)-4-oxoquinazolin-3*(*4*H)*-yl)-*N*-phenylacetamide **11b**

Ratio of compound **10a**: *p*-nitrobenzaldehyde was 1: 1.65 and heated under reflux for 18 h. **11b** was obtained as a canary yellow powder (0.113 g, 48.18%), m.p. 325-327 °C. ^{1}H NMR (400 MHz, DMSO-*d*$_6$) δ (ppm): 10.51 (1H, s, N**H**), 8.27 (2H, d, *J* = 8.0 Hz, 2,6-**H$_2$** nitrostyryl), 8.19-8.02 (4H, m, 3,5-**H$_2$** nitrostyryl, 5-**H** quinazolinone and =C**H**-nitrostyryl), 7.90 (1H, t, *J* = 8.0 Hz, 7-**H** quinazolinone), 7.79 (1H, d, *J* = 8.0 Hz, 8-**H** quinazolinone), 7.69-7.53 (4H, m, 2,6-**H$_2$** phenylacetamide, 6-**H** quinazolinone and quinazolinone-C**H**=), 7.33 (2H, t, *J* = 7.6 Hz, 3,5-**H$_2$** phenylacetamide), 7.07 (1H, t, *J* = 7.6 Hz, 4-**H** phenylacetamide), 5.26 (2H, s, C**H$_2$**CO). ^{13}C NMR (100 MHz, DMSO-*d*$_6$) δ (ppm): 166.23, 161.75, 152.59, 147.51, 142.21, 139.17, 138.16, 135.33, 129.70, 129.34, 127.75, 127.43, 126.83, 124.77, 124.41, 124.00, 120.39, 119.56, 46.88. EI-MS: *m/z*: 426.53 [M$^+$]. Anal. calcd. for $C_{24}H_{18}N_4O_4$: C, 67.60; H, 4.25; N, 13.14. Found: C, 67.30; H, 4.61; N, 13.40.

5.1.9.3 (*E*)-2-(2-(3-Bromostyryl)-4-oxoquinazolin-3(*4H*)-yl)-*N*-phenylacetamide **11c**

Ratio of compound **10a**: *m*-bromobenzaldehyde was 1: 2.3 and heated under reflux for 48 h. **11c** was obtained as a yellowish white powder (0.148 g, 29.22%), m.p. 299-301 °C. ^{1}H NMR (400 MHz, DMSO-*d*$_6$) δ (ppm): 10.52 (1H, s, N**H**), 8.13 (2H, s, =C**H-**bromostyryl and 5-**H** quinazolinone), 8.01-7.71 (4H, m, 2,6-**H$_2$** bromostyryl and 7,8-**H$_2$** quinazolinone), 7.68-7.45 (5H, m, 4-**H** bromostyryl, 2,6-**H$_2$** phenylacetamide, 6-**H** quinazolinone and quinazolinone-C**H**=), 7.44-7.21 (3H, m, 5-**H** bromostyryl and 3,5-**H$_2$** phenylacetamide), 7.08 (1H, s, 4-**H** phenylacetamide), 5.26 (2H, s, C**H$_2$**CO). ^{13}C NMR (100 MHz, DMSO-*d*$_6$) δ (ppm): 166.31, 161.81, 152.83, 147.61, 139.17, 139.12, 138.17, 135.25, 132.70, 131.37, 130.54, 129.34, 128.16, 127.63, 127.14, 126.82, 124.01, 122.86, 121.86, 120.28, 119.58, 46.8. EI-MS: *m/z*: 460.52 [M$^+$]. Anal. calcd. for $C_{24}H_{18}BrN_3O_2$: C, 62.62; H, 3.94; N, 9.13. Found: C, 62.32; H, 4.2; N, 9.41.

5.1.9.4 (*E*)-2-(2-(3-Nitrostyryl)-4-oxoquinazolin-3(4*H*)-yl)-*N*-phenylacetamide **11d**

Ratio of compound **10a**: *m*-nitrobenzaldehyde was 1: 1.4 and heated under reflux for 48 h. **11d** was obtained as a yellowish white powder (0.235 g, 50 %), m.p. 298-301 °C. ^{1}H NMR (400 MHz, DMSO-*d*$_6$) δ (ppm): 10.51 (1H, s, N**H**), 8.68 (1H, s, 2-**H** nitrostyryl), 8.43-7.98 (4H, m, 4,6-**H$_2$** nitrostyryl and 5,7-**H$_2$** quinazolinone), 7.97-7.44 (7H, m, =C**H-**nitrostyryl, 5-**H** nitrostyryl, 2,6-**H$_2$** phenylacetamide, quinazolinone-C**H**= and 6,8-**H$_2$** quinazolinone), 7.32 (2H, s, 3,5-**H$_2$** phenylacetamide), 7.06 (1H, s, 4-**H** phenylacetamide), 5.27 (2H, s, C**H$_2$**CO).^{13}C NMR (100 MHz, DMSO-*d*$_6$) δ (ppm): 166.30, 161.79, 152.74, 148.88, 147.57, 139.18, 138.39, 137.54, 135.29, 135.03, 130.76, 129.33, 127.68, 127.27, 126.82, 124.36, 123.99, 123.28, 122.81, 120.34, 119.54, 46.91. EI-MS: *m/z*: 426.59 [M$^+$]. Anal. calcd. for $C_{24}H_{18}N_4O_4$: C, 67.6; H, 4.25; N, 13.14. Found: C, 67.35; H, 4.53; N, 13.34.

5.1.9.5 (*E*)-2-(2-(2-(Benzo[*d*][1,3]dioxol-5-yl)vinyl)-4-oxoquinazolin-3(4*H*)-yl)-*N*-phenylacetamide **11e**

Ratio of compound **10a**: piperonal was 1: 4.5 and heated under reflux 18 h. **11e** was obtained as a dark green powder (0.150 g, 32%), m.p. 288-290 °C. ^{1}H NMR (400 MHz, DMSO-d6) δ (ppm): 10.33 (1H, s, N**H**), 8.50-6.74 (14H, m, =C**H-**benzodioxol**,** 4,6,7-**H$_3$** benzodioxol, 2,3,4,5,6-**H$_5$** phenylacetamide, quinazolinone-C**H**= and 5,6,7,8-**H$_4$** quinazolinone), 6.09 (2H, s, OC**H$_2$**O), 5.23 (2H, s, C**H$_2$**CO). ^{13}C NMR (100 MHz, DMSO-*d*$_6$) δ (ppm): 166.31, 161.90, 153.25, 149.25,

148.52, 147.80, 140.77, 139.25, 135.14, 130.24, 129.33, 127.44, 126.77, 126.69, 125.14, 123.93, 120.07, 119.51, 118.01, 108.95, 107.05, 101.99, 46.75. EI-MS: *m/z*: 425.28[M^+]. Anal. calcd. for $C_{25}H_{19}N_3O_4$: C, 70.58; H, 4.5; N, 9.88. Found: C, 70.88; H, 4.78; N, 10.15.

5.1.9.6 (*E*)-2-(2-(3-Methoxystyryl)-4-oxoquinazolin-3(4*H*)-yl)-*N*-phenylacetamide **11f**

Ratio of compound **10a**: *m*-methoxybenzaldehyde was 1: 5.1 and heated under reflux for 18 h. **11f** was obtained as a beige powder (0.130 g, 28.72 %), m.p. 265-267 °C. ^{1}H NMR (400 MHz, DMSO-*d*$_6$) δ (ppm): 10.51 (1H, s, N**H**), 8.14 (1H, d, *J* = 8.0 Hz, 5-**H** quinazolinone), 8.00-7.82 (2H, m, =C**H**-methoxystyryl and 7-**H** quinazolinone), 7.73 (1H, d, *J* = 8.0 Hz, 8-**H** quinazolinone), 7.66-7.49 (3H, m, 2,6-**H$_2$** phenylacetamide and 6-**H** quinazolinone), 7.47-7.26 (6H, m, 2,5,6-**H$_3$** methoxystyryl, 3,5-**H$_2$** phenylacetamide and quinazolinone-C**H**=), 7.12-6.94 (2H, m, 4-**H** methoxystyryl and 4-**H** phenylacetamide), 5.25 (2H, s, C**H$_2$**CO), 3.79 (3H, s, C**H$_3$**). ^{13}C NMR (100 MHz, DMSO-*d*$_6$) δ (ppm): 166.27, 161.86, 160.07, 153.00, 147.67, 140.77, 139.11, 137.04, 135.24, 130.39, 129.34, 129.34, 127.57, 127.01, 126.82, 124.05, 121.14, 120.42, 120.18, 119.59, 115.94, 113.73, 55.65, 46.71. EI-MS: *m/z*: 411.46 [M^+]. Anal. calcd. for $C_{25}H_{21}N_3O_3$: C, 72.98; H, 5.14; N, 10.21. Found: C, 73.0; H, 5.45; N, 10.49.

5.1.9.7 (*E*)-2-(2-(4-Methoxystyryl)-4-oxoquinazolin-3(4*H*)-yl)-N-phenylacetamide **11g**

Ratio of compound **10a**: *p*-methoxybenzaldehyde was 1: 5 and heated under reflux for 10 h. **11g** was obtained as a canary yellow powder (0.202 g, 44.6 %), m.p. 276-278 °C. ^{1}H NMR (400 MHz, DMSO-*d*$_6$) δ (ppm): 10.49 (1H, s, N**H**), 8.13 (1H, d, *J* = 8.0 Hz, 5-**H** quinazolinone), 7.95 (1H, d, *J* = 15.2 Hz, =C**H**-methoxystyryl), 7.86 (1H, t, *J* = 8.0 Hz, 7-**H** quinazolinone), 7.78 (2H, d, *J* = 8.0 Hz, 2,6-**H$_2$** methoxystyryl), 7.73 (1H, d, *J* = 8.0 Hz, 8-**H** quinazolinone), 7.61 (2H, d, *J* = 8.0 Hz, 2,6-**H$_2$** phenylacetamide), 7.51 (1H, t, *J* = 8.0 Hz, 6-**H** quinazolinone), 7.33 (2H, t, *J* = 8.0 Hz, 3,5-**H$_2$** phenylacetamide), 7.25 (1H, d, *J* = 15.2 Hz, quinazolinone-C**H**=), 7.08 (1H, t, *J* = 8.0 Hz, 4-**H** phenylacetamide), 7.00 (2H, d, *J* = 8.0 Hz, 3,5-**H$_2$** methoxystyryl), 5.23 (2H, s, C**H$_2$**CO), 3.81 (3H, s, C**H$_3$**). ^{13}C NMR (100 MHz, DMSO-*d*$_6$) δ (ppm): 166.29, 161.91, 161.10, 153.36, 147.84, 140.66, 139.21, 135.15, 133.67, 130.39, 129.33, 128.37, 127.44, 126.79, 126.65, 123.97, 120.05, 119.57, 117.48, 114.80, 55.79, 46.72. EI-MS: *m/z*: 411.23 [M^+]. Anal. calcd. for $C_{25}H_{21}N_3O_3$: C, 72.98; H, 5.14; N, 10.21. Found: C, 73.1; H, 5.42; N, 10.46.

5.1.9.8 *(E)*-2-(2-(4-(Dimethylamino)styryl)-4-oxoquinazolin-3(4*H*)-yl)-*N*-phenylacetamide **11h**

Ratio of compound **10a**: *p*-dimethylaminobenzaldehyde was 1: 3.6 and heated under reflux for 21 h. **11h** was obtained as an orange powder (0.297 g, 63.6 %), m.p. 275-278 °C. ^{1}H NMR (400 MHz, DMSO-d_6) δ (ppm): 10.50 (1H, s, N**H**), 7.24-8.30 (11H, m, =C**H**-dimethylaminostyryl, 2,6-**H$_2$** dimethylaminostyryl, 2,3,5,6-**H$_4$** phenylacetamide and 5,6,7,8-**H$_4$** quinazolinone), 7.08 (2H, s, 4-**H** phenylacetamide and quinazolinone-C**H**=), 6.75 (2H, s, 3,5-**H$_2$** dimethylaminostyryl), 5.22 (2H, s, C**H$_2$**CO), 2.99 (6H, s, N(C**H$_3$**)$_2$). ^{13}C NMR (100 MHz, DMSO-d_6) δ (ppm): 165.56, 161.23, 152.93, 151.02, 147.28, 140.97, 138.46, 134.28, 129.47, 128.56, 126.48, 126.00, 125.40, 123.20, 122.43, 119.04, 118.82, 113.05, 111.52, 45.83, 40.18 (over laid on DMSO peak). EI-MS: *m/z*: 424.55 [M$^+$]. Anal. calcd. for $C_{26}H_{24}N_4O_2$: C, 73.56; H, 5.70; N, 13.20. Found: C, 73.75; H, 5.51; N, 13.02.

5.1.9.9 (*E*)-*N*-(4-Methoxyphenyl)-2-(4-oxo-2-styrylquinazolin-3(4*H*)-yl)acetamide **11i**

Ratio of compound **10b**: benzaldehyde was 1: 20.8 and heated under reflux for 28 h. **11i** was obtained as a greenish white powder (0.347 g, 76.7%), m.p. 284-287°C. ^{1}H NMR (400 MHz, DMSO-d_6) δ (ppm): 10.36 (1H, s, N**H**), 8.14 (1H, d, *J* = 8.0 Hz, 5-**H** quinazolinone), 7.97 (1H, d, *J* = 15.2 Hz, =C**H**-styryl), 7.91-7.73 (4H, m, 7,8-**H$_2$** quinazolinone and 2,6-**H$_2$** styryl), 7.59-7.35 (7H, m, 2,6-**H$_2$** methoxyphenyl, quinazolinone-C**H**=, 6-**H** quinazolinone and 3,4,5-**H$_3$** styryl), 6.90 (2H, d, *J* = 8.0 Hz, 3,5-**H$_2$** methoxyphenyl), 5.21 (2H, s, C**H$_2$**CO), 3.72 (3H, s, OC**H$_3$**). ^{13}C NMR (100 MHz, DMSO-d_6) δ (ppm): 165.72, 161.87, 155.84, 153.08, 147.67, 140.73, 135.66, 135.22, 132.25, 130.25, 129.36, 128.61, 127.56, 126.99, 126.81, 121.17, 120.19, 114.42, 55.62, 46.58. EI-MS: *m/z*: 411.46 [M$^+$]. Anal. calcd. for $C_{25}H_{21}N_3O_3$: C, 72.98; H, 5.14; N, 10.21. Found: C, 73.10; H, 5.4; N, 10.01.

5.1.9.10 (*E*)-*N*-(4-Methoxyphenyl)-2-(2-(4-nitrostyryl)-4-oxoquinazolin-3(4*H*)-yl)acetamide **11j**

Ratio of compound **10b**: *p*-nitro benzaldehyde was 1: 1.3 and heated under reflux for 18 h. **11j** was obtained as a yellow powder (0.151 g, 30 %), m.p. 314-316 °C. ^{1}H NMR (400 MHz, DMSO-d_6) δ (ppm): 10.38 (1H, s, N**H**), 8.28 (2H, d, *J* = 8.4 Hz, 3,5-**H$_2$** nitrostyryl), 8.20 – 8.01 (3H, m, =C**H**- nitrostyryl and 2,6-**H$_2$** nitrostyryl), 7.89 (1H, t, *J* = 8.0 Hz, 7-**H** quinazolinone), 7.78 (1H, d, *J* = 8.0 Hz, 8-**H** quinazolinone), 7.65 (1H, d, *J* = 15.2 Hz, quinazolinone-C**H**=), 7.60-7.46 (3H, m, 2,6-**H$_2$** methoxyphenyl and 6-**H** quinazolinone), 6.90 (2H, d, *J* = 8.0 Hz, 3,5-**H$_2$** methoxyphenyl), 5.24 (2H, s, C**H$_2$**CO), 3.72 (3H, s, OC**H$_3$**). ^{13}C NMR (100 MHz, DMSO-d_6) δ (ppm): 165.69, 161.74, 155.81, 152.60, 147.99, 147.51, 142.23, 138.09, 135.29, 132.32, 129.68,

127.74, 127.40, 126.84, 124.83, 124.42, 121.08, 120.41, 114.42, 55.62, 46.71. EI-MS: *m/z*: 456.07 [M^+]. Anal. calcd. for $C_{25}H_{20}N_4O_5$: C, 65.78; H, 4.42; N, 12.27. Found: C, 66.00; H, 4.45; N, 12.48.

5.1.9.11 (*E*)-2-(2-(3-Bromostyryl)-4-oxoquinazolin-3(4*H*)-yl)-*N*-(4-methoxyphenyl)acetamide **11k**

Ratio of compound **10b**: *m*-bromobenzaldehyde was 1: 2.3 and heated under reflux for 18 h. **11k** was obtained as an off-white powder (0.150 g, 27.81 %), m.p. 303-306 °C. ^{1}H NMR (400 MHz, DMSO-d_6) δ (ppm): 10.37 (1H, s, N**H**), 8.18-8.10 (2H, m, 2-**H** bromostyryl, 5-**H** quinazolinone), 7.97-7.84 (2H, m, 7-**H** quinazolinone and =C**H**-bromostyryl), 7.82-7.72 (2H, m, quinazolinone-C**H**= and 8-**H** quinazolinone),7.62-7.45 (5H, m, 4,6-**H$_2$** bromostyryl, 2,6-**H$_2$** methoxyphenyl and 6-**H** quinazolinone), 7.40 (1H, t, *J* = 8.0 Hz, 5-**H** bromostyryl), 6.90 (2H, d, *J* = 8.0 Hz, 3,5-**H$_2$** methoxyphenyl), 5.22 (2H, s, C**H$_2$**CO), 3.72 (3H, s, OC**H$_3$**). ^{13}C NMR (100 MHz, DMSO-d_6) δ (ppm): 165.76, 161.80, 155.83, 152.83, 147.60, 139.04, 138.19, 135.22, 132.69, 132.30, 131.38, 130.52, 128.14, 127.62, 127.12, 126.82, 122.86, 121.91, 121.11, 120.29, 114.42, 55.62, 46.67. EI-MS: *m/z*: 490.17 [M^+]. Anal. calcd. for $C_{25}H_{20}BrN_3O_3$: C, 61.24; H, 4.11; N, 8.57. Found: C,61.42; H, 4.33; N, 8.47.

5.1.9.12 (*E*)-*N*-(4-Methoxyphenyl)-2-(2-(3-nitrostyryl)-4-oxoquinazolin-3(4*H*)-yl)acetamide **11l**

Ratio of compound **10b**: *m*-nitrobenzaldehyde was 1: 2.8 and heated under reflux for 28 h. **11l** was obtained as a pale-yellow powder (0.237 g, 47.2%), m.p. 298-300 °C. ^{1}H NMR (400 MHz, DMSO-d_6) δ (ppm): 10.38 (1H, s, N**H**), 8.69 (1H, s, 2-**H** nitrostyryl), 8.27 (1H, d, *J* = 8.0 Hz, 4-**H** nitrostyryl), 8.22 (1H, d, *J* = 8.0 Hz, 6-**H** nitrostyryl), 8.15 (1H, d, *J* = 8.0 Hz, 5-**H** quinazolinone), 8.07 (1H, d, *J* = 15.2 Hz, =C**H**-nitrostyryl), 7.88 (1H, t, *J* = 8.0 Hz, 7-**H** quinazolinone), 7.80-7.69 (2H, m, 5-**H** nitrostyryl and 8-**H** quinazolinone), 7.64 (1H, d, *J* = 15.2 Hz, quinazolinone-C**H**=), 7.58-7.49 (3H, m, 2,6-**H$_2$** methoxyphenyl and 6-**H** quinazolinone), 6.89 (2H, d, *J* = 8.0 Hz, 3,5-**H$_2$** methoxyphenyl), 5.25 (2H,s, C**H$_2$**CO), 3.72 (3H, s, OC**H**$_3$). ^{13}C NMR (100 MHz, DMSO-d_6) δ (ppm): 165.75, 161.79, 155.82, 152.74, 148.87, 147.56, 138.32, 137.54, 135.26, 135.00, 132.29, 130.76, 127.67, 127.25, 126.82, 124.35, 123.31, 122.76, 121.09, 120.36, 114.41, 55.61, 46.47. EI-MS: *m/z*: 456.22 [M^+]. Anal. calcd. for $C_{25}H_{20}N_4O_5$: C, 65.78; H, 4.42; N, 12.27. Found: C, 65.98; H, 4.15; N, 12.0.

5.1.9.13 (*E*)-2-(2-(2-(Benzo[*d*][1,3]dioxol-5-yl)vinyl)-4-oxoquinazolin-3(4*H*)-yl)-*N*-(4-methoxyphenyl)acetamide **11m**

Ratio of compound **10b**: piperonal was 1: 6.4 and heated under reflux for 18 h. **11m** was obtained as a dark green powder (0.148 g, 29.54%), m.p. 314-317 °C. ^{1}H NMR (400 MHz, DMSO-*d*$_6$) δ (ppm): 10.33 (1H, s, N**H**), 8.12 (1H, d, *J* = 8.0 Hz, 5-**H** quinazolinone), 7.95-7.81 (2H, m, =C**H**-benzodioxol and 7-**H** quinazolinone), 7.72 (1H, d, *J* = 8.0 Hz, 8-**H** quinazolinone), 7.62-7.47 (4H, m, 2,6-**H$_2$** methoxyphenyl, quinazolinone-C**H**= and 6-**H** quinazolinone), 7.32-7.21 (2H, m, 4,6-**H$_2$** benzodioxol), 6.98 (1H, d, *J* = 8.0 Hz, 7-**H** benzodioxol), 6.90 (2H, d, *J* = 8.0 Hz, 3,4-**H$_2$** methoxyphenyl), 6.09 (2H, s, OC**H$_2$**O), 5.20 (2H, s, C**H$_2$**CO), 3.72 (3H, s, OC**H$_3$**). ^{13}C NMR (100 MHz, DMSO-*d*$_6$) δ (ppm): 165.77, 161.90, 155.77, 153.26, 149.25, 148.53, 147.79, 140.70, 135.12, 132.38, 130.25, 127.44, 126.79, 126.67, 124.11, 121.04, 120.09, 118.06, 114.41, 108.97, 107.04, 102.00, 55.61, 46.58. EI-MS: *m/z*: 455.19 [M$^+$]. Anal. calcd. for $C_{26}H_{21}N_3O_5$: C, 68.56; H, 4.65; N, 9.23. Found: C, 68.78; H, 4.81; N, 9.00.

5.1.9.14 (*E*)-*N*-(4-Methoxyphenyl)-2-(2-(3-methoxystyryl)-4-oxoquinazolin-3(4*H*)-yl)acetamide **11n**

Ratio of compound **10b**: *m*-methoxybenzaldehyde was 1: 9.5 and heated under reflux for 25 h. **11n** was obtained as a greenish white powder (0.200 g, 41.2%), m.p. 280-282 °C. ^{1}H NMR (400 MHz, DMSO-*d*$_6$) δ (ppm): 10.35 (1H, s, N**H**), 8.14 (1H, s, 5-**H** quinazolinone), 8.04-7.66 (3H, m, =C**H**-methoxystyryl and 7,8-**H$_2$** quinazolinone), 7.63-7.17 (7H, m, 2,6-**H$_2$** methoxyphenyl, 4,5,6-**H$_3$** methoxystyryl, quinazolinone-C**H**= and 6-**H** quinazolinone), 7.13-6.62 (3H, m, 4,5-**H$_2$** methoxyphenyl and 2-**H** methoxystyryl), 5.21 (2H, s, C**H$_2$**CO), 3.79 (3H, s, OC**H$_3$**), 3.72 (3H, s, OC**H$_3$**). ^{13}C NMR (100 MHz, DMSO-*d*$_6$) δ (ppm): 165.75, 161.84, 160.08, 155.82, 153.01, 147.69, 140.68, 137.09, 135.19, 132.30, 130.37, 127.57, 127.11, 126.96, 126.83, 121.10, 120.51, 120.23, 115.92, 114.42, 113.77, 55.67, 55.61, 46.58. EI-MS: *m/z*: 441.47 [M$^+$]. Anal. calcd. for $C_{26}H_{23}N_3O_4$: C, 70.74; H, 5.25; N, 9.52. Found: C, 70.9; H, 5.00; N, 9.33.

5.1.9.15 (*E*)-*N*-(4-Methoxyphenyl)-2-(2-(4-methoxystyryl)-4-oxoquinazolin-3(4*H*)-yl)acetamide **11o**

Ratio of compound **10b**: *p*-methoxybenzaldehyde was 1: 6.8 and heated under reflux for 43 h. **11o** was obtained as a yellow powder (0.292 g, 60%), m.p. 274-276 °C. ^{1}H NMR (400 MHz, DMSO-*d*$_6$) δ (ppm): 10.34 (1H, s, N**H**), 8.12 (1H, d, *J* = 8.0 Hz, 5-**H** quinazolinone), 7.94 (1H, d,

J = 15.2 Hz, =C**H**-methoxystyryl), 7.85 (1H, t, *J* = 8.0 Hz, 7-**H** quinazolinone), 7.75 (3H, m, 2,6-**H₂** methoxystyryl and 8-**H** quinazolinone), 7.51 (3H, d, *J* = 8.0 Hz, 3,5-**H₂** methoxystyryl and 6-**H** quinazolinone), 7.23 (1H, d, *J* = 15.2 Hz, quinazolinone-C**H**=), 7.00 (2H, d, *J* = 8.0 Hz, 2,6-**H₂** methoxyphenyl), 6.90 (2H, d, *J* = 8.0 Hz, 3,5-**H₂** methoxyphenyl), 5.19 (2H, s, C**H₂**CO), 3.81 (3H, s, OC**H₃**), 3.72 (3H, s, OC**H₃**). ^{13}C NMR (100 MHz, DMSO-*d₆*) δ (ppm): 165.75, 161.91, 161.09, 155.81, 153.35, 147.83, 140.59, 135.12, 132.34, 130.36, 128.38, 127.43, 126.80, 126.63, 121.12, 120.08, 117.51, 115.00, 114.80, 114.42, 55.79, 55.62, 46.55. EI-MS: *m/z*: 441.56 [M^+]. Anal. calcd. for $C_{26}H_{23}N_3O_4$: C, 70.74; H, 5.25; N, 9.52. Found: C, 70.85; H, 5.03; N, 9.31.

5.1.9.16 *(E)*-2-(2-(4-(Dimethylamino)styryl)-4-oxoquinazolin-3(4*H*)-yl)-*N*-(4 methoxyphenyl)acetamide **11p**

Ratio of compound **10b**: *p*-dimethylaminobenzaldehyde was 1: 3.9 and heated under reflux for 18 h. **11p** was obtained as a yellow powder (0.149 g, 29.8 %), m.p. 272-275 °C. ^{1}H NMR (400 MHz, DMSO-*d₆*) δ (ppm): 10.34 (1H,s, N**H**), 8.10 (1H, s, 5-**H** quinazolinone), 7.92 (1H, d, *J* = 14.8 Hz, =C**H**-dimethylaminostyryl), 7.82 (1H, s, 7-**H** quinazolinone), 7.75-7.34 (6H, m, 2,6-**H₂** dimethylaminostyryl, 2,6-**H₂** methoxyphenyl and 7,8-**H₂** quinazolinone), 7.04 (1H, d, *J* = 14.8 Hz, quinazolinone-C**H**=), 6.91 (2H, d, *J* = 8.0 Hz, 3,5-**H₂** methoxyphenyl), 6.74 (2H, s, 3,5-**H₂** dimethylaminostyryl), 5.18 (2H, s, C**H₂**CO), 3.73 (3H, s, OC**H₃**), 2.99 (6H, s, N(C**H₃**)**₂**). ^{13}C NMR (100 MHz, DMSO-*d₆*) δ (ppm): 165.80, 162.01, 155.84, 153.71, 151.85, 148.05, 141.71, 135.03, 132.37, 130.23, 127.24, 126.84, 126.22, 123.20, 121.14, 119.81, 114.42, 113.85, 112.30, 55.62, 46.43, 40.18 (over laid on DMSO peak). EI-MS: *m/z*: 454.51 [M^+]. Anal. calcd. for $C_{27}H_{26}N_4O_3$: C, 71.35; H, 5.77; N, 12.33. Found: C, 71.51; H, 5.52; N, 12.07.

5.1.9.17 (*E*)-*N*-(4-Chlorophenyl)-2-(4-oxo-2-styrylquinazolin-3(4*H*)-yl)acetamide **11q**

Ratio of compound **10c**: benzaldehyde was 1: 21.6 and heated under reflux for 22 h. **11q** was obtained as a bright yellow powder (0.336 g, 73.45%), m.p. around 307 °C. ^{1}H NMR (400 MHz, DMSO-*d₆*) δ (ppm): 10.65 (1H, s, N**H**), 8.42-6.98 (15H, m, 2,3,5,6-**H₄** chlorophenyl, =C**H**-styryl, quinazolinone-C**H**=, 5,6,7,8-**H₄** quinazolinone and 2,3,4,5,6-**H₅** styryl), 5.24 (2H, s, C**H₂**CO). ^{13}C NMR (100 MHz, DMSO-*d₆*) δ (ppm): 166.50, 161.86, 153.07, 147.70, 140.84, 138.15, 135.68, 135.23, 130.23, 129.32, 129.26, 128.69, 127.59, 127.54, 126.97, 126.79, 121.13, 120.18, 46.88. EI-MS: *m/z*: 415.41 [M^+]. Anal. calcd. for $C_{24}H_{18}ClN_3O_2$: C, 69.31; H, 4.36; N, 10.10. Found: C, 69.25; H, 4.10; N, 10.30.

5.1.9.18 (*E*)-*N*-(4-Chlorophenyl)-2-(2-(3-nitrostyryl)-4-oxoquinazolin-3(4*H*)-yl)acetamide **11r**

Ratio of compound **10c**: *m*-nitrobenzaldehyde was 1: 1.5 and heated under reflux for 22 h. **11r** was obtained as a yellowish white powder (0. 243 g, 47.9 %), m.p. 325-328 °C. ^{1}H NMR (400 MHz, DMSO-d_6) δ (ppm): 10.66 (1H, s, N**H**), 8.69 (1H, s, 2-**H** nitrostyryl), 8.29 (1H, d, *J* = 8.0 Hz, 4-**H** nitrostyryl), 8.23 (1H, d, *J* = 8.0 Hz, 6-**H** nitrostyryl), 8.15 (1H,d, *J* = 8.0 Hz, 5-**H** quinazolinone), 8.08 (1H, d, *J* = 15.2 Hz, =C**H**-nitrostyryl), 7.90 (1H, t, *J* = 8.0 Hz, 7-**H** quinazolinone), 7.81-7.70 (2H, m, quinazolinone-C**H**= and 8-**H** quinazolinone), 7.69-7.61 (3H, m, 2,6-**H$_2$** chlorophenyl and 5-**H** nitrostyryl), 7.56 (1H,t, *J* = 8.0 Hz, 6-**H** quinazolinone), 7.39 (2H, d, *J* = 8.5 Hz, 3,5-**H$_2$** chlorophenyl), 5.27 (2H,s, C**H$_2$**CO). ^{13}C NMR (100 MHz, DMSO-d_6) δ (ppm): 166.53, 161.79, 152.73, 148.89, 147.57, 138.47, 138.14, 137.53, 135.33, 135.06, 130.77, 129.28, 127.71, 127.54, 127.32, 126.83, 124.40, 123.25, 122.86, 121.11, 120.31, 47.03. EI-MS: *m/z*: 460.34 [M$^+$]. Anal. calcd. for $C_{24}H_{17}ClN_4O_4$: C, 62.55; H, 3.72; N, 12.16. Found: C, 62.46; H, 3.99; N, 12.31.

5.1.9.19 (*E*)-2-(2-(3-Bromostyryl)-4-oxoquinazolin-3(4*H*)-yl)-*N*-(4-chlorophenyl)acetamide **11s**

Ratio of compound **10c**: *m*-bromobenzaldehyde was 1: 14.7 and heated under reflux for 22 h. **11s** was obtained as a khaki powder (0.306 g, 56.22 %), m.p. 316-318 °C. ^{1}H NMR (400 MHz, DMSO-d_6) δ (ppm): 10.67 (1H, s, N**H**), 8.38-7.08 (14H, m, 2,4,5,6-**H$_4$** bromostyryl, =C**H**-bromostyryl, 2,3,5,6-**H$_4$** chlorophenyl, quinazolinone-C**H**= and 5,6,7,8-**H$_4$** quinazolinone), 5.25 (2H, s, C**H$_2$**CO). ^{13}C NMR (100 MHz, DMSO-d_6) δ (ppm): 166.54, 161.81, 152.82 147.61, 139.18, 138.17, 135.29, 132.72, 131.38, 130.57, 129.28, 128.70, 128.21, 127.64, 127.53, 127.17, 126.80, 122.86, 121.84, 121.11, 120.24, 46.96. EI-MS: 493.87 *m/z*: [M$^+$]. Anal. calcd. for $C_{24}H_{17}BrClN_3O_2$: C, 58.26; H, 3.46; N, 8.49. Found: C, 58.45; H, 3.62; N, 8.71.

5.1.9.20 *(E)*-2-(2-(2-(Benzo[*d*][1,3]dioxol-5-yl)vinyl)-4-oxoquinazolin-3*(4H)*-yl)-*N*-(4-chlorophenyl)acetamide **11t**

Ratio of compound **10c**: piperonal was 1: 15.6 and heated under reflux for 35 h. **11t** was obtained as a dark green powder (0.348 g, 68.8 %), m.p. 317-319 °C. ^{1}H NMR (400 MHz, DMSO-d_6) δ (ppm): 10.62 (1H, s, N**H**), 8.12 (1H, d, *J* = 8.0 Hz, 5-**H** quinazolinone), 7.97-7.80 (2H, m, =C**H**-benzodioxol and 7-**H** quinazolinone), 7.72 (1H, d, *J* = 8.0 Hz, 8-**H** quinazolinone), 7.68-7.57 (3H, m, 2,6-**H$_2$** chlorophenyl and quinazolinone-C**H**=), 7.50 (1H, t, *J* = 8.0 Hz, 6-**H** quinazolinone), 7.39 (2H, d, *J* = 8.0 Hz, 3,5-**H$_2$** chlorophenyl), 7.32-7.20 (2H, m, 4,6-**H$_2$** benzodioxol), 6.98 (1H, d, *J* = 8.0 Hz, 7-**H** benzodioxol), 6.09 (2H, s, OC**H$_2$**O), 5.21 (2H, s, C**H$_2$**CO). ^{13}C NMR (100 MHz, DMSO-d_6) δ (ppm): 166.17, 161.53, 152.84, 149.15, 148.12, 147.39, 140.55, 140.42, 137.84,

134.86, 134.74, 129.84, 128.89, 127.09, 126.38, 124.80, 120.69, 119.66, 117.59, 108.60, 106.66, 101.65, 46.51. EI-MS: *m/z*: 459.78 [M^+]. Anal. calcd. for $C_{25}H_{18}ClN_3O_4$: C, 65.29; H, 3.95; N, 9.14. Found: C, 65.51; H, 4.1; N, 9.32.

5.1.9.21 *(E)-N*-(4-Chlorophenyl)-2-(2-(4-methoxystyryl)-4-oxoquinazolin-3(4*H)*-yl)acetamide **11u**

Ratio of compound **10c**: *p*-methoxybenzaldehyde was 1: 8.5 and heated under reflux for 22 h. **11u** was obtained as a yellow powder (0.230 g, 46.9%), m.p. 289-292 °C. ^{1}H NMR (400 MHz, DMSO-d_6) δ (ppm): 10.64 (1H, s, N**H**), 8.12 (1H, d, *J* = 8.0 Hz, 5-**H** quinazolinone), 7.95 (1H, d, *J* = 15.1 Hz, =C**H**-methoxystyryl), 7.85 (1H, t, *J* = 8.0 Hz, 7-**H** quinazolinone), 7.81-7.70 (3H, m, 2,6-**H$_2$** methoxystyryl and 8-**H** quinazolinone), 7.65 (2H, d, *J* = 8.0 Hz, 2,6-**H$_2$** chlorophenyl), 7.51 (1H, t, *J* = 8.0 Hz, 6-**H** quinazolinone), 7.39 (2H, d, *J* = 8.0 Hz, 3,5-**H$_2$** chlorophenyl), 7.25 (1H, d, *J* = 15 Hz, quinazolinone-C**H**=), 7.00 (2H, d, *J* = 8.0 Hz, 3,5-**H$_2$** methoxystyryl), 5.22 (2H, s, C**H$_2$**CO), 3.81 (3H,s, OC**H$_3$**). ^{13}C NMR (100 MHz, DMSO-d_6) δ (ppm): 166.52, 161.92, 161.11, 153.34, 147.83, 140.73, 138.17, 135.17, 130.42, 129.26, 128.36, 127.52, 127.45, 126.77, 126.66, 121.13, 120.02, 117.43, 114.78, 55.78, 46.82. EI-MS: *m/z*: 445.39 [M^+]. Anal. calcd. for $C_{25}H_{20}ClN_3O_3$: C, 67.34; H, 4.52; N, 9.42. Found: C, 67.1; H, 4.33; N, 9.19.

5.1.9.22 *(E)-N*-(4-Chlorophenyl)-2-(2-(3-methoxystyryl)-4-oxoquinazolin-3*(4H)*-yl)acetamide **11v**

Ratio of compound **10c**: *m*-methoxybenzaldehyde was 1: 9.5 and heated under reflux for 24 h. **11v** was obtained as a yellowish white powder (0.295 g, 60%), m.p. 302-304 °C. ^{1}H NMR (400 MHz, DMSO-d_6) δ (ppm): 10.65 (1H, s, N**H**), 8.14 (1H, d, *J* = 8.0 Hz, 5-**H** quinazolinone), 7.94 (1H, d, *J* = 14.8 Hz, =C**H**-methoxystyryl), 7.87 (1H, t, *J* = 8.0 Hz, 7-**H** quinazolinone), 7.76 (1H, d, *J* = 8.0 Hz, 8-**H** quinazolinone), 7.64 (2H, d, *J* = 8.0 Hz, 2,6-**H$_2$** chlorophenyl), 7.53 (1H, t, *J* = 8.0 Hz, 6-**H** quinazolinone), 7.44-7.32 (6H, m, 3,5-**H$_2$** chlorophenyl, 2,5,6-**H$_3$** methoxystyryl and quinazolinone-C**H**=), 6.99 (1H, d, *J* = 8.0 Hz, 4-**H** methoxystyryl), 5.24 (2H, s, C**H$_2$**CO), 3.80 (3H, s, OC**H$_3$**). ^{13}C NMR (100 MHz, DMSO-d_6) δ (ppm): 166.51, 161.85, 160.08, 153.00, 147.69, 140.81, 138.13, 137.06, 135.25, 130.36, 129.27, 127.58, 127.54, 127.00, 126.80, 121.12, 120.45, 120.18, 115.88, 113.90, 55.68, 46.86. EI-MS: *m/z*: 445.27 [M^+]. Anal. calcd. for $C_{25}H_{20}ClN_3O_3$: C, 67.34; H, 4.52; N, 9.42. Found: C, 67.19; H, 4.32; N, 9.18.

5.1.9.23 (*E*)-*N*-(4-Chlorophenyl)-2-(2-(4-(dimethylamino)styryl)-4-oxoquinazolin-3(4*H*)-yl)acetamide **11w**

Ratio of compound **10c**: *p*-dimethylaminobenzaldehyde was 1: 3.9 and heated under reflux for 18 h. **11v** was obtained as an orange powder (0.200 g, 39.6%), m.p.277-280 °C. ^{1}H NMR (400 MHz, DMSO-*d*$_6$) δ (ppm): 10.63 (1H, s, N**H**), 8.09 (1H, d, *J* = 8.0 Hz, 5-**H** quinazolinone), 7.91 (1H, d, *J* = 14.9 Hz, =C**H**-dimethylaminostyryl), 7.82 (1H, t, *J* = 8.0 Hz, 7-**H** quinazolinone), 7.76 – 7.57 (5H, m, 2,3,5,6-**H$_4$** chlorophenyl and 8-**H** quinazolinone), 7.52-7.33 (3H, m, 2,6-**H$_2$** dimethylaminostyryl and 6-**H** quinazolinone), 7.05 (1H, d, *J* = 14.9 Hz, quinazolinone-C**H**=), 6.72 (2H, d, *J* = 8.0 Hz, 3,5-**H$_2$** dimethylaminostyryl), 5.20 (2H, s, C**H$_2$**CO), 2.98 (6H, s, N(C**H$_3$**)$_2$). ^{13}C NMR (100 MHz, DMSO-*d*$_6$) δ (ppm): 166.56, 162.00, 153.70, 151.81, 148.05, 141.80, 138.19, 135.08, 130.28, 129.26, 127.49, 127.26, 126.76, 126.19, 123.20, 121.13, 119.77, 113.79, 112.27, 46.70, 40.18 (over laid on DMSO peak). EI-MS: *m/z*: 458.29 [M$^+$]. Anal. calcd. for $C_{26}H_{23}ClN_4O_2$: C, 68.04; H, 5.05; N, 12.21. Found: C, 68.30; H,5.21; N, 12.46.

5.2. Biological evaluation

5.2.1 RecQ helicases inhibitory assay

5.2.1.1 Recombinant Proteins

Methods for expression and purification of the recombinant human proteins BLM-HD, RECQ1-HD and WRN-HD are described in Chen *et al.* (2021). [14]

5.2.1.2 Malachite-green ATP turnover assay

Commercially available PiColorLock Gold Phosphate Detection System from Novus Biologicals was used, and manufacturer's recommended protocol was followed. These assays were conducted in 96-well clear flat-bottomed plates, using a wavelength of 630 nm for measurement of the absorbances in a CLARIOstar multimode plate reader (BMG Labtech). The used buffer was 50 mM NaCl, 50 mM Tris-HCl pH 7.5, 0.05% v/v Tween-20, 2 mM MgCl2 and 0.5 mM TCEP. SsDNA-20mer and 165 µl of BLM-HD (at concentrations of 121 nM and 2.4 nM, respectively) were pre-incubated with 10 µl of the compounds (2 mM stock dissolved in 100 % v/v DMSO, over a range of final concentrations up to 100 µM) for 15 min at room temperature. Then, 25 µl of Mg-ATP substrate (at 16 mM) was added. The reactions were stopped after 20 min, by the addition of 50 µl Gold mix (PiColorLock: Accelerator reagents ratio equals 100:1). After 2 min, 20 µl of

stabiliser solution was added to each well. The absorbance measurements were taken after another 30 min. Assay conditions: 2 nM BLM-HD, 100 nM ssDNA-20mer and 2 mM Mg-ATP in a reaction volume of 200 ml over a 20-min incubation period. [14] In the standard turnover assay, an ATP concentration of 16 mM was used as mentioned. This was increased to 80 mM for the competitive experiments.

5.2.1.3 Topoisomerase I DNA-unwinding assay

The assay was performed using DNA Unwinding Assay kits from Abcam (ab270004; Cambridge, UK) and Inspiralis (DUKSR001; Norwich, UK), respectively, and the manufacturer's recommended protocols were followed. The resultant samples were applied to a 1% w/v agarose gel (in 1 x TAE buffer), separated by electrophoresis, stained with ethidium bromide, and then visualised with a UV-transilluminator/digital gel documentation system. [14]

5.2.1.4 Fluorescence-based DNA unwinding assay

Methodology is based on that previously reported by Rosenthal et al., 2010 [12] and Chen et al., 2021 [14] but adopts a continuous readout rather than an endpoint format.

Oligonucleotides FORK-A and FORK-B were annealed at a concentration of 100 µM using a slow-cooling cycle programmed into a PCR thermal cycler, in a buffer containing 20 mM HEPES.NaOH pH 7.5, 50 mM NaCl and 1 mM $MgCl_2$.

FORK A: 5'-**X**GAACGAACACATCGGGTACGTTTTTTTTTTTTTTTTTTTTTTTTTTT-3'
FORK B: 5'-TTTTTTTTTTTTTTTTTTTTTTTTTTTTTTCGTACCCGATGTGTTCGTTC**Y**-3'

X = Black Hole Quencher 2 (BHQ2) and Y = tetramethylrhodamine (TAMRA).

Briefly, assays were carried out in 96-well flat-bottom black plates, with measurements taken every 30 seconds using a CLARIOstar multimode plate reader (BMG Labtech, at excitation and emission wavelengths of 540 and 590 nm respectively. Assay buffer: 50 mM HEPES.NaOH pH 7.5, 50 mM NaCl, 2 mM $MgCl_2$, 0.01% v/v TWEEN-20, 0.5 mM TCEP, 3.5% v/v DMSO. Assay conditions: 100 nM annealed DNA substrate, 125 µM Mg-ATP, 12.5 nM BLM-HD, 280 µM **11g** in a reaction volume of 100 µl.

5.2.1.5 western blot assay

The assay was performed according to the referenced protocols [69-71] and the detailed experimental data are available in the Supplementary File (**Pages 111-114**).

5.2.2 In vitro antitumor activity versus NCI 60 cancer cell lines

Evaluation of the preliminary *in vitro* anticancer activity of the target compounds was performed against 60 cancer cell lines, representing nine different human tissues, at the National Cancer Institute (NCI) Developmental Therapeutic Program using its protocols. [37-41] SRB assay was employed. The obtained results are growth percentages (G%) relative to the no-drug control and relative to the time zero number of cells. The growth inhibition percentage (GI%) was calculated from mean growth percentages values as (100 – G%). [67] The target compounds that met certain criteria defined by the DTP NCI were promoted to the five-dose screening stage by the NCI to assess the dose-response curves in the 60-cell line panel. Five 10-fold serial dilutions (100, 10, 1.0, 0.1, and 0.01 μM) for each compound were tested against each cell line to determine the growth percentage after treatment for 48 h. Different parameters were determined from the dose-response relationship. GraphPad Prism 9.0 was used to compute the values of GI_{50} and LC_{50} parameters. Five 10-fold serial dilutions (100, 10, 1.0, 0.1, and 0.01 μM) for each compound were tested against each cell line to determine the growth percentage after treatment for 48 h. Different parameters were determined from the dose-response relationship. GraphPad Prism 9.0 was used to compute the values of GI_{50} and LC_{50} parameters.

5.2.3. Investigation of the apoptotic effect of 11g

5.2.3.1 The real-time polymerase chain reaction (RT-PCR) of the tested genes

The expression levels of proapoptotic genes like P53, Bax, caspases 3,8, 9 as well as anti-apoptotic genes as Bcl-2 were measured to explore the apoptotic pathway; their sequences in forward and reverse direction are presented in the supporting information file (**Table S4**). HCT-116 and MDA-MB-231/ATCC cells were treated with compound **11g** at their IC_{50} values for 48 h. After the treatment, cells were collected, the RT-CPR reaction was carried out following RNA extraction, and cDNA was synthesized. Then, the Ct values were gathered to calculate the relative genes' expression in all samples by normalization to the β-actin housekeeping gene. [68]

5.2.3.2 The Annexin V/PI staining analysis and cell cycle analysis

Six-well culture plates were seeded with HCT-116 cells ($3\text{-}5\times10^5$ cells/well) and incubated overnight. Compound **11g** was used to treat cells for 48 hours at the IC_{50} concentration. Then, the

cells and the media supernatants were collected and washed with ice-cold PBS. The next step was suspending the cells in 100 µL of annexin binding buffer solution "25 mM $CaCl_2$, 1.4 M NaCl, and 0.1 M Hepes/ NaOH, pH 7.4" and incubation with "Annexin V-FITC solution (1: 100) and propidium iodide (PI)" at a concentration equals 10 µg mL^{-1} in the dark for 30 min. Stained cells were then acquired by Cytoflex FACS machine. Data were analyzed using cytExpert software. [68]

5.2.4. In vitro cytotoxicity for compound 11g against human normal cell (normal colon cells)

Normal colon (FHC) cells were procured from American Type Culture Collection (ATTC, USA) and maintained in a complete medium of DMEM/F12 medium L-Glutamine (Lonza Verviers SPRL, Belgium, cat#12-604F) supplemented with 10% fetal bovine serum (FBS, Sigma-Aldrich, MO, USA) and 1% penicillin-streptomycin (Lonza, Belgium). Following routine tissue culture work, cells were plated at a density equal $5x10^4$ cells in triplicates in a plate of 96 wells, and incubated at 37 ºC in 5% carbon dioxide atmosphere (NuAire). After 48h-incubation, cells were treated with the compounds at concentrations [100, 25, 6.25, 1.6, and 0.4 µM]. Cell viability was assessed after 48 h using the MTT solution (Promega, USA). [69] Absorbance was measured (at 570 nm) using an ELISA microplate reader (BIO-RAD, model iMark, Japan). The viability was calculated relative to control was determined using the GraphPad prism 7.

5.2.5. In silico studies

5.2.5.1. Predicted ADME properties

Chemdraw 12.0 was used to convert the molecular structures of **4a-c**, **6a-c**, and **11a-w** into SMILES database. The obtained database was used as input information in the web-based Swiss-ADME tool, https://www.swissadme.ch/index.php, for calculating the physicochemical descriptors, evaluating pharmacokinetics and drug-likeness of the compounds. [50, 51] Also, permeability through human gastrointestinal tract (GIT) and blood–brain barrier (BBB) was predicted using the same Swiss-ADME tool.

5.2.5.2. Molecular docking simulation study

The molecular Operating Environment software (MOE 2020), [58] was used to explore the binding modes. BLM, WRN, and RECQ1 crystal structures (PDB ID: 4CGZ, 6YHR and 2V1X respectively) were downloaded from the research Collaboratory for structural bioinformatics (RCSB) Protein Data Bank in the form of PDB files, [55-57] Proteins and ligands were prepared using the default options available in the program. For validation of the models, redocking

processes were performed and the results obtained were within the accepted range. Then the docking simulation process was performed according to previous protocol, [70] and the 2D ligand-receptor interactions were generated and visualized using Discovery Studio v20.1.019295.

6. Acknowledgement

- Anju Paul and Antony W. Oliver acknowledge funding from a Wellcome ISSF award 204833/Z/16/Z made to Professor Laurence H Pearl at the University of Sussex.
- Faculty of Pharmacy - Tanta University funding the chemistry part.

7. References

[1] H. Lu, A.J. Davis, Human RecQ Helicases in DNA Double-Strand Break Repair, Frontiers in Cell and Developmental Biology, 9 (2021) 640755.

[2] J. Maity, S. Horibata, G. Zurcher, J.-M. Lee, Targeting of RecQ Helicases as a Novel Therapeutic Strategy for Ovarian Cancer, Cancers, 14 (2022) 1219.

[3] V. Urban, J. Dobrovolna, P. Janscak, Distinct functions of human RecQ helicases during DNA replication, Biophysical Chemistry, 225 (2017) 20-26.

[4] V.A. Bohr, Rising from the RecQ-age: the role of human RecQ helicases in genome maintenance, Trends in Biochemical Sciences, 33 (2008) 609-620.

[5] D.L. Croteau, V. Popuri, P.L. Opresko, V.A. Bohr, Human RecQ helicases in DNA repair, recombination, and replication, Annual review of biochemistry, 83 (2014) 519-552.

[6] F.A. Alzahrani, F. Ahmed, M. Sharma, M. Rehan, M. Mahfuz, M.N. Baeshen, Y. Hawsawi, A. Almatrafi, S.A. Alsagaby, M.A. Kamal, Investigating the pathogenic SNPs in BLM helicase and their biological consequences by computational approach, Scientific Reports, 10 (2020) 12377.

[7] E. Kaur, R. Agrawal, S. Sengupta, Functions of BLM helicase in cells: is it acting like a double-edged sword?, Frontiers in genetics, 12 (2021) 634789.

[8] D.S. Chandrashekar, B. Bashel, S.A.H. Balasubramanya, C.J. Creighton, I. Ponce-Rodriguez, B.V. Chakravarthi, S.J.N. Varambally, UALCAN: a portal for facilitating tumor subgroup gene expression and survival analyses, Neoplasia, 19 (2017) 649-658.

[9] Q. Li, P. Zhang, Y.-N. Zhang, H.-X. Hu, J.-F. Yan, A.-H. Shen, B.-R. Hu, Aberrant Expression of BLM Correlates with Malignant Progression and Immune Infiltration in Pancreatic Adenocarcinoma, Cancer Screening, 2 (2022) 14-29.

[10] K. Kitano, Structural mechanisms of human RecQ helicases WRN and BLM, Frontiers in genetics, 5 (2014) 366.

[11] R.J. Bennett, J.L. Keck, Structure and function of RecQ DNA helicases, Critical Reviews in Biochemistry and Molecular Biology, 39 (2004) 79-97.

[12] A.S. Rosenthal, T.S. Dexheimer, G. Nguyen, O. Gileadi, A. Vindigni, A. Simeonov, A. Jadhav, I. Hickson, D.J. Maloney, Discovery of ML216, a small molecule inhibitor of bloom (BLM) helicase, Probe Reports from the NIH Molecular Libraries Program, (2013).

[13] G.H. Nguyen, T.S. Dexheimer, A.S. Rosenthal, W.K. Chu, D.K. Singh, G. Mosedale, C.Z. Bachrati, L. Schultz, M. Sakurai, P. Savitsky, A small molecule inhibitor of the BLM helicase modulates chromosome stability in human cells, Chemistry & Biology, 20 (2013) 55-62.

[14] X. Chen, Y.I. Ali, C.E.L. Fisher, R. Arribas-Bosacoma, M.B. Rajasekaran, G. Williams, S. Walker, J.R. Booth, J.J.R. Hudson, S.M. Roe, L.H. Pearl, S.E. Ward, F.M.G. Pearl, A.W. Oliver, Uncovering an allosteric mode of action for a selective inhibitor of human Bloom syndrome protein, elife, 10 (2021) e65339.

[15] Q.-K. Yin, C.-X. Wang, Y.-Q. Wang, Q.-L. Guo, Z.-L. Zhang, T.-M. Ou, S.-L. Huang, D. Li, H.-G. Wang, J.-H. Tan, S.-B. Chen, Z.-S. Huang, Discovery of Isaindigotone Derivatives as Novel Bloom's Syndrome Protein (BLM) Helicase Inhibitors That Disrupt the BLM/DNA Interactions and Regulate the Homologous Recombination Repair, Journal of Medicinal Chemistry, 62 (2019) 3147-3162.

[16] C.-X. Wang, Z.-L. Zhang, Q.-K. Yin, J.-L. Tu, J.-E. Wang, Y.-H. Xu, Y. Rao, T.-M. Ou, S.-L. Huang, D.J.J.o.M.C. Li, Design, synthesis, and evaluation of new quinazolinone derivatives that inhibit bloom syndrome protein (BLM) helicase, trigger DNA damage at the telomere region, and synergize with PARP inhibitors, Journal of Medicinal Chemistry, 63 (2020) 9752-9772.

[17] S.K. Wahan, B. Sharma, P.A. Chawla, Medicinal perspective of quinazolinone derivatives: Recent developments and structure–activity relationship studies, Journal of Heterocyclic Chemistry, 59 (2022) 239-257.

[18] R. Rezaeinasab, E. Jafari, G. Khodarahmi, Quinazolinone-based hybrids with diverse biological activities: A mini-review, Journal of Research in Medical Sciences, (2022).

[19] A.M. Alsibaee, H.M. Al-Yousef, H.S. Al-Salem, Quinazolinones, the Winning Horse in Drug Discovery, Molecules, 28 (2023) 978.

[20] S. Chakraborty, K. Dutta, P. Gupta, A. Das, A. Das, S.K. Ghosh, B.S. Patro, Targeting RECQL5 Functions, by a Small Molecule, Selectively Kills Breast Cancer in Vitr o and in Vivo, Journal of Medicinal Chemistry, 64 (2021) 1524-1544.

[21] M.K. Thakkar, J. Lee, S. Meyer, V.Y. Chang, RecQ Helicase Somatic Alterations in Cancer, Frontiers in Molecular Biosciences, 9 (2022) 887758.

[22] Y. Lin, H. Wang, X. Wang, M. Li, H. Chen, J. Peng, Low expression of RecQ-like helicase 5 is associated with poor prognosis in patients with gastric cancer, Oncology Letters, 19 (2020) 985-991.

[23] C.-X. Wang, Z.-L. Zhang, Q.-K. Yin, J.-L. Tu, J.-E. Wang, Y.-H. Xu, Y. Rao, T.-M. Ou, S.-L. Huang, D. Li, Design, Synthesis, and Evaluation of New Quinazolinone Derivatives that Inhibit Bloom Syndrome Protein (BLM) Helicase, Trigger DNA Damage at the Telomere Region, and Synergize with PARP Inhibitors, Journal of Medicinal Chemistry, 63 (2020) 9752-9772.

[24] G. Rotas, A. Kimbaris, G. Varvounis, Synthesis of a novel pyrrolo [1, 2-c][1.3] benzodiazepine analogue of VPA-985, Tetrahedron, 67 (2011) 7805-7810.

[25] C.C. Llopart, J.A. Joule, Synthetic studies related to the akuammiline alkaloids, Arkivoc, 10 (2004) 20-38.

[26] M.N. Noolvi, H.M. Patel, Synthesis, method optimization, anticancer activity of 2, 3, 7-trisubstituted quinazoline derivatives and targeting EGFR-tyrosine kinase by rational approach: 1st Cancer Update, Arabian Journal of Chemistry, 6 (2013) 35-48.

[27] M.N. Noolvi, H.M. Patel, V. Bhardwaj, A. Chauhan, Synthesis and in vitro antitumor activity of substituted quinazoline and quinoxaline derivatives: search for anticancer agent, European Journal of Medicinal chemistry, 46 (2011) 2327-2346.

[28] M.F. Zayed, S. Ahmed, S. Ihmaid, H.E.A. Ahmed, H.S. Rateb, S.R.M. Ibrahim, Design, Synthesis, Cytotoxic Evaluation and Molecular Docking of New Fluoroquinazolinones as Potent Anticancer Agents with Dual EGFR Kinase and Tubulin Polymerization Inhibitory Effects, International Journal of Molecular Sciences, 19 (2018) 1731.

[29] H.M. Abdel-Rahman, M. Abdel-Aziz, J.C. Canzoneri, B.D. Gary, G.A. Piazza, Novel Quinazolin-4 (3H)-one/Schiff Base Hybrids as Antiproliferative and Phosphodiesterase 4 Inhibitors: Design, Synthesis, and Docking Studies, Archiv der Pharmazie, 347 (2014) 650-657.

[30] M.F. Zayed, H.S. Rateb, S. Ahmed, O.A. Khaled, S.R.M. Ibrahim, Quinazolinone-Amino Acid Hybrids as Dual Inhibitors of EGFR Kinase and Tubulin Polymerization, Molecules, 23 (2018) 1699.

[31] M. Patel, M. Chhasatia, P. Parmar, Antibacterial and DNA interaction studies of zinc (II) complexes with quinolone family member, ciprofloxacin, European Journal of Medicinal Chemistry, 45 (2010) 439-446.

[32] S. Benhammadi, S. Iraten, A.A. Othman, Synthetic Studies and Antibacterial Activity of Nucleobases and their N-and S-Glucosides from 2-Amino Benzoic Acid and its Benzamido Derivatives, Oriental Journal of Chemistry, 32 (2016) 2567-2576.

[33] M.T. Sulthana, V. Alagarsamy, K. Chitra, Design, Synthesis, Pharmacological Evaluation, In silico Modeling, Prediction of Toxicity and Metabolism Studies of Novel 1-(substituted)-2-methyl-3-(4-oxo-2-phenyl quinazolin-3 (4H)-yl) isothioureas, Medicinal Chemistry, 17 (2021) 352-368.

[34] S.S. Kulkarni, S. Singh, J.R. Shah, W.-K. Low, T.T. Talele, Synthesis and SAR optimization of quinazolin-4 (3H)-ones as poly (ADP-ribose) polymerase-1 inhibitors, European Journal of Medicinal Chemistry, 50 (2012) 264-273.

[35] J.A. de Sousa Luis, H.D. da Silva Souza, B.F. Lira, F. da Silva Alves, P.F. de Athayde-Filho, T.K. de Souza Lima, J.C. Rocha, F.J.B.M. Junior, L. Scotti, M.T. Scotti, Combined structure- and ligand-based virtual screening aiding discovery of selenoglycolicamides as potential multitarget agents against Leishmania species, Journal of Molecular Structure, 1198 (2019) 126872.

[36] H.S.A. ElZahabi, M.S. Nafie, D. Osman, N.H. Elghazawy, D.H. Soliman, A.A.H. El-Helby, R.K. Arafa, Design, synthesis and evaluation of new quinazolin-4-one derivatives as apoptotic enhancers and autophagy inhibitors with potent antitumor activity, European Journal of Medicinal Chemistry, 222 (2021) 113609.

[37] P. Skehan, R. Storeng, D. Scudiero, A. Monks, J. McMahon, D. Vistica, J.T. Warren, H. Bokesch, S. Kenney, M.R. Boyd, New Colorimetric Cytotoxicity Assay for Anticancer-Drug Screening, JNCI: Journal of the National Cancer Institute, 82 (1990) 1107-1112.

[38] M.R. Boyd, K.D. Paull, Some practical considerations and applications of the National Cancer Institute in vitro anticancer drug discovery screen, Drug Development Research, 34 (1995) 91-109.

[39] R.H. Shoemaker, The NCI60 human tumour cell line anticancer drug screen, Nature Reviews Cancer, 6 (2006) 813-823.

[40] M.C. Alley, D.A. Scudiero, A. Monks, M.L. Hursey, M.J. Czerwinski, D.L. Fine, B.J. Abbott, J.G. Mayo, R.H. Shoemaker, M.R. Boyd, Feasibility of drug screening with panels of human tumor cell lines using a microculture tetrazolium assay, Cancer Research, 48 (1988) 589-601.

[41] M.R. Grever, S.A. Schepartz, B.A. Chabner, The National Cancer Institute: cancer drug discovery and development program, in: In: Seminars in oncology, 1992, pp. 622-638.

[42] S. Dutertre, M. Ababou, R. Onclercq, J. Delic, B. Chatton, C. Jaulin, M. Amor-Gueret, Cell cycle regulation of the endogenous wild type Bloom's syndrome DNA helicase, Oncogene, 19 (2000) 2731-2738.

[43] S. Sengupta, A. Shimamoto, M. Koshiji, R. Pedeux, M. Rusin, E.A. Spillare, J.C. Shen, L.E. Huang, N.M. Lindor, Y. Furuichi, C.C. Harris, Tumor suppressor p53 represses transcription of RECQ4 helicase, Oncogene, 24 (2005) 1738-1748.

[44] N. van Wietmarschen, W.J. Nathan, A. Nussenzweig, The WRN helicase: resolving a new target in microsatellite unstable cancers, Current Opinion in Genetics & Development, 71 (2021) 34-38.

[45] S. Shechter, S. Ya'ar Bar, H. Khattib, M.J. Gage, D. Avni, Riok1, A Novel Potential Target in MSI-High p53 Mutant Colorectal Cancer Cells, Molecules, 28 (2023) 4452.

[46] E.M. Chan, T. Shibue, J.M. McFarland, B. Gaeta, M. Ghandi, N. Dumont, A. Gonzalez, J.S. McPartlan, T. Li, Y. Zhang, WRN helicase is a synthetic lethal target in microsatellite unstable cancers, Nature, 568 (2019) 551-556.

[47] E.M. Chan, T. Shibue, J.M. McFarland, B. Gaeta, M. Ghandi, N. Dumont, A. Gonzalez, J.S. McPartlan, T. Li, Y. Zhang, J. Bin Liu, J.-B. Lazaro, P. Gu, C.G. Piett, A. Apffel, S.O. Ali, R. Deasy, P. Keskula, R.W.S. Ng, E.A. Roberts, E. Reznichenko, L. Leung, M. Alimova, M. Schenone, M. Islam, Y.E. Maruvka, Y. Liu, J. Roper, S. Raghavan, M. Giannakis, Y.-Y. Tseng, Z.D. Nagel, A. D'Andrea, D.E. Root, J.S. Boehm, G. Getz, S. Chang, T.R. Golub, A. Tsherniak, F. Vazquez, A.J. Bass, WRN helicase is a synthetic lethal target in microsatellite unstable cancers, Nature, 568 (2019) 551-556.

[48] C. Frei, S.M. Gasser, RecQ-like helicases: the DNA replication checkpoint connection, Journal of Cell Science, 113 (2000) 2641-2646.

[49] L. Dutrieux, Y.-L. Lin, M. Lutzmann, R. Rodriguez, M. Cogné, P. Pasero, J. Moreaux, Transcription/Replication Conflicts in Tumorigenesis and Their Potential Role as Novel Therapeutic Targets in Multiple Myeloma, Cancers, 13 (2021) 3755.

[50] A. Daina, O. Michielin, V. Zoete, SwissADME: a free web tool to evaluate pharmacokinetics, drug-likeness and medicinal chemistry friendliness of small molecules, Scientific Reports, 7 (2017) 1-13.

[51] A. Daina, V. Zoete, A boiled-egg to predict gastrointestinal absorption and brain penetration of small molecules, ChemMedChem, 11 (2016) 1117-1121.

[52] C.A. Lipinski, F. Lombardo, B.W. Dominy, P.J. Feeney, Experimental and computational approaches to estimate solubility and permeability in drug discovery and development settings, Advanced Drug Delivery Reviews, 23 (1997) 3-25.

[53] T.M. Sodano, L.A. Combee, C.R.J. Stephenson, Recent advances and outlook for the isosteric replacement of anilines, ACS Medicinal Chemistry Letters, 11 (2020) 1785-1788.

[54] Z.-Y. Yang, Z.-J. Yang, J.-H. He, A.-P. Lu, S. Liu, T.-J. Hou, D.-S. Cao, Benchmarking the mechanisms of frequent hitters: limitation of PAINS alerts, Drug Discovery Today, 26 (2021) 1353-1358.

[55] J.A. Newman, P. Savitsky, C.K. Allerston, A.H. Bizard, Ö. Özer, K. Sarlos, Y. Liu, E. Pardon, J. Steyaert, I.D. Hickson, Crystal structure of the Bloom's syndrome helicase indicates a role for the HRDC domain in conformational changes, Nucleic Acids Research, 43 (2015) 5221-5235.

[56] J.A. Newman, A.E. Gavard, S. Lieb, M.C. Ravichandran, K. Hauer, P. Werni, L. Geist, J. Böttcher, J.R. Engen, K. Rumpel, Structure of the helicase core of Werner helicase, a key target in microsatellite instability cancers, Life Science Alliance, 4 (2021).

[57] A.C. Pike, B. Shrestha, V. Popuri, N. Burgess-Brown, L. Muzzolini, S. Costantini, A. Vindigni, O. Gileadi, Structure of the human RECQ1 helicase reveals a putative strand-separation pin, Proceedings of the National Academy of Sciences, 106 (2009) 1039-1044.

[58] C.C.G.U. Molecular Operating Environment (MOE), 1010 Sherbooke St. West, Suite #910, Montreal, QC, Canada, H3A 2R7, 2023.

[59] X. Wang, S. Shang, Q. Tian, Y. Wang, H. Wu, Z. Li, S. Zhou, H. Liu, Z. Dai, W. Luo, D. Li, X. Xiao, S. Wang, J. Yuan, Imidazolium chloride as an additive for synthesis of 4 (3H)-quinazolinones using anthranilamides and DMF derivatives, Tetrahedron, 76 (2020) 131480.

[60] A. Ouahrouch, M. Taourirte, J.W. Engels, S. Benjelloun, H.B. Lazrek, Synthesis of new 1, 2, 3-triazol-4-yl-quinazoline nucleoside and acyclonucleoside analogues, Molecules, 19 (2014) 3638-3653.

[61] X. Guo, Q. Yang, J. Xu, L. Zhang, H. Chu, P. Yu, Y. Zhu, J. Wei, W. Chen, Y. Zhang, Design and bio-evaluation of indole derivatives as potent Kv1. 5 inhibitors, Bioorganic & Medicinal Chemistry, 21 (2013) 6466-6476.

[62] R.P. Modh, S.P. Kumar, Y.T. Jasrai, K.H. Chikhalia, Design, Synthesis, Biological Evaluation, and Molecular Modeling of Coumarin–P iperazine Derivatives as Acetylcholinesterase Inhibitors, Archiv der Pharmazie, 346 (2013) 793-804.

[63] M.G. Salem, Y.M. Abdel Aziz, M. Elewa, M.S. Nafie, H.A. Elshihawy, M.M. Said, Synthesis, molecular modeling, selective aldose reductase inhibition and hypoglycemic activity of novel meglitinides, Bioorganic Chemistry, 111 (2021) 104909.

[64] G.S. Pedgaonkar, J.P. Sridevi, V.U. Jeankumar, S. Saxena, P.B. Devi, J. Renuka, P. Yogeeswari, D. Sriram, Development of 2-(4-oxoquinazolin-3 (4H)-yl) acetamide derivatives as novel enoyl-acyl carrier protein reductase (InhA) inhibitors for the treatment of tuberculosis, European Journal of Medicinal chemistry, 86 (2014) 613-627.

[65] Zotta, Investigations on the 4-Quinazolone Series. Note II. N-substituted amides of 2-methyl-4-quinazolone-3-(il)-acetic acid, Farmacia, 25 (1977) 207-209.

[66] Zotta, Investigation of the 4-quinazolone series. The N-substituted amides of 2-methyl-4-quinazolone-3 (il)-acetic acid, Farmacia, 27 (1979) 65-68.

[67] S.M. Aboukhatwa, P.A. Sidhom, A. Angeli, C.T. Supuran, H.O. Tawfik, Terminators or guardians? design, synthesis, and cytotoxicity profiling of chalcone-sulfonamide hybrids, ACS omega, 8 (2023) 7666-7683.

[68] R. Elrayess, M.S. Elgawish, M.S. Nafie, N. Ghareb, A.S. Yassen, 2-Phenylquinazolin-4 (3H)-one scaffold as newly designed, synthesized VEGFR-2 allosteric inhibitors with potent cytotoxicity through apoptosis, Archiv der Pharmazie, 356 (2023) e2200654.

[69] T. Mosmann, Rapid colorimetric assay for cellular growth and survival: Application to proliferation and cytotoxicity assays, Journal of Immunological Methods, 65 (1983) 55-63.

[70] S.M. Aboukhatwa, A.O. Ibrahim, H. Aoyama, A.S. Al-Behery, M.A. Shaldam, G. El-Ashmawy, H.O. Tawfik, Nicotinonitrile-derived apoptotic inducers: Design, synthesis, X-ray crystal structure and Pim kinase inhibition, Bioorganic Chemistry, 129 (2022) 106126.